Distribution Agreement

In presenting this thesis or dissertation as a partial fulfillment of the requirements for an advanced degree from Emory University, I hereby grant to Emory University and its agents the non-exclusive license to archive, make accessible, and display my thesis or dissertation in whole or in part in all forms of media, now or hereafter known, including display on the world wide web. I understand that I may select some access restrictions as part of the online submission of this thesis or dissertation. I retain all ownership rights to the copyright of the thesis or dissertation. I also retain the right to use in future works (such as articles or books) all or part of this thesis or dissertation.

Signature:

_____ _____

Sara N. Bramlett **Date**

Characterization of RGS14 in the Adult Mouse Brain and its Role in Limiting Cocaine-Induced Behavioral Adaptations

By

Sara N. Bramlett

Doctor of Philosophy

Graduate Division of Biological and Biomedical Sciences
Molecular and Systems Pharmacology

_____
John Hepler, Ph.D.
Advisor

_____
Shannon Gourley, Ph.D.
Committee Member

_____
Randy Hall, Ph.D.
Committee Member

_____
David Weinshenker, Ph.D.
Committee Member

Accepted:

_____
Kimberly Jacob Arriola, Ph.D., MPH
Dean of the James T. Laney School of Graduate Studies

_____
Date

Characterization of RGS14 in the Adult Mouse Brain and its Role in Limiting Cocaine-Induced Behavioral Adaptations

By

Sara N. Bramlett
B.S., Michigan State University, 2013

Advisor: John R. Hepler, Ph.D.

An abstract of a dissertation submitted to the Faculty of the James T. Laney School of Graduate Studies of Emory University in partial fulfillment of the requirements for the degree of Doctor of Philosophy

Graduate Division of Biological and Biomedical Sciences
Molecular and Systems Pharmacology
2024

Abstract

Characterization of RGS14 in the Adult Mouse Brain and its Role in Limiting Cocaine-Induced Behavioral Adaptations

By Sara N. Bramlett

Regulator of G protein signaling 14 (RGS14) is a multifunctional signaling protein that acts as a natural suppressor of synaptic plasticity, particularly in the hippocampus. Previously, RGS14 was found primarily in the postsynaptic dendrites of pyramidal neurons in hippocampal area CA2, but more recent studies have shown that RGS14 is expressed in multiple neuron populations throughout the hippocampus (CA1 and CA2), caudate nucleus, putamen, globus pallidus, substantia nigra, and amygdala. Additionally, RGS14 is present in limbic regions associated with reward behavior and addiction, such as the central amygdala and nucleus accumbens (NAc). Here, we provide comprehensive mapping of RGS14 in the adult mouse brain, revealing its widespread expression. Strong RGS14 staining is observed in neuron populations of the hippocampal formation, amygdala, septum, bed nucleus of the stria terminalis, and NAc, as well as in axon fiber tracts, including the dorsal fornix and fimbria. These findings suggest that RGS14 modulates core cognitive functions such as sensory perception, emotion, memory, and motivation by regulating plasticity in these regions.

Further, we explored the role of RGS14 in cocaine-induced plasticity in emotional-motivational circuits. Using immunofluorescence and dopamine receptor reporter mice, we found that RGS14 is localized to neurons expressing D1 and D2 dopamine receptors in NAc neurons and is upregulated in the NAc of mice with chronic cocaine history. RGS14-deficient mice exhibited significantly enhanced cocaine-induced locomotor sensitization, conditioned place preference, and conditioned locomotor activity compared to wild-type controls. These results suggest that endogenous RGS14 suppresses cocaine-induced neuroplasticity in emotional and motivational circuits, acting as a protective factor against maladaptive changes that contribute to addiction. Together, these findings reveal that RGS14 plays a key role in regulating both normal and drug-induced plasticity in regions of the brain that govern cognition, motivation, and addiction-related behaviors.

Characterization of RGS14 in the Adult Mouse Brain and its Role in Limiting Cocaine-Induced Behavioral Adaptations

By

Sara N. Bramlett
B.S., Michigan State University, 2013

Advisor: John R. Hepler, Ph.D.

A dissertation submitted to the Faculty of the James T. Laney School of Graduate Studies of Emory University in partial fulfillment of the requirements for the degree of Doctor of Philosophy

Graduate Division of Biological and Biomedical Sciences
Molecular and Systems Pharmacology
2024

Table of Contents

		Page
Chapter 1: Introduction		
1.1	Regulator of G protein Signaling 14: structure and binding partners	1
1.2	RGS14 regulation of postsynaptic signaling and plasticity	3
1.3	Tissue distribution of RGS14	4
1.4	RGS14 in the limbic system	7
1.5	RGS14 in the basal ganglia	11
1.6	Addiction pathology and possible roles of RGS14	13
1.7	Research objectives	18
Chapter 2: Methods		
2.1	Subjects	20
2.2	Immunohistochemistry	20
2.3	Fluorescent imaging and image processing	22
2.4	Assessment of relative protein levels	23
2.5	Drugs	24
2.6	Locomotor sensitization	24
2.7	Conditioned place preference	25
2.8	Statistics	26
Chapter 3: Characterization of RGS14 in the adult mouse brain		
3.1	Heat atlas of RGS14 protein	28
3.2	Olfactory areas	33
3.3	Isocortex	33
3.4	Septal regions	42

3.5 Amygdaloid complex & extended amygdala 43

3.6 Hippocampal formation 44

3.7 Basal ganglia and midbrain 45

3.8 Discussion 59

3.8.1. RGS14 in the hippocampal formation, septal regions, and basolateral amygdala 60

3.8.2. RGS14 in the extended amygdala 63

3.8.3. RGS14 in the basal ganglia 65

3.8.4. Caveats and limitations 66

3.8.5. Conclusions 68

Chapter 4: Endogenous RGS14 suppresses cocaine-induced emotionally-motivated behaviors in female mice

4.1 RGS14 localizes to D1R- and D2R-expressing cells in the nucleus accumbens 69

4.2 RGS14 is upregulated following cocaine challenge in the nucleus accumbens of mice with a chronic cocaine history 71

4.3 Enhanced locomotor sensitization to cocaine in RGS14-KO mice 71

4.4 RGS14 loss increases the expression of cocaine-induced locomotor sensitization 74

4.5 RGS14 loss alters the temporal dynamics of cocaine-induced locomotor activation 75

4.6 RGS14 loss augments the magnitude and duration of cocaine-conditioned place preference 81

4.7 RGS14 loss augments the magnitude and duration of cocaine-conditioned locomotor hyperactivity 82
4.8 RGS14 regulates cocaine-conditioned place preference and cocaine-conditioned locomotor activation through dissociable mechanisms 84
4.9 Cocaine conditioning overcomes stronger inherent place aversion in RGS14-KO mice 84
4.10 RGS14 and pERK colocalize in distinct neurons in the nucleus accumbens and extended amygdala following cocaine 89
4.10.1. RGS14 and pERK colocalize in patches in nucleus accumbens core and shell 90
4.10.2. RGS14 and pERK colocalize in dorsal BNSTov and BNSTju 91
4.10.3. RGS14 and pERK colocalize in the lateral-capsular central amygdala 96
4.11 Discussion 99
4.11.1. RGS14 actions in the nucleus accumbens and regulation of locomotor activity 99
4.11.2. RGS14 actions outside of the nucleus accumbens and cocaine-conditioned place preference 101
4.11.3. Dissociation of RGS14 actions on cocaine-induced limbic and motor system adaptations 103
4.11.4. RGS14 in addiction and anxiety in women and girls 103
4.11.5. Caveats and limitations 105
4.11.6. Conclusions 106

Chapter 5: Final discussion, conclusions, and future directions

5.1 Overview of brain RGS14 expression and possible functional implications 107

5.2 Possible differential regulation of signaling in nucleus accumbens D1- and D2-MSN 108

5.3 Implications for RGS14 in human disease and future directions 111

List of Tables and Figures

Page

Tables

Table 1: Summary of RGS14 immunoreactivity in adult mouse brain: allocortex and isocortex 41

Table 2: Summary of RGS14 immunoreactivity in adult mouse brain: limbic system, basal ganglia, and midbrain 57

Table 3: Summary of RGS14 immunoreactivity in adult mouse brain: fiber tracts 58

Table 4: Locomotor sensitization statistics: induction 79

Table 5. Locomotor sensitization statistics: challenge 80

Table 6. Conditioned place preference statistics 88

Figures

Figure 1: RGS14 domains and binding partners 2

Figure 2: RGS14 regulation of postsynaptic signaling and plasticity 5

Figure 3: Reported tissue expression of RGS14 in adult primate and rodent 6

Figure 4: Major neurocircuits affected by RGS14 (existing model) 14

Figure 5: Heat atlas of RGS14 protein levels in adult mouse brain: rostral to medial 29

Figure 6: Heat atlas of RGS14 protein levels in adult mouse brain: medial to caudal 31

Figure 7: RGS14 immunoreactivity is widespread and moderate across olfactory areas 35

Figure 8: RGS14 immunoreactivity is low in prefrontal and frontal cortices 37

Figure 9: RGS14 immunoreactivity is moderate in parietal-temporal and occipital cortices 39

Figure 10: RGS14 immunoreactivity is intense in the lateral septal complex 47

Figure 11: RGS14 immunoreactivity is intense in select subregions of the amygdaloid complex and extended amygdala 49
Figure 12: RGS14 immunoreactivity is high throughout the hippocampus proper 51
Figure 13: RGS14 immunoreactivity is widespread and moderate in retrohippocampal regions 53
Figure 14: RGS14 immunoreactivity is variable across the basal ganglia 55
Figure 15: RGS localizes to D1R and D2R-expressing cells in the nucleus accumbens 70
Figure 16: RGS14 is upregulated in nucleus accumbens core and shell 2 hours after cocaine challenge in cocaine-experienced mice 72
Figure 17: Locomotor sensitization to cocaine is enhanced in RGS14-KO mice 77
Figure 18: RGS14 loss enhances cocaine-conditioned place preference and locomotor hyperactivity 86
Figure 19: RGS14 colocalizes with pERK1/2 in ventromedial NAc following cocaine 92
Figure 20: RGS14 colocalizes with pERK in dorsal BNSTov and BNSTju following cocaine 95
Figure 21: RGS14 colocalizes with pERK in lateral-capsular central amygdala following cocaine 98
Figure 22: Simplified anatomo-functional neurocircuitry diagram of prominent RGS14-expressing regions in the adult mouse brain (updated model) 109
Figure 23: RGS14 may be regulating cocaine-induced dopamine signaling differently in striatal D1- and D2-MSNs 112

List of Abbreviations

ACC: anterior cingulate cortex, **ANOVA**: analysis of variance, **AUD**: auditory cortex, **AgI**: agranular insular cortex, **AON**: anterior olfactory nucleus, **BLA(a,p)**: basolateral amygdala- (anterior, posterior), **BNST(ju,ov)**: bed nucleus of the stria terminals- (juxtacapsular, oval), **CA(1,2,3)**: hippocampal field *cornu ammonis* (1, 2, 3), **CaM**: calmodulin, **CaMKII**: calmodulin-dependent kinase II, **CeA**: central amygdala, **Ce(C,L,M)**: central amygdala- (capsular, lateral, medial), **COA(pm)**: cortical amygdalar area- (posterior; medial zone), **Coc**: cocaine, **CPP**: conditioned place preference, **CPu**: caudoputamen, **CRF**: corticotropin-releasing factor, **CRFR1**: CRF type I receptor, **D1R**: D1 dopamine receptor, **D2R**: D2 dopamine receptor, **(D1,D2)-MSN**: (D1R, D2R)-containing medium spiny neuron, **DG**: dentate gyrus, **dHIPP**: dorsal hippocampus, **ECT**: ectorhinal cortex, **ENT(l,m)**: entorhinal cortex- (lateral, medial), **EPd**: endopiriform nucleus- dorsal, **ERK**: extracellular signal-regulated kinase, **FC**: fasciola cinerea, **FS**: fundus of the striatum, **GAP**: GTPase accelerating protein, **GP**: globus pallidus, **GPCR**: G protein-coupled receptor, **GPR**: G protein regulatory (motif), **GU**: gustatory cortex, **IG**: induseum griseum, **ju**: juxtacapsular nucleus of the BNST, **LA**: lateral amygdala, **LR**: L507R mutant, **LS**: lateral septal nucleus, **LUT**: look-up table, **LTD**: long-term depression, **LTP(-IE)**: long-term potentiation (of intrinsic excitability), **MeA(pd)**: medial amygdala- (posterodorsal), **MO**: motor cortex, **MSN**: medium spiny projection neuron, **NAc(C,S)**: nucleus accumbens- (core, shell), **NDB**: nucleus of the diagonal band, **NES**: nuclear export sequence, **NGS**: normal goat serum, **NHERF1**: NHERF family PDZ scaffold protein 1, **NLOT**: nucleus of the lateral olfactory tract, **NLS**: nuclear localization sequence, **OT**: olfactory tubercle, **ov**: oval nucleus of the BNST, **PAA**: piriform-amygdalar area, **PBS**: phosphate-buffered saline, **PERI**:

perirhinal cortex, **PFA**: paraformaldehyde, **PIR**: piriform cortex, **PL**: prelimbic cortex, **POST**: postsubiculum, **PP1**: protein phosphatase 1, **PTL:** posterior parietal association cortex, **RGS(14)**: regulator of G protein signaling (14), **RGS14-KO**: RGS14-knockout, **RN**: red nucleus, **RSPv**: retrosplenial cortex- ventral, **Sal**: saline, **SF**: septofimbrial nucleus, **SFO**: subfornical organ, **SH**: septohippocampal nucleus, **SI**: substantia innominata, **SN(c,r)**: substantia nigra- (pars compacta, pars reticulata), **SS**: somatosensory cortex, **STEP**: striatal-enriched protein tyrosine phosphatase, **SUB(d,v)**: subiculum- (dorsal, ventral), **TeA**: temporal association cortex, **TR**: postpiriform transition cortex, **TRS**: triangular nucleus of the septum, **TTd**: taenia tecta- dorsal, **vHIPP**: ventral hippocampus, **VIS**: visual cortex, **VISC**: visceral cortex, **VP**: ventral pallidum, **VTA**: ventral tegmental area, **WT**: wild-type, **XPO1**: exportin1.

Chapter 1: Introduction

This chapter contains figures and text that have been modified from the published manuscripts:

Harbin, N. H., **Bramlett, S. N**., Montanez-Miranda, C., Terzioglu, G., & Hepler, J. R. (2021). RGS14 Regulation of Post-Synaptic Signaling and Spine Plasticity in Brain. *International Journal of Molecular Sciences*, *22*(13). https://doi.org/10.3390/ijms22136823.

Montanez-Miranda, C., **Bramlett, S. N.**, & Hepler, J. R. (2023). RGS14 expression in CA2 hippocampus, amygdala, and basal ganglia: Implications for human brain physiology and disease. Hippocampus, 33(3), 166–181. https://doi.org/10.1002/hipo.23492.

1.1 Regulator of G protein signaling 14: structure and binding partners

The Regulators of G protein Signaling (RGS) are a family of proteins that negatively regulate G protein-coupled receptor (GPCR)-G protein signaling events (Hollinger et al., 2001; Sjögren, 2011; Stewart & Fisher, 2015). Their eponymous RGS domain facilitates GTP hydrolysis by active Gα-GTP subunits, greatly accelerating conversion to the inactive GDP-bound state, a function known as GTPase accelerating protein, or GAP, activity. RGS proteins negatively modulate G protein-coupled receptor (GPCR)-G protein signaling via their RGS14 domain GAP activity, which speeds up reassociation of heterotrimeric G protein subunits and recoupling with GPCRs, terminating signaling. While many RGS proteins are dedicated GAPs consisting of a single RGS domain, some are much larger and more complex featuring multiple domains and binding partners. One such complex RGS protein is RGS14, a multifunctional scaffolding protein enriched in the brain (Hollinger et al., 2001).

Figure 1 shows a diagram of RGS14 protein structure and intracellular binding partners, with approximate locations of binding domains and motifs. In addition to an RGS domain which confers

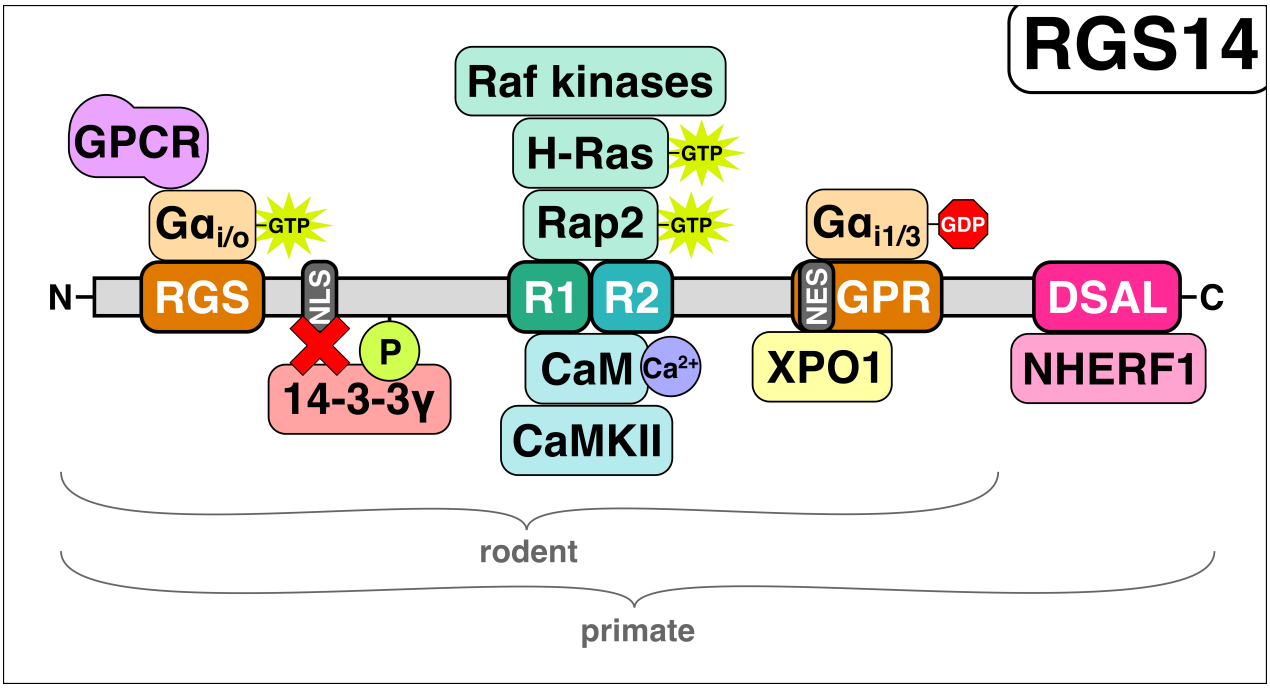


Figure 1. RGS14 domains and binding partners. Approximate locations of RGS14 binding domains, motifs, and localization sequences (white text) and known protein binding partners. See text for descriptions. Abbreviations: **CaM**: calmodulin, **CaMKII**: calcium-calmodulin dependent kinase II, **DSAL**: aspartate-serine-alanine-lysine (PDZ-binding motif), **GPCR**: G protein-coupled receptor, **GPR**: G protein regulatory motif, **NES**: nuclear export sequence, **NHERF1**: NHERF family PDZ scaffold protein 1, **NLS**: nuclear localization sequence, **R1/R2**: Ras/Rap binding domains R1/R2, **RGS**: regulator of G protein signaling binding domain, **XPO1**: exportin1.

inactivating GAP activity on GTP-bound Gαi/o proteins, RGS14 also contains tandem binding domains for Ras/Rap (R1 and R2) that bind and sequester active GTP-bound small G proteins H-Ras and Rap2 and interact with calcium-bound calmodulin (Ca2+/CaM) to suppresses extracellular signal-regulated kinase (ERK) and calcium signaling (Evans et al., 2018a; Evans et al., 2018b; Shu et al., 2010; Vellano et al., 2013). RGS14 shuttles to and from the nucleus via recognition of its nuclear localization sequence (NLS) for import and for export (Squires et al., 2020). RGS14 nuclear import is blocked by binding of the regulatory protein 14-3-3γ at phosphorylated Ser218, possibly due to occlusion of the nearby NLS (Gerber et al., 2018). RGS14 nuclear export is prevented by exportin1 (XPO1) obstruction of the NES, which is located near the C-terminus, within the G protein regulatory (GPR) motif (Squires et al., 2020). The L507R reporter mouse line used in the studies herein contains a leucine-to-arginine point mutation within the NES that disrupts sequence recognition. The GPR, also known as GoLoco motif binds inactive GDP-bound Gαi1/3, a function likely important for subcellular localization of RGS14 (Brown et al., 2016; Hollinger et al., 2001). The C-terminus of the primate RGS14 variant also contains a PDZ-binding motif (DSAL) shown to regulate renal phosphate update via binding NHERF family PDZ scaffold protein 1 (NHERF1) (Friedman et al., 2022)

1.2 RGS14 regulation of postsynaptic signaling and plasticity

RGS14 regulates postsynaptic signaling and plasticity in the hippocampus (Evans et al., 2018b; Harbin et al., 2021; Samadi et al., 2023; Shu et al., 2010; Vellano et al., 2011, Vellano et al., 2013). RGS14 is highly enriched in dendritic spines of hippocampal area CA2 where it naturally suppresses ERK- and calcium-dependent long-term potentiation (LTP) and structural plasticity linked to spatial learning (Evans et al., 2018b; Lee et al., 2010). A schematic of RGS14

interactions with proteins involved in intracellular regulation of postsynaptic plasticity is shown in Figure 2.

In addition to suppression of LTP, RGS14 was also shown to be necessary for metabotropic glutamate receptor-dependent long-term depression (LTD) in CA2 in a manner that presumably involves positive modulation of striatal-enriched protein tyrosine phosphatase (STEP) activity (Samadi et al., 2023). We previously reported colocalized RGS14 and STEP immunoreactivity in CA2 and other limbic regions (Foster et al., 2021) The mechanism by which RGS14 mediates LTD in CA2 is unknown, but potential hints can be found in an interactome analysis revealing the existence of RGS14 in protein complexes with regulatory and catalytic subunits of protein phosphatase 1 (PP1) (Evans et al., 2018a). Activation of STEP by PP1 dephosphorylation at Ser221 permits STEP to inactivate signaling molecules involved in synaptic potentiation and growth, including ERK and the non-receptor tyrosine kinase Fyn (Goebel-Goody et al., 2012). It is possible that RGS14 scaffolding facilitates LTD in CA2 by localizing PP1 to dendritic spines to optimally position it to bind and activate STEP.

1.3 Tissue distribution of RGS14

The RGS domain is evolutionarily conserved among vertebrate and invertebrate species (Vatner et al., 2018). RGS14 specifically is conserved in vertebrates such as chimpanzee, rhesus macaque, dog, cow, mouse, rat, chicken, zebrafish, and frog, and in invertebrates as an early homologue (ncbi.nlm.nih.gov/homologene). RGS14 has been primarily studied in rodents and primates, where it was shown to be heavily expressed in the brain and lymphatic system, and to a lesser degree in organs such as the kidney, heart, liver, lungs, skin, and gonads (Fig. 3) (Agudelo et al., 2018; Kardestuncer et al., 1998; Snow et al., 1997). While RGS14 in peripheral tissue plays an important role in physiology, the present work focuses on RGS14 in the brain.

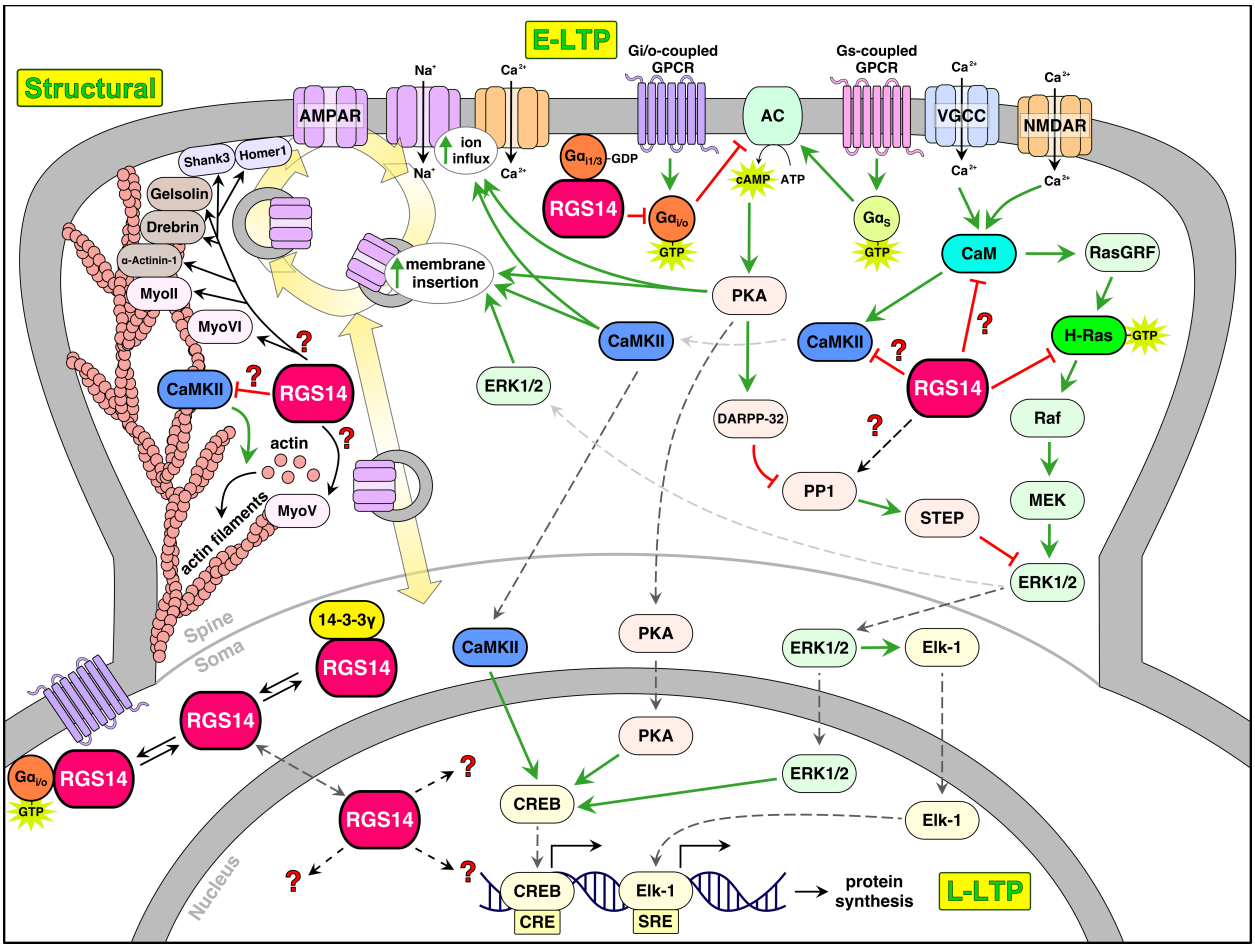


Figure 2. RGS14 regulation of postsynaptic signaling and plasticity. RGS14 binds many protein partners, directly or indirectly, to regulate signaling events and plasticity in the post synaptic dendritic spine (top) and in the soma where it shuttles in/out of the nucleus (bottom). Key: green line with arrow = activation (increase if inside bubble), red line with T arrow = inhibition, black dashed line with arrow = interaction or relationship (unspecified directionality), gray dashed line with arrow = movement, question mark = unknown or uncertain interaction. Refer to text and to Harbin et. al., 2021, for details.

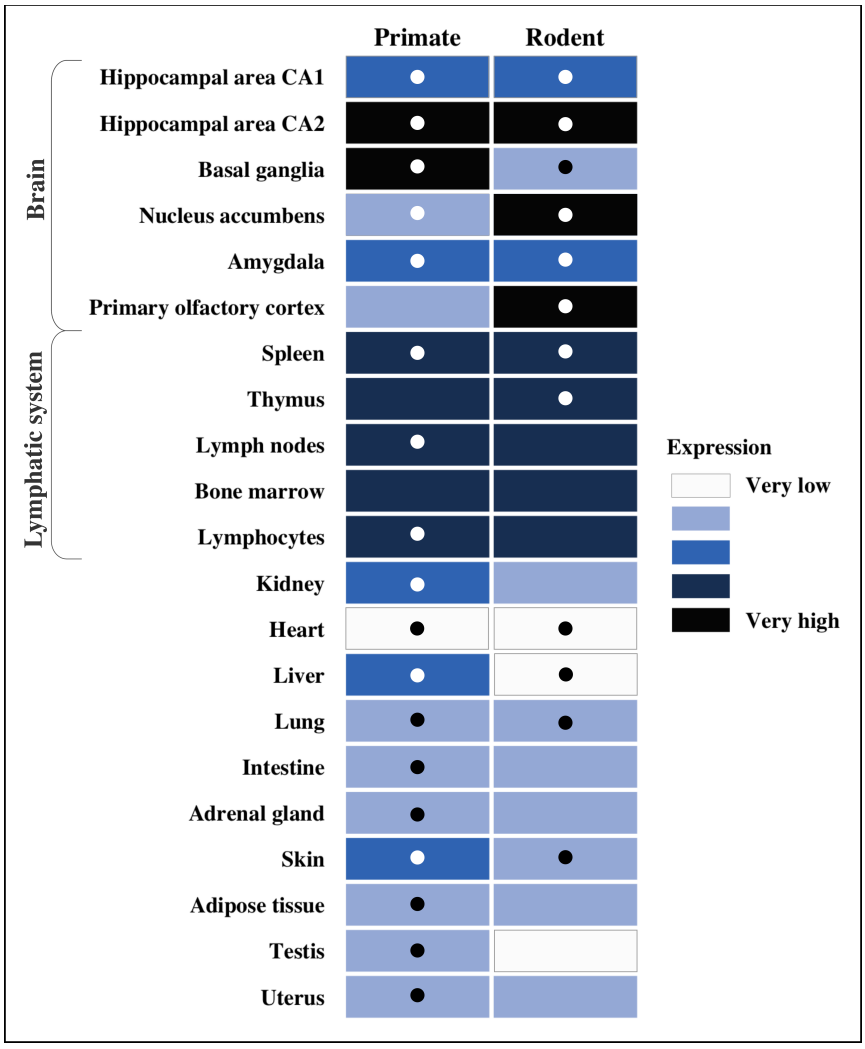


Figure 3. Reported tissue expression of RGS14 in adult primate and rodent. Cell shading indicates RGS14 mRNA expression across tissues. Dot indicates positive RGS14 protein expression data. See Harbin et al., 2021 for detailed list of data source aggregates.

A prior study from our group characterized the postnatal developmental expression of RGS14 in the mouse brain (Evans et al., 2014). RGS14 mRNA levels were found to be low and the protein was absent in the brain at birth. RGS14 protein was first detectable in early postnatal development (P7), with whole-brain levels of protein and mRNA increasing across development (P7–P21) until reaching a plateau in adulthood that persisted throughout maturity. In the primary olfactory areas, including the anterior olfactory nucleus and piriform cortex, and the olfaction-linked orbital and entorhinal cortices, protein expression was found to be upregulated during development and maintained to varying degrees into adulthood. Transient postnatal expression was observed in neocortical layers II/III and V. Hippocampal protein levels are initially low at P7 before climbing markedly throughout development to show prominent expression in adulthood, specifically in area CA2 and the fasciola cinerea (FC).

Adult rodents and primates share pronounced RGS14 expression in the hippocampus, striatum, and amygdala (Evans et al., 2014; Foster et al., 2021; Lee et al., 2010; Squires et al., 2018). Notable levels of RGS14 immunoreactivity are seen in the primary olfactory areas in adult rodents, staining that is absent in primates (Evans et al., 2014) Immunoblotting of hippocampal and striatal punches from mice and macaques revealed several apparent truncated RGS14 splice variants unique to the primate striatum (Squires et al., 2018).

1.4 RGS14 in the limbic system

The limbic system is a neuroanatomical network of discrete structures responsible for emotional processing, and plays a major role in attention, memory, and decision-making. We have demonstrated elevated RGS14 expression in the hippocampus and amygdala, the two largest limbic structures by volume (Foster et al., 2021; Squires et al., 2018).

The overarching role of the hippocampus involves the mapping of one's experiences to the environment. This type of cognition fundamentally requires the mechanisms of learning and memory, and as such, learning and memory have historically been attributed to and studied in the hippocampus. Our group has shown that RGS14 is strongly expressed in specific subregions of the hippocampus, notably in pyramidal cell bodies, axons, and dendrites throughout the entire rostro-caudal range of area CA2 and in the FC (Evans et al., 2014; Lee et al., 2010; Squires et al., 2018). RGS14 staining is also observed in the stratum oriens layer of area CA1, which is thought to be in neuronal processes originating from CA2, and sparsely in CA1 pyramidal cells in the rodent brain. In the primate hippocampus, RGS14 exhibits typical intense expression in area CA2 (Squires et al., 2018), consistent with studies in mice (Evans et al., 2014; Foster et al., 2021). However, RGS14 was also found to be substantially expressed in area CA1 of primates, where it is found pre- and post-synaptically in neuropil, pyramidal cell bodies, and proximal dendritic profiles (Squires et al., 2018).

Consistent with its expression in the hippocampus, RGS14 plays key roles in hippocampal-based learning and memory. Social memory is critically dependent on CA2 (Hitti & Siegelbaum, 2014; Meira et al., 2018; Smith et al., 2016; Stevenson & Caldwell, 2014; Young et al., 2006), and projections from CA2 onto ventral CA1 are necessary for dynamic aspects of social memory (Meira et al., 2018). CA2 mediates the formation and stabilization of the memory of the mother required for maternal preference in neonates, followed by nonfamilial preference in adulthood (Laham et al., 2021). Within the hippocampus, area CA2 is distinctly targeted by the magnocellular projection neurons from the paraventricular nucleus of the hypothalamus which produce the neuropeptides oxytocin and vasopressin, key effectors of social processing in mammals (Cui et al., 2013; Zhang & Hernández, 2013). In addition to social memory, CA2 neuronal ensembles encode

certain types of temporal and spatial information (Kay et al., 2016; Mankin et al., 2015). CA2 is also capable of driving spatial memory via inputs to CA1, though this is suppressed under normal conditions due to the unique resistance of CA2 neurons to LTP, which is partially imposed by RGS14 (Evans et al., 2015; Zhang & Hernández, 2013). RGS14 loss is linked to improved spatial memory, demonstrated by superior performance in the Morris water maze and novel object recognition task in mice with genetically-deleted RGS14 (RGS14-KO) mice (Lee et al., 2010), but impaired social recognition memory when measured in a social discrimination task (Samadi et al., 2023)

The amygdala is an almond-shaped cluster of cortical-adjacent nuclei critical to mediating behavioral and physiological responses to emotionally salient stimuli. Amygdaloid RGS14 in macaques is found in the basolateral, basomedial, and centrolateral subregions, as well as the amygdalostriatal transition area (Squires et al., 2018). RGS14 expression had not been as extensively explored throughout the rodent amygdala, though we did previously show dense RGS14 immunoreactivity in the central amygdala (CeA), specifically in the lateral CeA subregion (CeL) (Foster et al., 2021).

The RGS14-containing basomedial and basolateral amygdalar nuclei are components of the basolateral complex, which, in combination with the lateral nucleus, are collectively referred to as the basolateral amygdala (BLA). The BLA is responsible for the affective valuation of stimuli, as well as the acquisition and expression of both fear- and reward-based learning (Bliss-Moreau et al., 2011; Sun et al., 2020; Wassum & Izquierdo, 2015). This brain region is the primary input structure of the amygdala, receiving projections from sensory cortex, prefrontal cortex, hippocampus, and thalamus. In addition to its substantial intra-amygdaloid connections, the BLA sends projections back to the prefrontal cortex, hippocampus, and thalamus. It also extensively

innervates the nucleus accumbens (NAc), a ventral striatal region with key control over motivational drive, and BLA → NAc connections have been shown to mediate reward-seeking (Ambroggi et al., 2011; Kochli et al., 2020; Stuber et al., 2011).

The BLA is extensively interconnected with the extended amygdala macrostructure, which includes the CeA, bed nucleus of the stria terminalis (BNST), and substantia innominata (SI) and is involved in processing the emotional components of motivation. The CeA interfaces between the amygdala proper and the extended amygdala. It receives emotional information from the BLA and sends descending connections to the midbrain/brainstem to initiate physiological responses (e.g. changes in sympathetic nervous system tone) and to the NAc, BNST, and hypothalamus to initiate behavioral responses (e.g. approach or avoidance, motor activation or inhibition) (Gorka et al., 2018; Jiang et al., 2021; Pêgo et al., 2008; Terburg et al., 2018; Viviani et al., 2011). The CeA is best known for its role in behavioral, autonomic, and neuroendocrine stress responses (Callahan et al., 2013; Hitchcock & Davis, 1986; Kalin et al., 2004; Mogenson & Calaresu, 1973; Stock et al., 1978) The CeL in particular contains one of the largest populations of corticotropin-releasing factor (CRF)-immunoreactive neurons outside of the hypothalamus (Cassell et al., 1986; Cummings et al., 1983), and robust CeL RGS14 staining is seen in both macaques and mice (Foster et al., 2021; Squires et al., 2018). CRF is a stress-linked neuropeptide that is capable of profound changes in the brain due to its prolonged duration of action and wide field of influence (Mantsch, 2022). Evidence suggests that RGS14 tempers behavioral reactivity to stress; in RGS14-KO mice, both novelty stress and an anxiogenic dose of cocaine were shown to augment thigmotaxis, a metric for anxiety-like behavior in rodents (Foster et al., 2021).

We have established that RGS14 regulates hippocampal-based learning and memory (Lee et al., 2010), and RGS14 is well-positioned to regulate learning and memory based in the amygdala

as well. Fear conditioning critically involves synaptic plasticity of BLA outputs onto the CeA, and synaptic plasticity at local and long-range projection neurons in the CeL in particular has been shown to be essential for fear learning, fear memory recall, and behavioral fear responses (Ciocchi et al., 2010; Li et al., 2013; Penzo et al., 2014; Sun et al., 2020). Consistent with this idea, RGS14 loss increases freezing in a cued fear memory test in female mice (Alexander et al., 2019). Additionally, a non-synonymous coding single nucleotide polymorphism in the RGS14 gene is linked to increased freezing during both cued and contextual fear conditioning, which also suggests additional involvement of the hippocampus (Parker et al., 2012).

1.5 RGS14 in the basal ganglia

The basal ganglia are a set of interconnected subcortical nuclei principally involved processing motor function, including conscious motor behavior and motor learning, as well as related cognitive processes such as motivation and action selection. It is organized such that information enters the basal ganglia at the striatum, then travels outward through the pallidum and/or midbrain en route to the thalamus (Lanciego et al., 2012; Young et al., 2024). RGS14 immunoreactivity is seen in several basal ganglia structures, with the strongest signal found in the striatum and somewhat less in the internal and external globus pallidus (GP) and substantia nigra (SN) (Foster et al., 2021; Squires et al., 2018). Ultrastructural analysis of primate tissue revealed RGS14 immunoreactivity in the striatum in neurons morphologically consistent with medium spiny projection neurons (MSNs), and in axons and terminals of putative striatopallidal and striatonigral projection neurons in the GP and SN. Striatal RGS14 was found to be largely located in the cytosol of postsynaptic structures, though significant staining was also seen in the nucleus in primates that was not seen in rodents (Squires et al., 2018).

The striatum is the primary input node of the basal ganglia, integrating excitatory inputs predominantly from the limbic system and cortex with coincident neuromodulatory inputs from a variety of sources into a unified output that effects motor behavior. The ventral striatum, comprised of the NAc and olfactory tubercle (OT), primarily processes the more emotionally-driven basal ganglia functions including aspects of motivation and decision-making, while the dorsal striatum, consisting of the caudoputamen (CPu) (caudate nucleus and putamen in primates), is moreso involved in motor processing, including roles in conscious movement, habit formation, and procedural learning. The circuitry that commands behavioral responses to internal and external stimuli flows through broadly hierarchical loops that gradually shift the locus of control from ventral to dorsal striatum as behavior shifts from volitional to habitual (Belin & Everitt, 2008; Haber et al., 2000; Hunnicutt et al., 2016; Kalivas, 2009). This organization allows for behavioral flexibility or stability in the face of changing or stable contingencies, respectively (Cox & Witten, 2019; Schultz, 2016). RGS14 immunoreactivity is seen in both ventral and dorsal striatum in macaques and mice, though dorsal striatal signal is more intense than ventral in macaques, while the opposite was observed in mice (Foster et al., 2021; Squires et al., 2018).

There is a general dichotomy in striatal MSNs in terms of two main facets: whether their targets project to the thalamus directly or indirectly through an additional GABAergic basal ganglia connection (direct vs. indirect pathway MSNs), and whether they predominantly express D1 or D2 dopamine receptors (D1R & D2R) (D1-MSNs vs. D2-MSNs). Neurons of the dorsal striatum mostly follow a single dichotomy that extends to both facets: D1-MSNs project along direct pathways and D2-MSNs project along indirect pathways. Activation of dorsal striatal direct pathway/D1-MSNs removes basal inhibitory tone on the thalamus and ultimately drives motor activation, while the additional inhibitory connection present in indirect pathways means that

activation of dorsal striatal D2-MSNs maintains thalamic inhibition, promoting immobility. Hence, the basal ganglia pathways involving dorsal striatum are commonly referred to as the GO (direct) pathway and NO-GO (indirect) pathways.

On the other hand, these dichotomies partially overlap in MSNs of the ventral striatum. NAc D1- and D2-MSNs alike participate in basal ganglia direct and indirect pathways and cross paths in the ventral pallidum (Kupchik et al., 2015; Kupchik & Kalivas, 2017). This allows for coordinated effects of D1- and D2-MSN activation in the ventral striatum, unlike in dorsal striatum where the effects of D1- and D2-MSN activation along a given pathway strictly oppose each other (Kupchik et al., 2015; Zachry et al., 2024). The capacity of ventral striatal D1- and D2-MSNs to work both in concert and in opposition allows for sophisticated regulation of motor behavior, and their capacity for plasticity allows for behavioral strategies to be updated upon receiving new information, such as when a contingency changes.

The relative distribution of RGS14 in D1- and D2-MSNs in ventral and dorsal striatum is of interest, given that RGS14 is equipped to impact dopaminergic signaling differently within each MSN subtype. All known dopamine receptors are GPCRs, but D1R normally couples with Gs/olf while D2R couples with Gi/o (Beaulieu & Gainetdinov, 2011). If canonical signaling pathways are adhered to, it would mean that RGS14, due to the Gαi/o-GTP specificity of its RGS domain, has the capacity to directly curtail the acute effects of dopamine receptor activation in D2-MSNs only, and not in D1-MSNs. Striatal D1-MSNs, however, undergo ERK-dependent LTP when receiving coincident dopamine and glutamate input, which RGS14 may also be functioning to suppress.

1.6 Addiction pathology and possible roles of RGS14

Shown in Figure 4 is the existing model of major anatomo-functional relationships between known RGS14-containing brain regions that served as the conceptual basis for the current work.

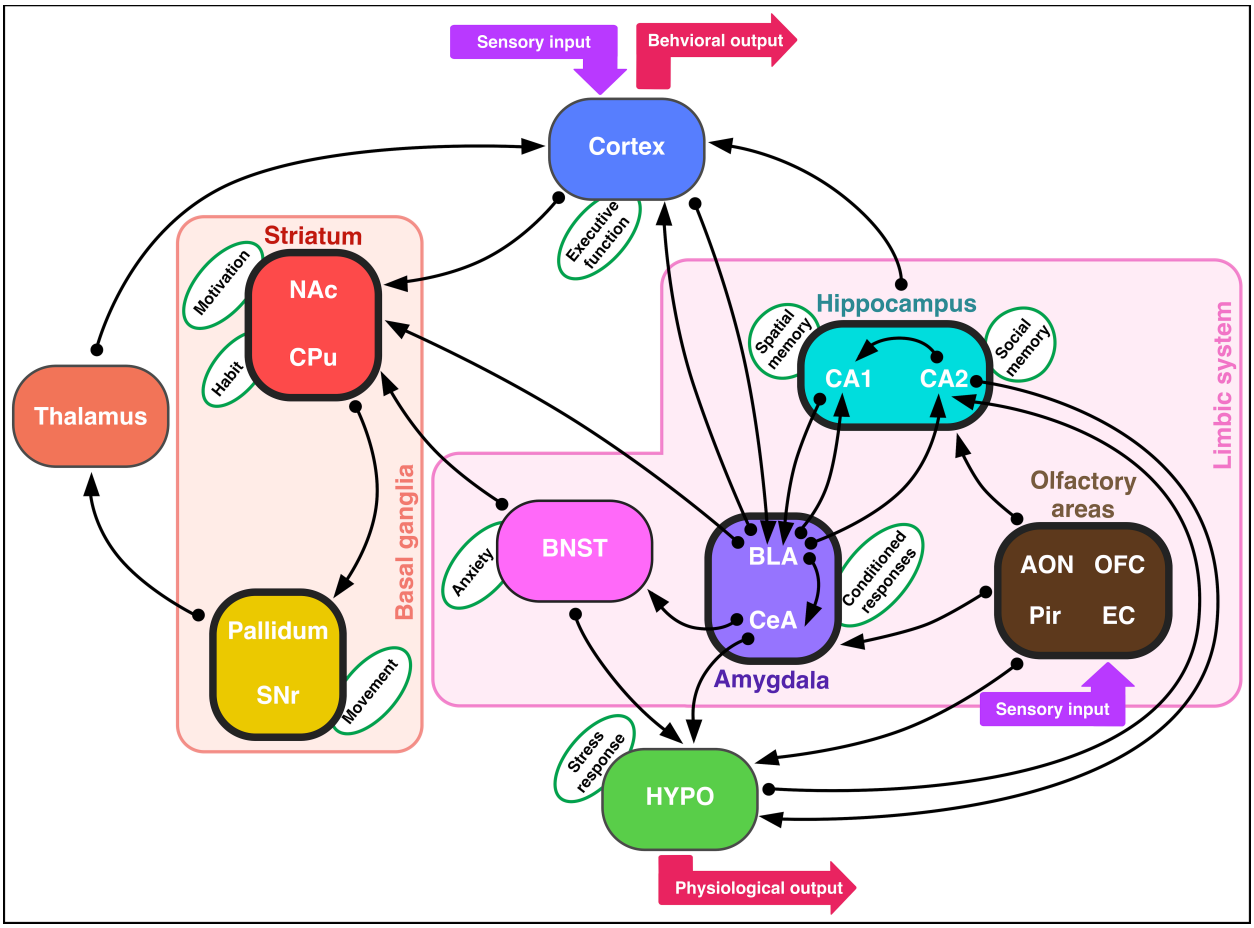


Figure 4. Major neurocircuits affected by RGS14 (existing model). Thick box borders indicate RGS14-expressing regions. Behavior is driven by a complex signaling flow between regions including the cortex, limbic system, basal ganglia, thalamus, and hypothalamus. As a general overview, external information is first processed cortically (including olfactory cortex), then flows to the limbic system for emotional interpretation, then to the basal ganglia for processing of motivation and physical movement, then to the thalamus and back to the cortex for behavioral execution or inhibition. Limbic regions are also highly interconnected with the hypothalamus, which drives the physiological stress response. RGS14 may affect the synaptic strength of these connections at several points throughout the limbic system and basal ganglia. Abbreviations: AON, anterior olfactory nucleus; BLA, basolateral amygdala; BNST, bed nucleus of the stria terminalis; CeA, central amygdala; CPu, caudoputamen (rodents) or caudate and putamen (primates); EC, entorhinal cortex; HYPO, hypothalamus; NAc, nucleus accumbens; OFC, orbitofrontal cortex; Pir, piriform cortex; SNr, substantial nigra pars reticulata.

RGS14 immunoreactivity was identified in several major limbic structures of rodents and primates, including the hippocampus, amygdala, and olfactory cortex, reflecting known or possible roles in modulating memory and emotional processing. It was also seen in the basal ganglia, including in the ventral and dorsal striatum, globus pallidus, and substantia nigra, reflecting possible roles in motivation and motor function. This suggests an overarching role of RGS14 in modulating cognitive processing of external and internal experiences, including emotional processing, and the ultimate behavioral and physiological responses that they elicit. Novelty-induced hypolocomotion and high-dose cocaine-induced hyperlocomotion were observed in RGS14-KO mice, indicating that RGS14 is regulating immediate, short-term signaling in these circuits (Foster et al., 2021).

However, the hypothetical capacity to limit potentiation of connections between these regions puts RGS14 in a position that could be uniquely critical for opposing many of the maladaptive neuroplastic changes that underlie addiction.

Addiction is a disease in which compulsive drug use gives rise to compounding harmful consequences to health and well-being. All known addictive drugs directly or indirectly enhance dopamine signaling in the NAc, which induces feelings of reward that serve as the initial motivating factor for continued drug use (Hall et al., 1994; Nestler, 2005). Repeated drug use gradually usurps control of motivated behavior in part because switches the processing of behaviors surrounding drug use from ventral striatum (NAc) to dorsal, which is a key mechanism of progression from the acquisition to the maintenance stage of addiction as learned behaviors associated with drug use solidify and become habitual (Everitt & Robbins, 2016). This is accompanied by homeostatic adaptations to chronic reward system overactivation, including blunted reward function (e.g. decreased NAc dopamine neurotransmission) which results in

escalation of drug use due to a greater intake being required to achieve the same positive subjective effects (i.e. the "high") (de Guglielmo et al., 2019; Liu et al., 1989). Increased recruitment of stress response systems (e.g. increased CRF release from the CeA) occurs as an allostatic adaptation to reduced reward function, and causes withdrawal from drug to induce negative affective and interoceptive states that further drive compulsive drug use and relapse (de Guglielmo et al., 2019; Liu et al., 1989; Volkow et al., 1993, Volkow et al., 1996, Volkow et al., 2007) This shift in motivation for drug use from the appetitive effects of drug reward to the aversive effects of drug withdrawal is underlaid by a shift in processing from the BLA to the extended amygdala (Koob & Le Moal, 2008; Koob & Volkow, 2016).

Addictive drugs reconfigure the brain in part by engaging mechanisms of synaptic plasticity, including LTP and long-term depression (LTD) at select synapses in the basal ganglia and limbic regions (Glangetas et al., 2013; Harris & Winder, 2018; Russo et al., 2010). The highly addictive psychostimulant cocaine enhances extracellular levels of dopamine and other monoamine neurotransmitters throughout the brain by directly blocking their presynaptic reuptake to alter both acute neuronal excitability and neuroplasticity (Hummel & Unterwald, 2002; Jones et al., 2009; Pan et al., 2008). Monoamine neurotransmission in emotional-motivational brain circuits supports transient and lasting behavioral adaptations through different mechanisms, and it is the capacity of cocaine to engage dopamine-driven synaptic plasticity that allows the drug to usurp cognitive processing and behavior to support its continued use (Chiara & Impérato, 1988; Di Chiara & Imperato, 1988; Kalivas & O'Brien, 2008; Salamone, 1994; Salamone & Correa, 2012). Dopamine receptors are highly expressed in limbic and basal ganglia regions, particularly in the striatum, making these regions uniquely susceptible to the effects of cocaine (Beaulieu & Gainetdinov, 2011).

Acute behavioral effects of cocaine occur mostly through transient changes in ion channel conductivity, while effects on learning and memory are tied to convergent signaling with glutamate receptors onto activation of phosphorylated extracellular signaling regulated kinase (ERK) (Berke & Hyman, 2000; Cahill et al., 2014; Pascoli et al., 2014; Speranza et al., 2021). Studies show that in hippocampal area CA2, RGS14 suppresses post-synaptic ERK-dependent LTP and is also essential for mGluR-dependent LTD (Lee et al., 2010; Samadi et al., 2023). Transient increases in ERK activity lead to short-lived enhancements of neuronal excitability mostly through actions at ion channels in dendrites and spines (Hu & Gereau, 2003; Tompkins et al., 2016), while persistent ERK overactivation promotes nuclear translocation and stabilization of neuroplastic changes via modification of transcription factor activity (Lidke et al., 2010; Shindo et al., 2016). By altering ERK and calcium signaling in CA2 and other regions, evidence suggest that RGS14 has the overall metaplastic effect of suppressing post-synaptic spine growth (Evans et al., 2018b).

Evidence supports the notion that RGS14 suppresses postsynaptic growth related to emotion-driven learning, a critical mechanism of adaptive behavior (Wang & Cui, 2018). RGS14 is enriched in brain structures linked to reward, reinforcement, and addiction, including the ventral and dorsal striatum, BLA, CeA, and hippocampus (Foster et al., 2021; Squires et al., 2018). We previously reported that genetic deletion of RGS14 (RGS14-KO) enhances Morris water maze performance in mice (Lee et al., 2010), while another group reported elevated fear conditioning in RGS14-KO females (Alexander et al., 2019), suggesting that RGS14 loss improves hippocampal- and amygdala-based learning and memory, the latter in a sex-dependent manner. RGS14-KO mice also exhibit greater locomotor activation and increased anxiety-like behavior in response to combined novelty and high-dose cocaine, accompanied by higher pERK1/2 and c-Fos immunoreactivity in the hippocampus and CeA (Foster et al., 2021). Addictive drugs were shown to strongly induce

pERK in the NAc and CeA (Valjent et al., 2004), regions that also highly express RGS14 (Foster et al., 2021). Together, these studies suggest that RGS14 may protect against developing addiction by serving as a natural suppressor of synaptic plasticity in emotion and motivation processing circuits, and that RGS14 dysfunction could promote vulnerability to addiction.

1.7 Research objectives

We previously reported the expression profile of RGS14 protein in the developing mouse brain, showing strong expression in hippocampal area CA2 and primary olfactory areas, piriform cortex, and entorhinal cortices (Evans et al., 2014). More recently, we also reported RGS14 immunoreactivity in discrete limbic structures in the adult mouse brain, where it modulates locomotor behavior linked to environmental novelty and cocaine (Foster et al., 2021). However, the protein distribution pattern of RGS14 throughout the adult mouse brain had not been well characterized. To fill this knowledge gap, we employed immunostaining and fluorescence microscopy using tissue from both wild-type (WT) and L507R (LR) mutant mice to provide a comprehensive map of the RGS14 protein expression profile in the adult mouse brain. RGS14 is a cytoplasmic-nuclear shuttling protein (Branch & Hepler, 2017; Cho et al., 2005), and the LR mutant features a CRISPR-generated alanine-to-arginine point mutation in the NES of the *rgs14* gene that disrupts nuclear export, thus trapping RGS14 protein inside the nucleus of its originating cell (Squires et al., 2020). Use of this RGS14-reporter mouse line benefits our approach in several ways: (1) it allows for the precise localization of RGS14-producing neuron populations, (2) the subcellular nuclear concentration of RGS14 in LR mice allows for detection in regions with low protein expression, and (3) the nuclear sequestration of RGS14 in LR mice permits their use as an additional negative control when comparing with WT immunoreactivity.

In a separate set of experiments, we examined RGS14 regulation of cocaine-induced behavioral plasticity and reward-based learning and explored potential molecular relationships in the extended amygdala and striatum. Prior work from our group showed that RGS14 loss enhances Morris water maze performance in mice (Lee et al., 2010), while another group reported elevated fear conditioning in RGS14-KO females (Alexander et al., 2019), suggesting that RGS14 loss improves hippocampal- and amygdala-based learning and memory, the latter in a sex-dependent manner. RGS14-KO mice also exhibit greater locomotor activation and increased anxiety-like behavior in response to combined novelty and acute cocaine, accompanied by higher pERK1/2 and c-Fos immunoreactivity in the hippocampus and CeA (Foster et al., 2021). Addictive drugs strongly induce pERK in the NAc and CeA (Valjent et al., 2004), regions that also highly express RGS14 (Foster et al., 2021). Together, these studies suggest that RGS14 may protect against developing addiction by serving as a natural suppressor of synaptic plasticity in emotion and motivation processing circuits, and that RGS14 dysfunction could promote vulnerability to addiction.

To investigate this hypothesis, we assessed cocaine-induced locomotor sensitization and conditioned place preference (CPP) in RGS14-KO mice and WT littermate controls. We also used immunostaining to evaluate relative RGS14 expression, and RGS14 and pERK1/2 colocalization following cocaine exposure in tissue from drug-naïve and cocaine-experienced WT mice, and to assess colocalization of RGS14 with D1R- and D2R-expressing cells in the striatum using tissue from *Drd1a*-tdTomato and *Drd2*-EGFP reporter mice. We focused on female mice in our investigation, in accordance with pilot data showing more profound effects of RGS14-KO on cocaine-induced plasticity in females than males.

Chapter 2: Materials & methods

2.1 Subjects

All animal housing and procedures were designed according to the National Institutes of Health Guidelines for the Care and Use of Laboratory Animals and were approved by the Emory University Institutional Animal Care and Use Committee. Mice homozygous for a RGS14-deleting mutation (RGS14-KO) were generated as described in Lee at al., 2010. Mice homozygous for a L507R point mutation (LR) were generated as described in Squires et al. 2020. RGS14-KO and LR mice were maintained on a C57BL/6J background. Adult (aged 3-7 months) RGS14-KO mice and wild-type (WT) littermates of both sexes were included in preliminary experiments, the results of which guided the decision to include only adult females in the experiments described in this text. All testing groups were comprised of an even distribution of WT and RGS14-KO subjects, as well as *Drd1a*-tdTomato and *Drd2*-EGFP mice (described in Shuen et al., 2008 and Gong et al., 2003). Mice were maintained on a 12-hour light/12-hour dark cycle while socially housed with free access to food and water, except during behavioral testing. All subjects were acclimated to housing in the testing room for >1 week prior to beginning experiments.

2.2 Immunohistochemistry

Subjects were injected with 200 mg/kg sodium pentobarbital and transcardially perfused with 4% paraformaldehyde in 0.01 M PBS. Extracted brains were submerged in paraformaldehyde solution for 24 hours for post-fixation, then floated in 15% sucrose/PBS for 24 hours followed by 30% sucrose/PBS for ≥24 hours until sunk. Brains were embedded in OCT on dry ice and coronally

section at 40 µm using a cryostat (-20°C). Sections were stored in PBS+0.025% sodium azide at 4°C.

Tissue sections for RGS14 detection were submersed in 10 mM sodium citrate buffer for the purpose of antigen retrieval (3 min at 100°C). They were then washed in PBS and blocked for 1 hour in 5% normal goat serum (NGS)/PBS (room temp), then incubated in mouse α-RGS14 (NeuroMab, Davis, CA, clone N133/21, RRID AB_2877352; 1:500) and rabbit α-pERK1/2 (anti-Phospho-p44/42 MAPK, Cell Signaling Technology, Danvers, MA, 1:500) primary antibodies in NGS/PBS at 4°C overnight. This monoclonal antibody was previously characterized in great depth and shown to be highly specific for rodent RGS14 comparing staining of wild-type and RGS14-KO mouse brains (Evans et al., 2014). The following day, the sections were washed in PBS and incubated in goat α-mouse AlexaFluor 488+ and goat α-rabbit AlexaFluor 568 (Invitrogen, 1:500) secondary antibodies in NGS/PBS for 2 hours at room temp, washed again in PBS, and mounted onto Superfrost Plus slides (Thermo Fisher Scientific, Waltham, MA). Once dry, slides were coverslipped with Fluoromount-G+DAPI mounting medium (Southern Biotech, Birmingham, AL) and stored at -4°C until imaging. An identical protocol was followed for negative control sections, excluding overnight incubation in primary antibody.

For visualization of RGS14 colocalization with D1 and D2 dopamine receptors in the striatum, free-floating paraformaldehyde-fixed tissue sections from *Drd1a*-tdTomato and *Drd2*-EGFP mice were incubated with mouse α-RGS14 primary antibody followed by either goat α-mouse AlexaFluor 488 (for *Drd1-tdTomato* tissue) or goat α-mouse AlexaFluor 568 (for *Drd2-EGFP* tissue) secondary antibody and mounted as described above.

2.3 Fluorescent imaging and image processing

Sections were imaged using two microscopes on separate occasions. Initially, they were imaged with a Leica DM6000 epifluorescent upright microscope at 5x and 10x magnification, using identical exposure settings between subjects for each anatomical region. Later, they were imaged with a Leica SP8 MP multiphoton confocal microscope using the tile function with automatic z-axis adjustment at each position to stitch together adjacent 10x magnified images (smooth stitching at 10% overlap). Exposure and image acquisition settings for heat atlas images were kept largely consistent. Certain sources of variability during heat atlas image acquisition were unavoidable, but were individually assessed and corrected for when possible. Their overall impact was determined to be minor if not negligible. Examples of such sources include between-session instrument variability, variation in autofluorecence intensity, and slight photobleaching effects in tissue imaged repeatedly.

Microscopy images were post-processed using ImageJ and figures were composed using Inkscape. All images were compared to negative controls (lacking primary antibody) to identify nonspecific staining. Apart from slight corrections for the aforementioned minor sources of variability, pixel value ranges were kept consistent between heat atlas images to allow for relative quantification of RGS14 levels throughout the brain from pseudo-standardized images. Pixel value ranges for non-heat atlas images were set relative to each image in order to maximize signal-to-noise, while still maintaining the appearance of identifying structural features. Heat atlas images were derived from a single WT female subject whose tissue had been sectioned at an optimal angle for alignment with the coronal Allen Mouse Brain Atlas. RGS14 expression in this mouse reflected that of the other WT subjects, and no sex differences were seen. Non-heat atlas images were obtained from a variety of subjects, both male and female.

The ImageJ pipeline for heat atlas images included: despeckle → gaussian blur filter → adjust brightness/contrast → apply heat map look-up table (LUT). The processed image was then overlaid onto the grayscale original image. The heat map LUT used is the Jet LUT native to ImageJ with the low end extended into black, which allows for transparency when overlaid. Heat atlas images were juxtaposed with matching Allen Mouse Brain Atlas graphics in Inkscape. Allen Brain Atlas graphics were manually warped using lattice deformation to align with heat atlas images. The ImageJ pipeline for non-heat atlas images included: despeckle → median filter → remove outliers (for artifact elimination) → adjust brightness/contrast → apply Virdis LUT. Occasionally, background was subtracted using a rolling ball filter in LR tissue images to reduce autofluorescence background. Image post-processing was performed with the explicit goal of providing data clarity while maintaining data integrity. Raw files of all images are available upon request.

All images were matched to the Allen Mouse Brain Atlas or the Paxinos and Franklin's mouse brain atlas for select regions. Regions exhibiting known or suspected false positive signal based on negative control staining were excluded from the report. Naming conventions followed the Allen Mouse Brain Atlas or the Paxinos and Franklin's mouse brain atlas for select regions.

2.4 Assessment of relative protein levels

Hemispheric images were acquired and pseudo-standardized as described above. The heat map LUT was applied to each image, and RGS14, as determined by relative fluorescence intensity, was assessed for each brain region. Relative protein was binned into five incremental levels, listed here in ranking order from lowest to highest protein levels by the terminology used to describe them in the text and the corresponding color in heat atlas and tables: light (dark blue), low (teal), moderate (green), high (yellow), and intense (red). To simplify the tabulated results, regions with

variable RGS14 levels were binned based on overall average level. Heat atlas images presented in the figures include a representational selection of those used to assess relative protein levels. Anatomy tables were composed using the gt and fontawesome packages for R. Behavior tables were composed using Microsoft Excel.

2.5 Drugs

Cocaine hydrochloride (5 mg/kg, i.p.; National Institute on Drug Abuse Drug Supply Program, Bethesda, MD) dissolved in saline, or saline alone, was administered at a volume of 10 mL/kg body weight. Testing began on subjects immediately following injection.

2.6 Locomotor sensitization

Subjects (n = 48) were handled for 1-2 min daily for 4 days preceding the start of the experiment. Locomotor chambers consisted of an enclosed 10”×18”×10” transparent polycarbonate box with corn cob bedding thinly layered over the floor. Locomotor chambers were surrounded by an apparatus projecting a horizontal 4×8 infrared photobeam grid connected to a monitoring system that records photobeam interference (Photobeam Activity System, San Diego Instruments, San Diego, CA). Two consecutive beam breaks constituted an ambulation, which were recorded in 5-min bins and used to quantify locomotor activity.

The paradigm consisted of the following consecutive phases: 3 days of habituation, 5 days of induction, 10 days of withdrawal, and 1 day of cocaine challenge. During habituation, all subjects received saline injections and then locomotor activity was recorded for 30 min. During induction, locomotor activity was recorded while subjects habituated to chambers for 90 min, then half of the subjects (12 WT, 12 RGS14-KO) received cocaine injections while the other half received saline and locomotor activity was recorded for an additional 60 min. During withdrawal, subjects were

left undisturbed in their home cages. During challenge, locomotor activity was recorded while subjects habituated to chambers for 90 min, then all subjects received cocaine injections and locomotor activity was recorded for an additional 60 min.

2.7 Conditioned place preference

Subjects (n = 32) were handled for 1-2 min daily for 7 days preceding the start of the experiment and habituated to injections with saline on the last 3 of the 7 days. Conditioned place preference apparatuses (San Diego Instruments, San Diego, CA) consisted of a 27”×8.375”×13.5” 3-compartment acrylic enclosure with side compartments each of length 10.75” and a center compartment of length 5.5”, separated by removable panels. Side compartments were distinguishable by visual and tactile cues: one side featured horizontally-striped outer walls and a smooth white floor, while the other side featured vertically-striped outer walls and a rough black floor. All surfaces were opaque except for chamber lids, which were transparent to allow for video tracking by overhead cameras. Mouse activity was recorded and processed into compartments defined manually prior to testing using ANY-maze automatic video tracking software (Stoelting Co., Wood Dale, IL). Time and distance in each compartment were used as metrics for place preference and locomotor activity, respectively.

Baseline place preference was established during a pre-test session, in which chamber separation panels were removed and subjects were placed in the center compartment and permitted to freely explore both sides of the apparatus for 15 min. A biased design was chosen for the paradigm, meaning that the side on which a subject spent the least amount of time during pre-test (i.e. the non-preferred side) was paired with cocaine during conditioning and the preferred side was paired with saline. Control subjects received saline on both sides.

Conditioning was carried out on a schedule of 2 sessions per subject per day, spaced ~4 hours apart, over 3 consecutive days. To avoid lingering psychoactive effects of drug during same-day conditioning sessions, saline pairing was done during the AM session and cocaine pairing was done during the PM session each day. During conditioning, chamber separation panels were put in place and subjects were injected with either cocaine or saline solution, then immediately placed in the side compartment assigned to the given treatment, where they remained for 30 min before being returned to their home cages. Post-conditioning tests (i.e. post-tests) were conducted the day after the final conditioning sessions and at two 10-day intervals thereafter. Subjects were left undisturbed in their home cages during the periods between post-tests. Post-test procedure was identical to pre-test.

2.8 Statistics

Statistical tests used to analyze locomotor sensitization and conditioned place preference data are listed in Supplementary Tables 1 & 2. Data was organized and analyzed in R using base R and the following packages: dplyr, tidyr, stats, rstatix, lmer, emmeans, afex, Rmisc, DescTools, outliers. Plots were generated using ggplot2. Tables were generated using Microsoft Excel. Homogeneity of variance was assessed using Levene's test, normality was assessed using the Shapiro-Wilk test and analysis of residuals, and outliers were assessed using Grubbs' test. Assumption violations were addressed by rank transformation of data and/or removal of outliers. Given the robustness of linear mixed-effects models to violations of homoskedasticity and normality (Schielzeth et al., 2020), modest failures of tests for these assumptions were discounted if the model was otherwise a good fit for the data based on residual analysis. Effects testing of linear mixed-effects models used the Satterthwaite method. Post-hoc contrasts were analyzed using estimated marginal means (emmeans package) and the Kenward-Roger approximation was

used for contrasts in linear mixed-effects models. For repeated measures analysis of variance (ANOVA), the Greenhouse–Geisser correction was applied in cases of sphericity violations.

Treatment group differences in RGS14 levels in NAc in WT subjects as measured by mean fluorescent density were analyzed by Welch's t-tests. The alpha level for all tests was 0.05.

Chapter 3: Characterization of RGS14 in the mouse brain

The protein distribution pattern of RGS14 throughout the adult mouse brain has not been fully characterized. To fill this knowledge gap, we employed immunostaining and fluorescence microscopy using tissue from WT and LR mutant mice to provide a comprehensive map of the RGS14 protein expression profile in the adult mouse brain.

3.1 Heat atlas of RGS14 expression

Figures 5 & 6 depict a series of RGS14-immunostained coronal sections through the rostro-caudal axis of the mouse brain up to the anterior region of the cerebellum. This comprehensive atlas of RGS14 protein levels reveals that RGS14 is more widely expressed in the adult mouse brain than previously known. Substantial RGS14 immunoreactivity is seen in regions of allocortex, septum, striatum, pallidum, and to a lesser extent ventral midbrain. Widespread, but lighter, immunoreactivity is seen across isocortex (also commonly referred to as neocortex). The protein is also found at varying degrees along many of the axonal fiber tracts that run between these regions. In terms of functional anatomy, RGS14 is largely found in regions of the limbic system and basal ganglia, as well as sensory, motor, and association cortices. The relative intensity of RGS14 immunoreactivity across all examined regions is summarized in Tables 1-3. The cellular localization of RGS14 labeling in specific regions throughout the rostrocaudal axis of the mouse brain is discussed in the following sections.

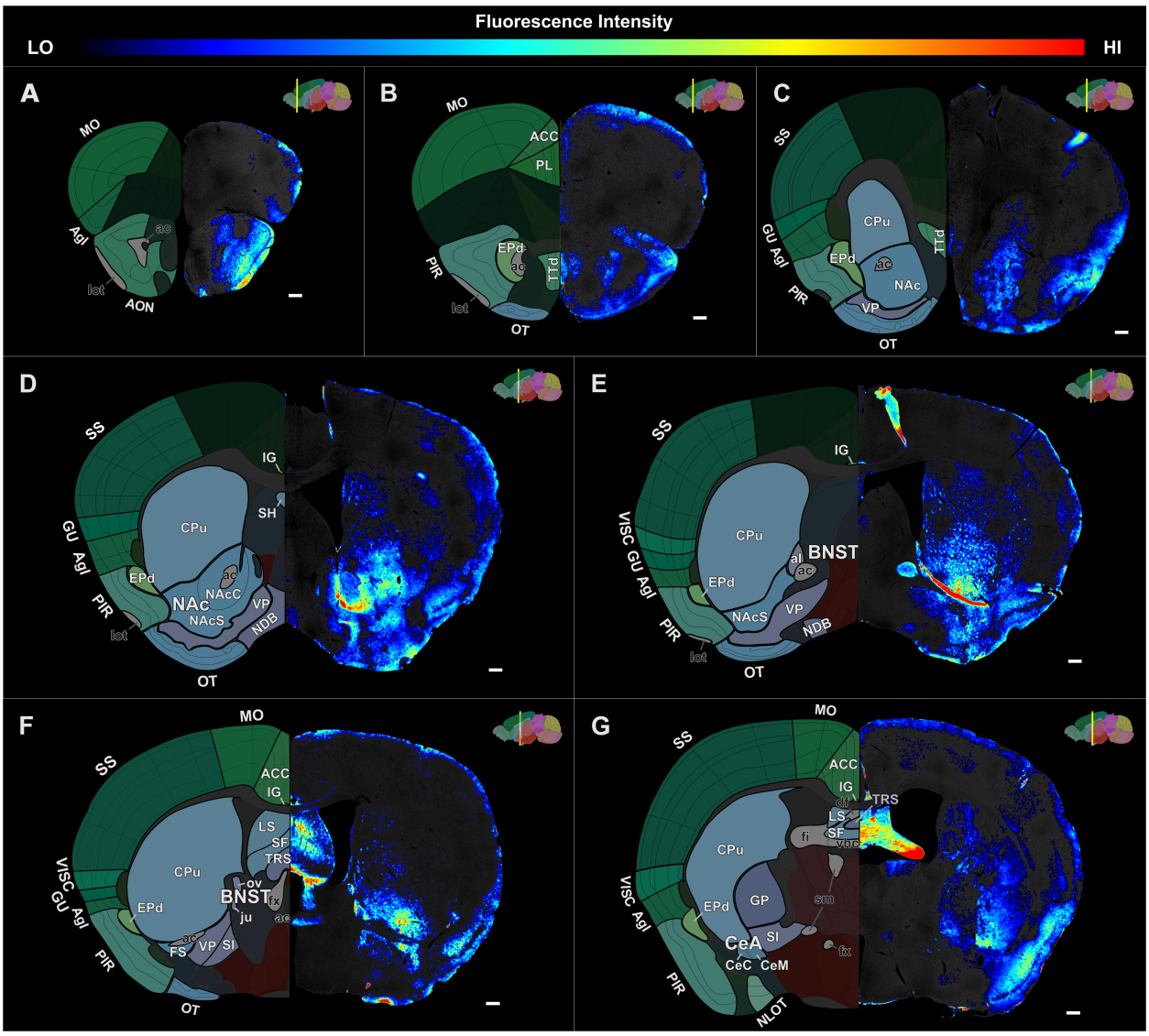


Figure 5: Heat atlas of RGS14 protein levels in adult mouse brain: rostral to medial. Relative fluorescence intensity in RGS14-immunostained coronal brain sections from a wild type (WT) mouse in series across the rostro-caudal axis (**A → G**). RGS14 (right) and anatomical annotations (left) from the Allen Mouse Brain Reference Atlas (atlas.brain-map.org). RGS14 immunoreactivity is seen within the confines of the regions labeled on the reference atlas. Notable immunoreactivity is seen in olfactory cortex, striatum, and septum, with lighter staining in isocortex. Light text indicates nuclei and subnuclei; dark text indicates fiber tracts. Yellow bar indicates sagittal position. Scale bar = 100 µm. Abbreviations: <u>regions</u>: **ACC**: anterior cingulate cortex, **AgI**: agranular insular cortex, **al**: anterolateral BNST, **AON**: anterior olfactory nucleus, **BNST**: bed nucleus of the stria terminals, **CeA**: central amygdala, **Ce(C,M)**: central amygdala- (capsular, medial), **CPu**: caudoputamen, **EPd**: endopiriform nucleus- dorsal, **FS**: fundus of the

striatum, **GP**: globus pallidus, **GU**: gustatory cortex, **IG**: induseum griseum, **ju**: juxtacapsular nucleus of BNST, **LS**: lateral septal nucleus, **MO**: motor cortex, **NAc(C,S)**: nucleus accumbens- (core, shell), **NDB**: nucleus of the diagonal band, **NLOT**: nucleus of the lateral olfactory tract, **OT**: olfactory tubercle, **ov**: oval nucleus of the BNST, **PIR**: piriform cortex, **PL**: prelimbic cortex, **SF**: septofimbrial nucleus, **SH**: septohippocampal nucleus, **SI**: substantia innominata, **SS**: somatosensory cortex, **TRS**: triangular nucleus of the septum, **TTd**: taenia tecta- dorsal, **VISC**: visceral cortex, **VP**: ventral pallidum; fiber tracts: **ac**: anterior commissure, **df**: dorsal fornix, **fi**: fimbria, **fx**: fornix (columns), **lot**: lateral olfactory tract, **sm**: stria medullaris, **vhc**: ventral hippocampal commissure.

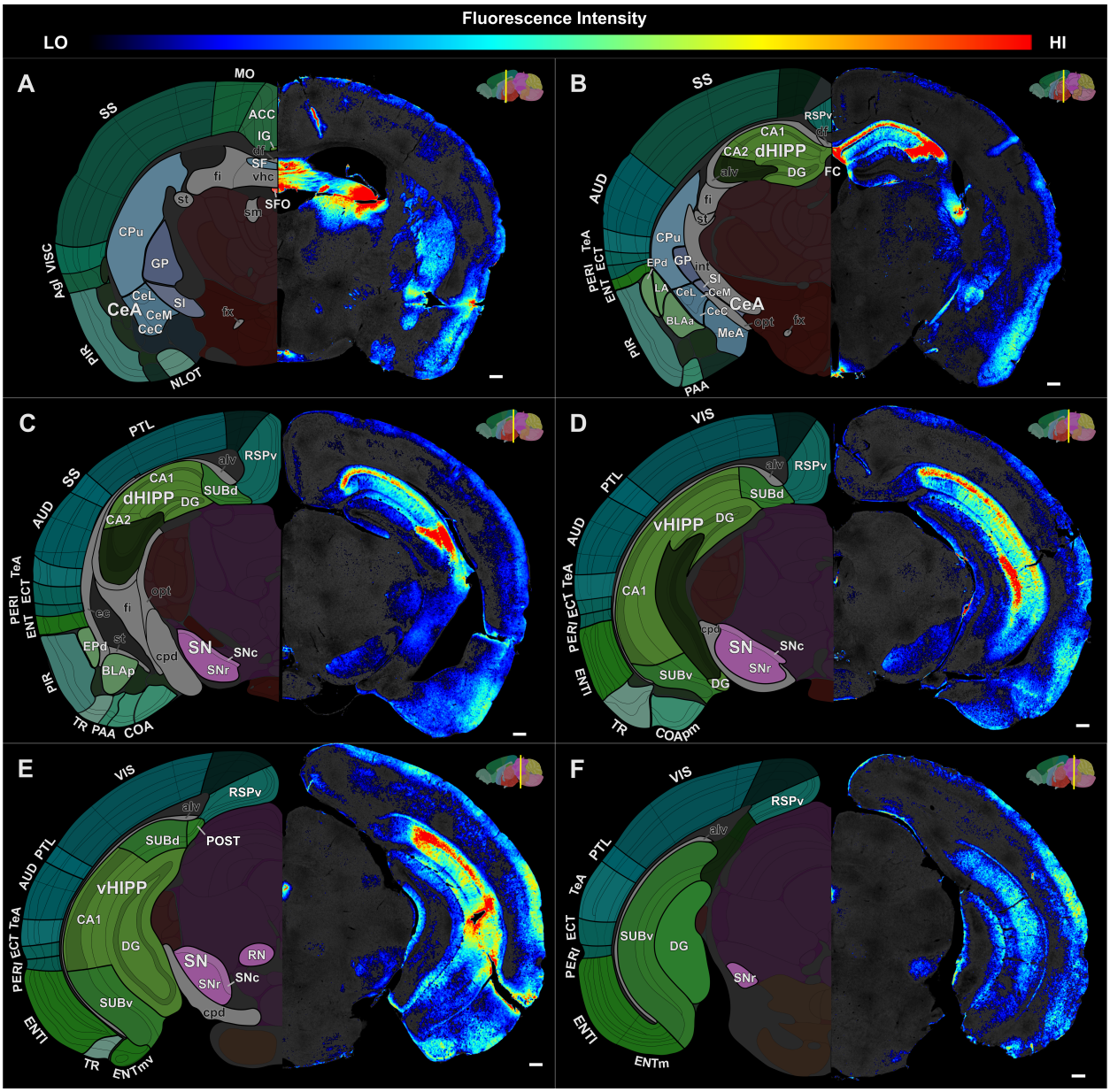


Figure 6: Heat atlas of RGS14 protein levels in adult mouse brain: medial to caudal. Relative fluorescence intensity in RGS14-immunostained coronal brain sections from a wild type (WT) mouse in series across the rostro-caudal axis (**A → F**). RGS14 (right) and anatomical annotations (left) from the Allen Mouse Brain Reference Atlas (atlas.brain-map.org). RGS14 immunoreactivity is seen within the confines of the regions labeled on the reference atlas. Notable RGS14 immunoreactivity is seen in septum, hippocampal formation, and amygdala, with lighter staining in isocortex and discrete midbrain subregions. Light text indicates nuclei and subnuclei; dark text indicates fiber tracts. Yellow bar indicates sagittal position. Scale bar = 100 µm. Abbreviations: regions: **ACC**: anterior cingulate cortex, **AUD**: auditory cortex, **AgI**: agranular insular cortex, **BLA(a,p)**: basolateral amygdala- (anterior, posterior), **CA(1,2)**:

hippocampal field *cornu ammonis* (1, 2), **CeA**: central amygdala, **Ce(C,L,M)**: central amygdala- (capsular, lateral, medial), **COA(pm)**: cortical amygdalar area- (posterior/medial zone), **CPu**: caudoputamen, **DG**: dentate gyrus, **dHIPP**: dorsal hippocampus, **ECT**: ectorhinal cortex, **ENT(l,m)**: entorhinal cortex- (lateral, medial), **EPd**: endopiriform nucleus- dorsal, **FC**: fasciola cinerea, **GP**: globus pallidus, **IG**: induseum griseum, **LA**: lateral amygdala, **MeA**: medial amygdala, **MO**: motor cortex, **NLOT**: nucleus of the lateral olfactory tract, **PAA**: piriform-amygdalar area, **PERI**: perirhinal cortex, **PIR**: piriform cortex, **POST**: postsubiculum, **PTL**: posterior parietal association cortex, **RN**: red nucleus, **RSPv**: retrosplenial cortex- ventral, **SF**: septofimbrial nucleus, **SFO**: subfornical organ, **SI**: substantia innominata, **SN(c,r)**: substantia nigra- (pars compacta, pars reticulata), **SS**: somatosensory cortex, **SUB(d,v)**: subiculum- (dorsal, ventral), **TeA**: temporal association cortex, **TR**: postpiriform transition cortex, **vHIPP**: ventral hippocampus, **VIS**: visual cortex, **VISC**: visceral cortex; fiber tracts: **alv**: alveus, **cpd**: cerebral peduncle, **df**: dorsal fornix, **ec**: external capsule, **fi**: fimbria, **fx**: fornix (columns), **int**: internal capsule, **opt**: optic tract, **sm**: stria medullaris, **st**: stria terminalis, **vhc**: ventral hippocampal commissure.

3.2 Olfactory areas

In the olfactory areas, RGS14 immunoreactivity is highest across ventrolateral allocortical regions, including the anterior olfactory nucleus (AON, Fig. 7B), piriform cortex (PIR, Fig. 7E & Fig. 8H), and postpiriform transition cortex (TR, Fig. 7K), where it is seen at moderate levels approximately evenly distributed been inner and outer layers. Staining in LR tissue shows RGS14-positive nuclei concentrated in the middle layer (PIR: Fig. 7F & Fig. 8I; TR: Fig. 7L), or the related inner layer for AON (Fig. 7C). RGS14 is present at moderate to low levels in the dorsal taenia tecta (TTd, Fig. 7B), and at low levels in the nucleus of the lateral olfactory tract (NLOT, Fig. 5G & Fig. 6A), and piriform-amygdalar area (PAA, Fig. 11E). LR tissue shows RGS14-positive nuclei in TTd (Fig. 7C), but not NLOT (not shown) or PAA (Fig. 11F), suggesting that RGS14 in NLOT and PAA is in axon and terminal processes. Lastly, light subcortical RGS14 immunostaining is seen in the dorsal endopiriform nucleus (EPd, Fig. 7H). LR staining shows RGS14-positive nuclei in EPd in a pattern that generally mirrors signal density in WT mice (Fig. 7I).

3.3 Isocortex

RGS14 immunoreactivity is broadly seen across the isocortex, though at much more modest levels than in allocortex. In WT mice, light signal is seen in the prefrontal cortex, specifically in the prelimbic (PL, Fig. 8B), anterior cingulate (ACC, Fig. 8E), and agranular insular areas (AgI, Fig. 8H), though is apparently absent in the infralimbic cortex (Fig. 8B). Signal is somewhat higher, though still low, in association areas beyond the frontal lobe, namely the temporal association (TeA) and posterior parietal association cortices (PTL, Fig. 6C-F). The strongest RGS14 labeling in association cortices is seen at moderate levels in the ectorhinal (ECT) and perirhinal cortex (PERI, Fig. 9H). This is unsurprising given the close anatomo-functional relationship of these regions with the hippocampal formation. Light signal is also seen exclusively

in the ventral subregion of the retrosplenial cortex (RSPv, Fig. 9B,E). RGS14 is seen in sensory cortical regions, including moderate levels in visual (VIS, Fig. 9E) and auditory (AUD, Fig. 9H) cortices and light levels in gustatory (GU, Fig. 8H), somatosensory (SS, Fig. 8K), and visceral (VISC, Fig. 5E-G & Fig. 6A) cortices. It is also found at varying, but overall low, levels in primary and secondary motor cortices (MOp & MOs, Fig. 8B,K). We previously noted a similar protein distribution pattern across the isocortex in adolescent mice, but it was transient and undetectable in adults (Evans et al., 2014).

The data from the LR mice in the present study show that, while mostly subtle, RGS14 is unequivocally expressed in the adult mouse isocortex. With the exception of gustatory cortex (Fig. 8I), our data reveal herein that all RGS14 immunoreactive isocortical regions also exhibit RGS14 nuclear localization (Table 1). Figure 9I particularly exemplifies the consistent pattern of the bulk of RGS14-positive nuclei residing in more superficial layers below layer I, presumably layer II/III, with fewer labeled nuclei in deeper layers. In WT mice, RGS14 is most concentrated in the superficial layers of sensory and motor cortices, but it is evenly distributed between superficial and deeper layers in association cortices (exemplified in Fig. 9H). Given that neurons in superficial layers are mainly involved in cortico-cortical communication, while deeper layer cells project to subcortical regions (Aboitiz, 1999), this pattern of localization may indicate that isocortical RGS14 functions regulate aspects of polymodal sensory processing, such as learning associations between polymodal stimuli and their capacity to drive behavior when experienced concurrently.

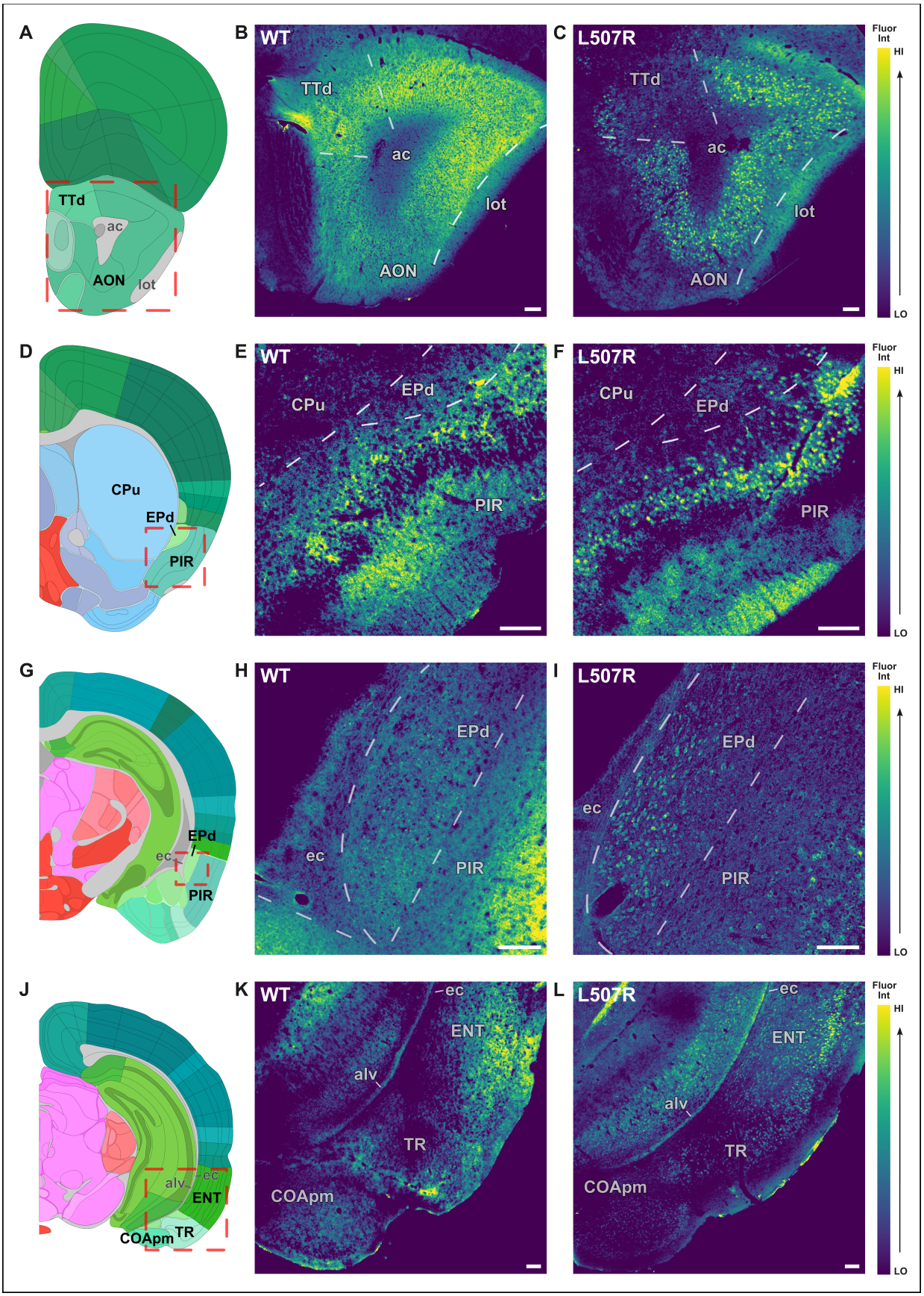

A
TTd
ac
AON
lot
B
WT
TTd
ac
lot
AON
C
L507R
TTd
ac
lot
AON
Fluor Int
HI
LO
D
CPu
EPd
PIR
E
WT
CPu
EPd
PIR
F
L507R
CPu
EPd
PIR
G
EPd
ec
PIR
H
WT
EPd
ec
PIR
I
L507R
EPd
ec
PIR
J
alv
cc
ENT
COApm
TR
K
WT
ec
ENT
alv
TR
COApm
L
L507R
ec
ENT
alv
TR
COApm

Figure 7: RGS14 immunoreactivity is widespread and moderate across olfactory areas. Relative fluorescence intensity in RGS14-immunostained tissue sections from wild type (WT) and L507R-reporter mice. Anatomical annotations (left; **A,D,G,J**) from the Allen Mouse Brain Reference Atlas (atlas.brain-map.org) aligned with confocal images of RGS14 immunoreactivity in LR reporter (middle; **B,E,H,K**) and WT mice (right; **C,F,I,L**). Red dashed box in atlas images indicates approximate anatomical location of tissue cross-sections in each row; black text indicates nuclei and subnuclei, gray text indicates fiber tracts. Scale bar = 100 μm. Abbreviations: **AON**: anterior olfactory nucleus, **COA(pm)**: cortical amygdalar area- (posterior/medial zone), **CPu**: caudoputamen, **EPd**: endopiriform nucleus- dorsal, **ENT**: entorhinal cortex, **PIR**: piriform cortex, **TR**: postpiriform transition cortex; **TTd**: taenia tecta-dorsal, fiber tracts: **ac**: anterior commissure, **alv**: alveus, **ec**: external capsule. **lot**: lateral olfactory tract.

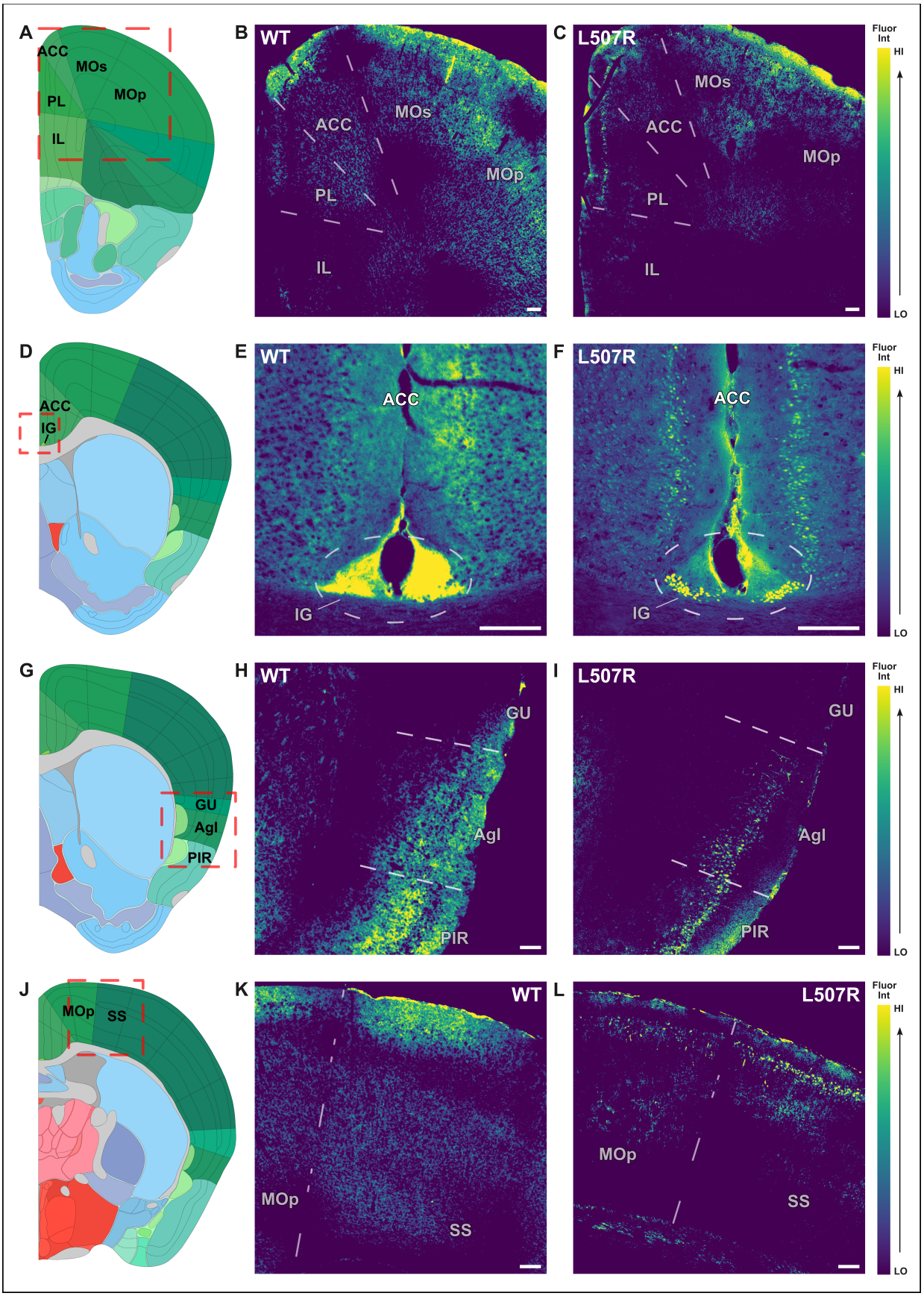

A
ACC
MOs
MOp
PL
IL
B
WT
ACC
MOs
MOp
PL
IL
C
L507R
MOs
ACC
MOp
PL
IL
Fluor Int
HI
LO
D
ACC
IG
E
WT
ACC
IG
F
L507R
ACC
IG
Fluor Int
HI
LO
G
GU
AgI
PIR
H
WT
GU
AgI
PIR
I
L507R
GU
AgI
PIR
Fluor Int
HI
LO
J
MOp
SS
K
WT
MOp
SS
L
L507R
MOp
SS
Fluor Int
HI
LO

Figure 8: RGS14 immunoreactivity is low in prefrontal and frontal cortices. Relative fluorescence intensity in RGS14-immunostained tissue sections from wild type (WT) and L507R-reporter mice. Anatomical annotations (left; **A,D,G,J**) from the Allen Mouse Brain Reference Atlas (atlas.brain-map.org) aligned with confocal images of RGS14 immunoreactivity in LR reporter (middle; **B,E,H,K**) and WT mice (right; **C,F,I,L**). Red dashed box in left panels indicates approximate anatomical location of tissue cross-sections in middle and right panels in each row. Scale bar = 100 μm. Abbreviations: **ACC**: anterior cingulate cortex, **AgI**: agranular insular cortex, **GU**: gustatory cortex, **IG**: induseum griseum, **IL**: infralimbic cortex, **MO(p,s)**: motor cortex- (primary, secondary), **PIR**: piriform cortex, **PL**: prelimbic cortex, **SS**: somatosensory cortex.

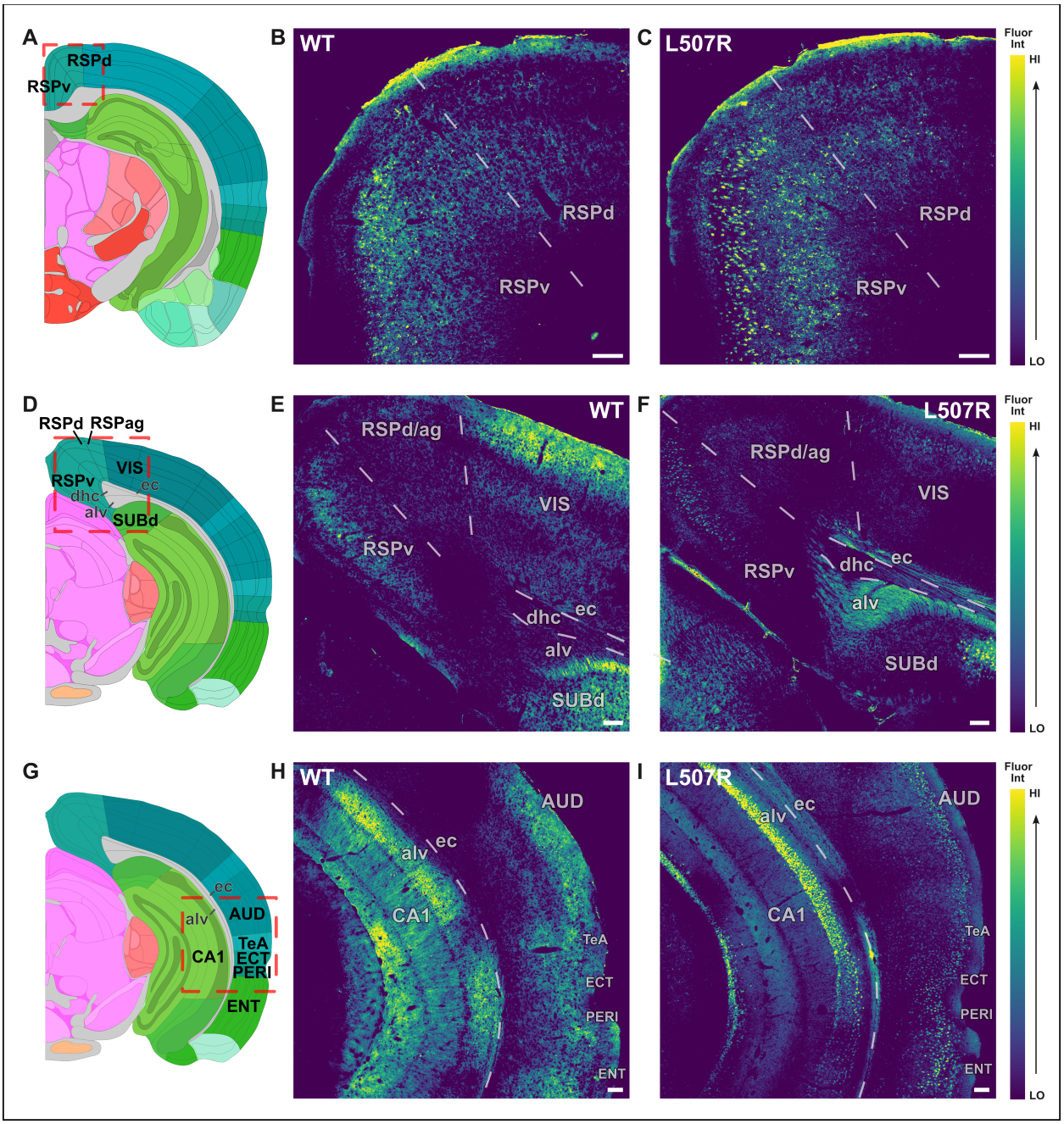


Figure 9: RGS14 immunoreactivity is moderate in parietal-temporal and occipital cortices. Relative fluorescence intensity in RGS14-immunostained tissue sections from wild type (WT) and L507R-reporter mice. Anatomical annotations (left; **A,D,G,J**) from the Allen Mouse Brain Reference Atlas (atlas.brain-map.org) aligned with confocal images of RGS14 immunoreactivity in LR reporter (middle; **B,E,H,K**) and WT mice (right; **C,F,I,L**). Red dashed box in atlas images indicates approximate anatomical location of tissue cross-sections in each row; black text indicates nuclei and subnuclei, gray text indicates fiber tracts. Scale bar = 100 µm. Abbreviations: **AUD**: auditory cortex, **CA1**:

hippocampal field *cornu ammonis* 1, **ECT**: ectorhinal cortex, **ENT**: entorhinal cortex, **PERI**: perirhinal cortex, **RSP(d,v,ag)**: retrosplenial cortex- (dorsal, ventral, agranular), **SUBd**: subiculum- dorsal, **TeA**: temporal association cortex, **VIS**: visual cortex; fiber tracts: **alv**: alveus, **dhc**: dorsal hippocampal commissure, **ec**: external capsule.

Table 1: Summary of RGS14 immunoreactivity in adult mouse brain: allocortex and isocortex. Relative expression determined from immunofluorescence heat atlas.

	BRAIN REGION		RGS14 EXPRESSION	
	STRUCTURE	**ABBV.**	**LEVEL**	**NUCLEAR**
OLFACTORY AREAS	Anterior olfactory nucleus	**AON**		✓
	Piriform cortex	**PIR**		✓
	Postpiriform transition cortex	**TR**		✓
	Nucleus of the lateral olfactory tract	**NLOT**		✗
	Piriform-amygdalar area	**PAA**		✗
	Taenia tecta, dorsal	**TTd**		✓
	Endopiriform nucleus, dorsal	**EPd**		✓
ISOCORTEX	Auditory cortex	**AUD**		✓
	Ectorhinal cortex	**ECT**		✓
	Perirhinal cortex	**PERI**		✓
	Visual cortex	**VIS**		✓
	Motor cortex	**MO**		✓
	Posterior parietal association cortex	**PTL**		✓
	Temporal association cortex	**TeA**		✓
	Agranular insular cortex	**AgI**		✓
	Anterior cingulate cortex	**ACC**		✓
	Gustatory cortex	**GU**		✗
	Prelimbic cortex	**PL**		✓
	Retrosplenial cortex, ventral	**RSPv**		✓
	Somatosensory cortex	**SS**		✓
	Visceral cortex	**VISC**		✓

3.4 Septal regions

The septum is a midline structure that consists of several limbic nuclei with fiber tracts of the fornix system interwoven between. Septal nuclei are heavily innervated by the hippocampus to incorporate memory into aspects of socially and emotionally motivated behaviors. We show here that the lateral septal complex is highly enriched in RGS14 immunoreactivity, in both regional nuclei and fiber tracts. The lateral septal complex features prominent RGS14 staining, particularly caudally. Of the lateral complex, the septofimbrial nucleus (SF) exhibits the most intense RGS14 immunoreactivity, especially in posterior portions (Fig. 10K). The lateral septal nucleus (LS) ranks closely behind SF in terms of RGS14 immunoreactivity, exhibiting high-level signal throughout the region (Fig. 10E,H). Tissue from LR mice shows RGS14-positive nuclei dispersed throughout SF (Fig. 10L) and LS (Fig. 10F). There is light RGS14 staining in the septohippocampal nucleus (SH) in WT mice (Fig. 10B), while the LR tissue shows a band of RGS14-positive nuclei along the hemispheric midline within SH (Fig. 10C). There is moderate signal in the triangular nucleus of the septum (TRS), but some degree of autofluorescence contamination from the surrounding regions might account for part of this labeling (Fig. 10H). There is light signal in the nucleus of the diagonal band (NDB), a medial septal region (Fig. 5D,E), in WT mice, but RGS14-positive nuclei are not detected in TRS or NDB in LR tissue (TRS: Fig. 10I; NDB: not shown).

Grouped in with the septal regions due to regional proximity but less so shared functionality or neurochemical similarity, the subfornical organ (SFO) exhibits intense RGS14 immunoreactivity that appears to be strongest in a select population of neurons (Fig. 10H,I). The fornix system tracts within the septum are strongly RGS14-immunoreactive as well (Fig. 5G & Fig. 6A). The murine dorsal fornix runs from the hippocampus along the septum, just ventral to the corpus collosum and medial to the SH (compare to Fig. 10B,C), following which it meets with

the anterior commissure and disperses out towards its target nuclei. While the tractology is complex and beyond the scope of this paper, it seems reasonable to suggest that these intra-septal tracts are a route through which RGS14 regulates communication between cortical and subcortical limbic regions.

3.5 Amygdaloid complex and extended amygdala

The intensity of RGS14 protein labeling in the amygdaloid complex is regionally specific and mostly mild, with the exception of a substantial high-signal "hotspot" in the lateral subdivision of the central amygdala (CeL). Signal in the surrounding medial and capsular subdivisions (CeM & CeC) is light, as is signal in the lateral amygdala (LA), posterodorsal medial amygdala (MeApd), and anterior basolateral amygdala (BLAa, Fig. 11E) though it is somewhat more substantial in the posterior basolateral amygdala (BLAp, Fig. 11H). Low signal is seen exclusively in the medial zone of the posterior cortical amygdalar area (COApm, Fig. 6D), but not the anterior COA or the lateral posterior zone (Fig. 11E). Analysis of LR tissue reveals that RGS14-positive nuclei are seen at a high density throughout the amygdala in a pattern that generally mirrors signal density in WT mice (Fig. 11F,I).

The extended amygdala is a macrostructure consisting of interconnected regions with shared embryonic origins and neurochemical features that includes the CeA, BNST, SI. Similar to CeA, RGS14 immunoreactivity in the bed nucleus of the stria terminalis (BNST) is dense and regionally restricted. Two distinct signal hotspots are seen at positions that correspond to the juxtacapsular and oval BNST subnuclei (BNSTju & BNSTov) (Fig. 11B), with little to no signal seen outside these specific subregions across the rest of the BNST. Analysis of the LR mice reveals densely-clustered RGS14-positive nuclei within both subregions in patterns that mirror signal density in WT mice (Fig. 11C). Light signal is seen across the substantia innominata (SI) (Fig. 5F,G & Fig.

6A,B). RGS14 signal detected in SI is non-nuclear, suggesting that it is located in terminal processes of SI afferents, some of which likely originate in upstream extended amygdala structures like the BNSTju (Francesconi et al., 2009).

3.6 Hippocampal formation

The intensity of RGS14 immunoreactivity is generally high throughout the hippocampal formation, though the bulk of the labeling in this region is seen in the hippocampus proper. In the CA fields in WT animals, intense signal is found in CA2 (Fig. 12E), with lesser but still high signal in CA1, while CA3 is apparently devoid of labeling (Fig. 12E,H). This distribution pattern remains the same throughout the dorsoventral extent of the hippocampus. The signal is strongest in the pyramidal layer, then dissipates outwards through processes extending into the stratum oriens and stratum radiatum/stratum lacunosum moleculare. In line with this, examination of LR tissue reveals RGS14-positive nuclei in the pyramidal layer of CA2 (Fig. 12F) and CA1 (Fig. 9I & Fig. 12H). In both WT and LR mice, intense signal and nuclear staining is also found within the fasciola cinerea (FC, Fig. 12B,C) and indusium griseum (IG, Fig. 8E,F & Fig. 10B,C). Diffuse low-level signal is seen throughout the dentate gyrus (DG) in the polymorph and, particularly, the molecular layers in WT animals (Fig. 12K), while in LR mice RGS14-positive nuclei are predominantly localized in the dorsolateral granule cell layer (stratum granulosum, Fig. 12L). Ostensibly, RGS14 produced in tightly-packed granule layer cells diffuses out into dendritic processes in the molecular layer.

Overall moderate, but variable levels of RGS14 immunoreactivity are seen in retrohippocampal regions. Moderate signal is seen throughout the entorhinal cortex (ENT, Fig. 7K & Fig. 13H) in WT mice. Staining in LR tissue reveals RGS14-positive nuclei in most, if not all, ENT layers, with the exception of the most superficial layer I (Fig. 7L & Fig. 13I). Staining in WT

subiculum is moderate in the ventral subregion (SUBv, Fig. 13E,H) but lighter in the dorsal subregion (SUBd, Fig. 9E & Fig. 13B). In LR tissue, RGS14-positive nuclei are seen exclusively in SUBv (Fig. 13F,I) but not in SUBd (Fig. 9F & Fig. 13C). A likely explanation is that RGS14 in SUBd is located within axonal and terminal processes from such SUBv and/or other projecting regions. Lastly, light staining is seen in the postsubiculum (POST, Fig. 13K) of WT mice, while RGS14-positive nuclei are dispersed across the region in LR animals (Fig. 13L).

3.7 Basal ganglia and midbrain

The basal ganglia is a functional group of connected nuclei involved in motor-, cognitive- and limbic-related behaviors that include the striatum, pallidum, and ventral midbrain. RGS14 labeling is broadly seen throughout the striatum of WT mice, but is significantly more abundant in the ventral striatum where rich plexuses of terminal and axon-like profiles display a semi-circular pattern in the nucleus accumbens core (NAcC, Fig. 5D,E & Fig. 14B,E) wrapping around the anterior commissure. Throughout the rostrocaudal extent of the caudatoputamen, (CPu) RGS14 immunostaining is strongly expressed in axon bundles giving rise to a patchy protein distribution pattern in dorsal and ventrolateral striatal regions that becomes more diffuse as the labeling invades the NAcC. In contrast to the high level of RGS14 immunoreactivity in the NAcC, the intensity of RGS14 staining in the surrounding nucleus accumbens shell (NAcS, Fig. 14B,E) is more modest. Low levels of labeling are seen in the olfactory tubercle (OT, Fig. 14B).

Apart from the striatum, low- RGS14 signal is seen across the ventral pallidum (VP, Fig. 5C-F & Fig. 14E), with lighter signal evident in the globus pallidus (GP, Fig. 14H). At the ventral midbrain level, we found a low level of diffuse neuropil RGS14 immunoreactivity throughout the substantia nigra pars reticulata (SNr) and patches of more intense staining in a dorsomedial region of the SN that likely corresponds to the pars compacta (SNc, Fig. 14K). We also found light

staining in the red nucleus (RN, Fig. 14K), a midbrain region involved in the descending dorsolateral motor pathways. Analysis of LR tissue reveals RGS14-positive nuclei in NAc, CPu, FS, and GP but none in OT, VP, SN, or RN (Fig. 14C,F,I,L). RGS14 signal is absent in OT and VP in LR tissue, suggesting that RGS14 protein in these regions is mainly expressed in axon and terminal processes (Fig. 14F). Unexpectedly, we observed perinuclear staining in midbrain LR tissue in both SN and RN (Fig. 14L). The reason for this result is unknown, but possible explanations are discussed below.

It should be stated that some signal was noted at times in thalamic and hypothalamic regions in WT animals. Due to issues with autofluorescence, we could not reliably distinguish this signal from background when compared to controls incubated with secondary antibody only. For this reason, we chose to exclude these observations from our results. This study did not examine RGS14 expression in the lower brainstem and spinal cord.

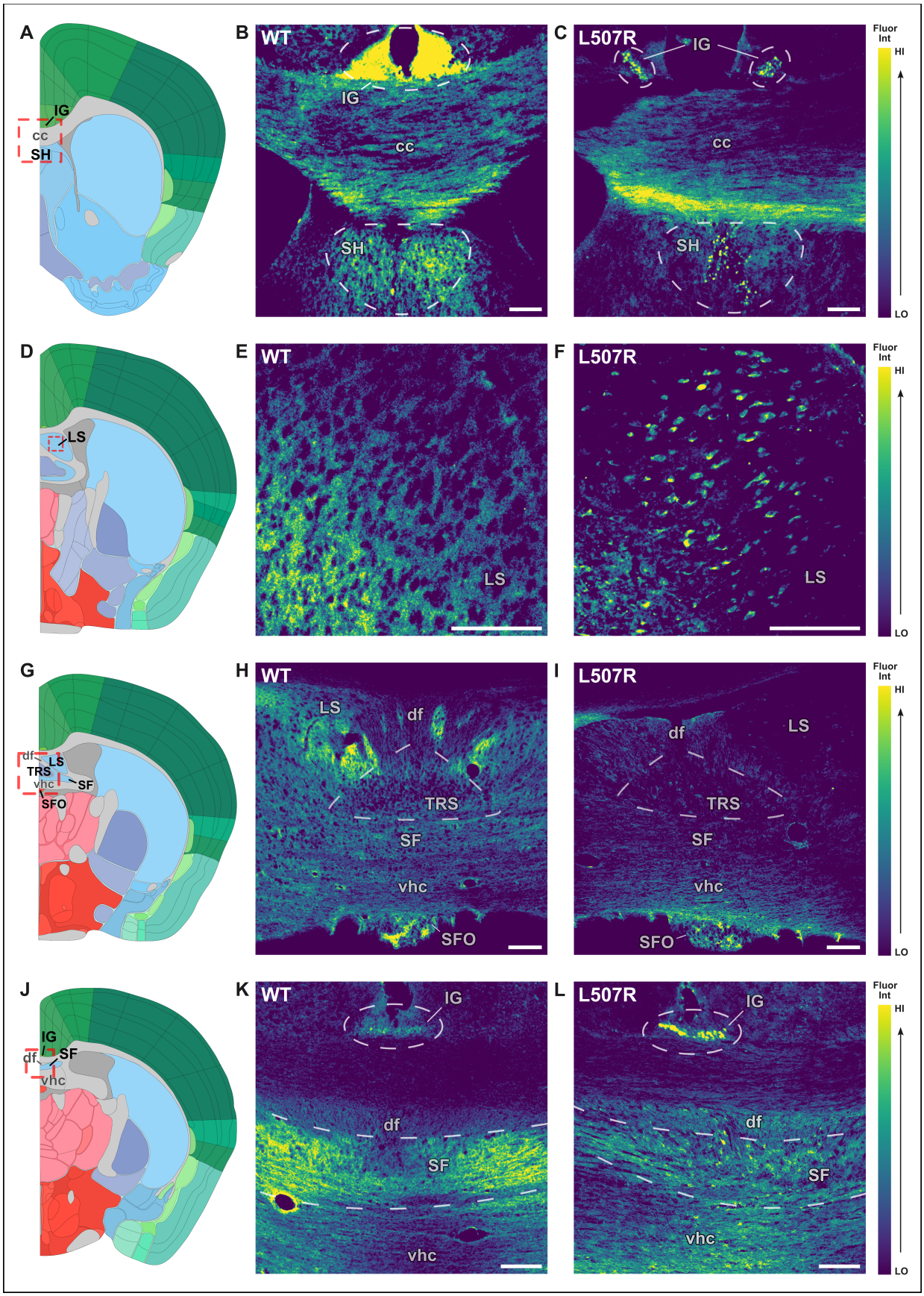

A
IG
cc
SH
B
WT
IG
cc
SH
C
L507R
IG
cc
SH
Fluor Int
HI
LO
D
LS
E
WT
LS
F
L507R
LS
Fluor Int
HI
LO
G
df
LS
TRS
vhc
SF
SFO
H
WT
LS
df
TRS
SF
vhc
SFO
I
L507R
df
LS
TRS
SF
vhc
SFO
Fluor Int
HI
LO
J
IG
SF
df
vhc
K
WT
IG
df
SF
vhc
L
L507R
IG
df
SF
vhc
Fluor Int
HI
LO

Figure 10: RGS14 immunoreactivity is intense in the lateral septal complex. Relative fluorescence intensity in RGS14-immunostained tissue sections from wild type (WT) and L507R-reporter mice. Anatomical annotations (left; **A,D,G,J**) from the Allen Mouse Brain Reference Atlas (atlas.brain-map.org) aligned with confocal images of RGS14 immunoreactivity in LR reporter (middle; **B,E,H,K**) and WT mice (right; **C,F,I,L**). Red dashed box in atlas images indicates approximate anatomical location of tissue cross-sections in each row; black text indicates nuclei and subnuclei, gray text indicates fiber tracts. Scale bar = 100 μm. Abbreviations: **IG**: induseum griseum, **LS**: lateral septal nucleus, **SF**: septofimbrial nucleus, **SFO**: subfornical organ, **SH**: septohippocampal nucleus, **TRS**: triangular nucleus of the septum; fiber tracts: **cc**: corpus callosum, **df**: dorsal fornix, **vhc**: ventral hippocampal commissure.

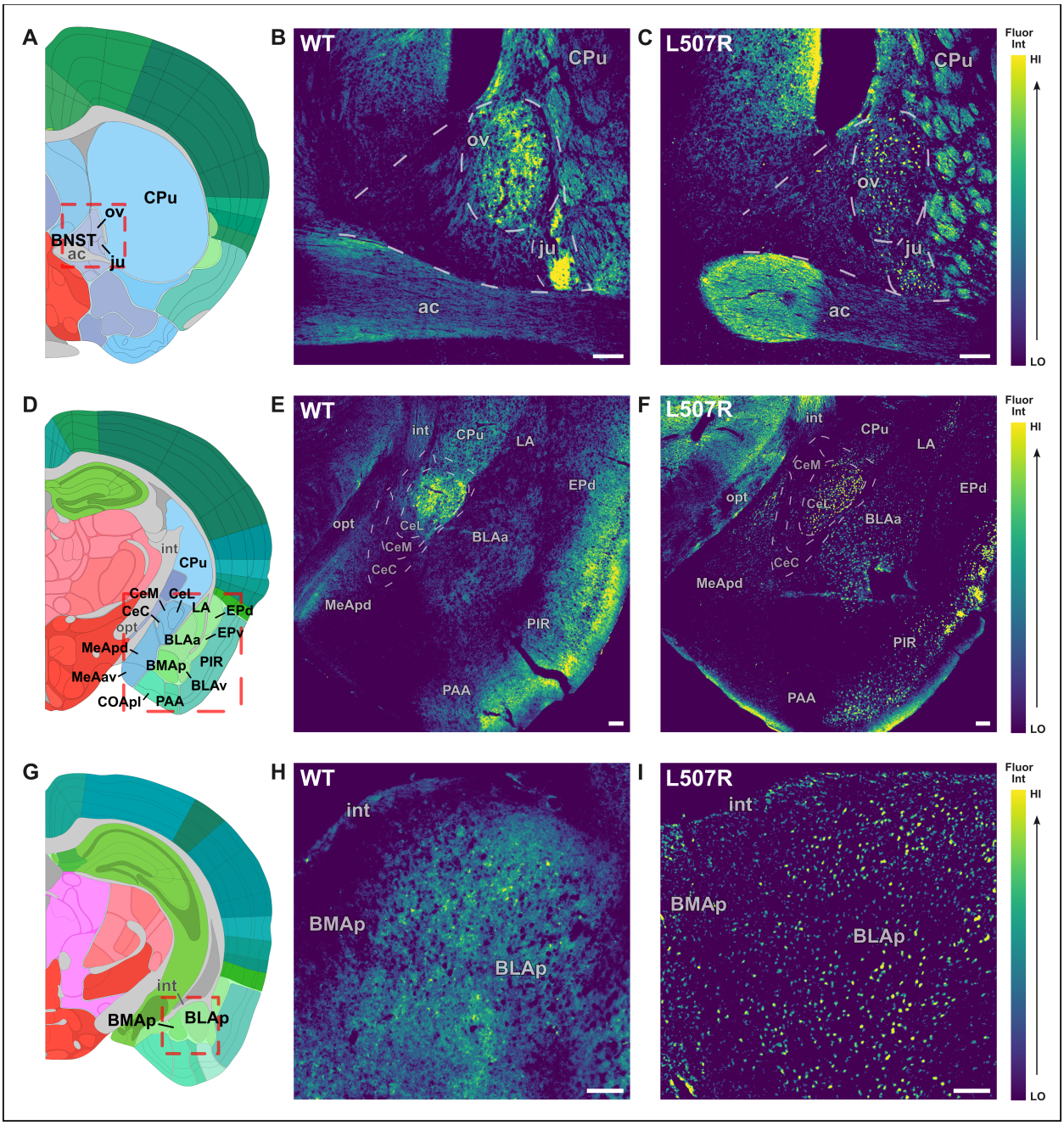


Figure 11: RGS14 immunoreactivity is intense in select subregions of the amygdaloid complex and extended amygdala. Relative fluorescence intensity in RGS14-immunostained tissue sections from wild type (WT) and L507R-reporter mice. Anatomical annotations (left; **A,D,G,J**) from the Allen Mouse Brain Reference Atlas (atlas.brain-map.org) aligned with confocal images of RGS14 immunoreactivity in LR reporter (middle; **B,E,H,K**) and WT mice (right; **C,F,I,L**). Red dashed box in atlas images indicates approximate anatomical location of tissue cross-sections in each row; black text indicates nuclei and subnuclei, gray text indicates fiber tracts. Scale bar = 100 µm. Abbreviations:

BLA(a,p,v): basolateral amygdala- (anterior, posterior, ventral), **BMAp**: basomedial amygdala- posterior, **BNST**: bed nucleus of the stria terminals, **Ce(C,L,M)**: central amygdala- (capsular, lateral, medial), **COApl**: cortical amygdalar area- posterior/lateral zone, **CPu**: caudoputamen, **EP(d,v)**: endopiriform nucleus- (dorsal, ventral), **ju**: juxtacapsular nucleus of BNST, **LA**: lateral amygdala, **NAc**: nucleus accumbens, **MeA(av,pd)**: medial amygdala- (anteroventral, posterodorsal), **ov**: oval nucleus of the BNST, **PAA**: piriform-amygdalar area, **PIR**: piriform cortex; fiber tracts: **ac**: anterior commissure, **int**: internal capsule, **opt**: optic tract.

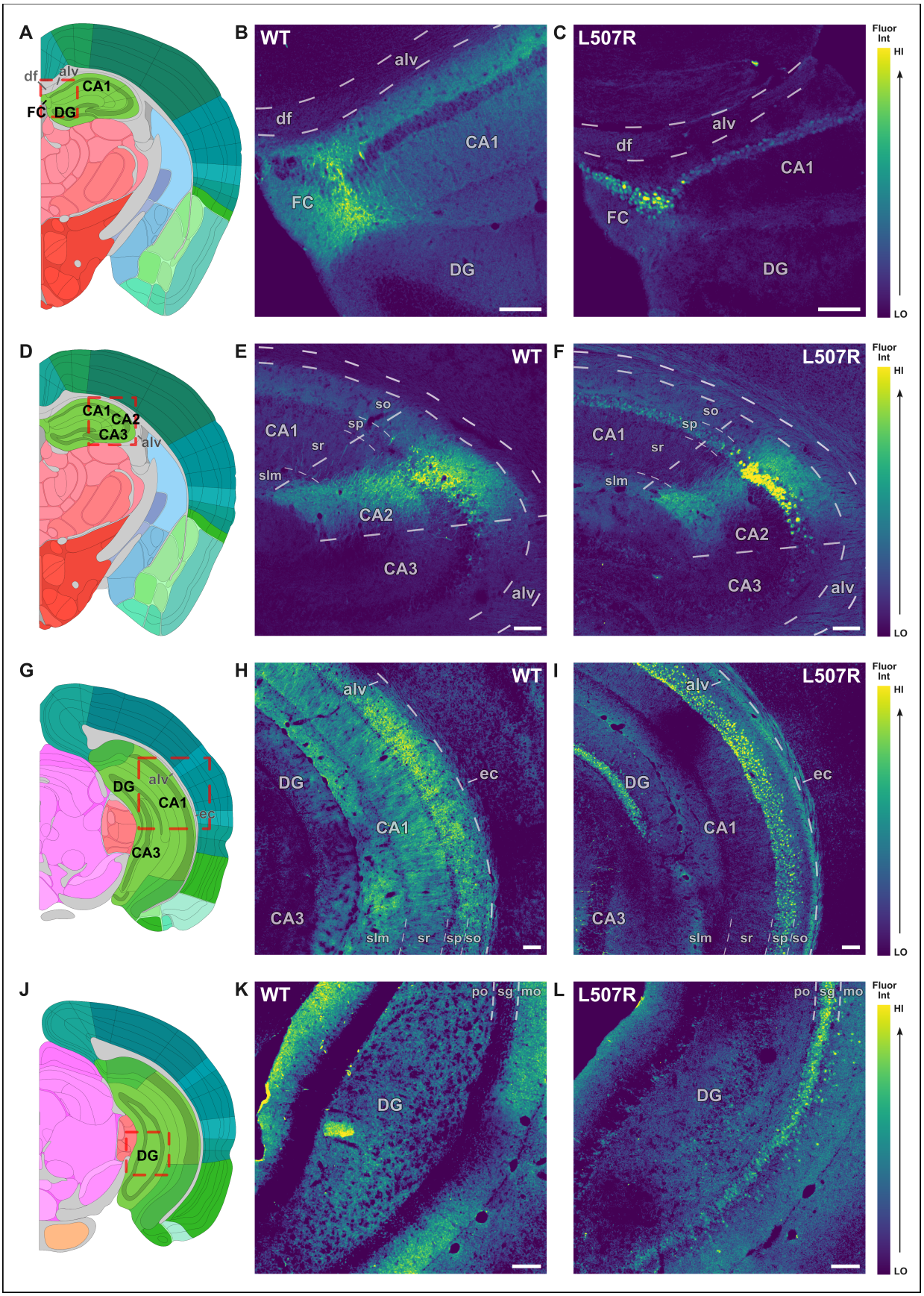

A
df
alv
CA1
FC
DG
B
WT
alv
df
CA1
FC
DG
C
L507R
alv
df
CA1
FC
DG
Fluor Int
HI
LO
D
CA1
CA2
CA3
alv
E
WT
so
sp
CA1
sr
slm
CA2
CA3
alv
F
L507R
so
sp
CA1
sr
slm
CA2
CA3
alv
Fluor Int
HI
LO
G
DG
alv
CA1
ec
CA3
H
WT
alv
DG
ec
CA1
CA3
slm
sr
sp/so
I
L507R
alv
DG
ec
CA1
CA3
slm
sr
sp/so
Fluor Int
HI
LO
J
DG
K
WT
po
sg
mo
DG
L
L507R
po
sg
mo
DG
Fluor Int
HI
LO

Figure 12: RGS14 immunoreactivity is high throughout the hippocampus proper. Relative fluorescence intensity in RGS14-immunostained tissue sections from wild type (WT) and L507R-reporter mice. Anatomical annotations (left; **A,D,G,J**) from the Allen Mouse Brain Reference Atlas (atlas.brain-map.org) aligned with confocal images of RGS14 immunoreactivity in LR reporter (middle; **B,E,H,K**) and WT mice (right; **C,F,I,L**). Red dashed box in atlas images indicates approximate anatomical location of tissue cross-sections in each row; black text indicates nuclei and subnuclei, gray text indicates fiber tracts. Scale bar = 100 μm. Abbreviations: **CA(1,2,3)**: hippocampal field *cornu ammonis* (1,2,3), **DG**: dentate gyrus, **FC**: fasciola cinerea; fiber tracts: **alv**: alveus, **df**: dorsal fornix, **ec**: external capsule; layers: **slm**: stratum lacunosum-moleculare, **sr**: stratum radiatum, **sp**: stratum pyramidale, **so**: stratum oriens; **po**: polymorph layer, **sg**: stratum granulosum, **mo**: molecular layer.

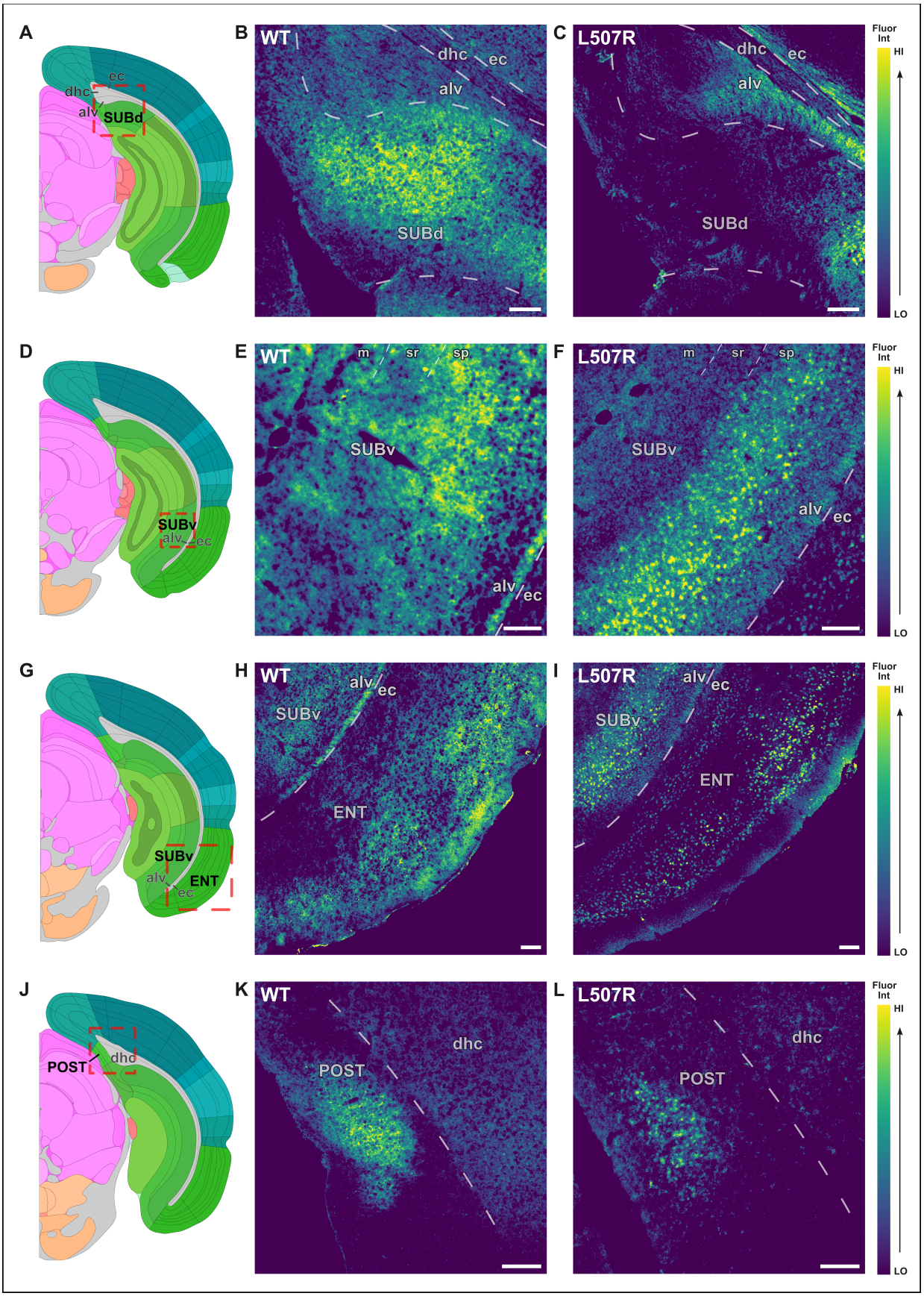

A
cc
dhc
alv
SUBd
B
WT
dhc
ec
alv
SUBd
C
L507R
dhc
ec
alv
SUBd
Fluor Int
HI
LO
D
SUBv
alv
ec
E
WT
m
sr
sp
SUBv
alv
ec
F
L507R
m
sr
sp
SUBv
alv
ec
Fluor Int
HI
LO
G
SUBv
alv
ENT
ec
H
WT
alv
ec
SUBv
ENT
I
L507R
alv
ec
SUBv
ENT
Fluor Int
HI
LO
J
POST
dhd
K
WT
dhc
POST
L
L507R
dhc
POST
Fluor Int
HI
LO

Figure 13: RGS14 immunoreactivity is widespread and moderate in retrohippocampal regions. Relative fluorescence intensity in RGS14-immunostained tissue sections from wild type (WT) and L507R-reporter mice. Anatomical annotations (left; **A,D,G,J**) from the Allen Mouse Brain Reference Atlas (atlas.brain-map.org) aligned with confocal images of RGS14 immunoreactivity in LR reporter (middle; **B,E,H,K**) and WT mice (right; **C,F,I,L**). Red dashed box in atlas images indicates approximate anatomical location of tissue cross-sections in each row; black text indicates nuclei and subnuclei, gray text indicates fiber tracts. Scale bar = 100 μm. Abbreviations: **ENT**: entorhinal cortex, **POST**: postsubiculum, **SUB(d,v)**: subiculum- (dorsal, ventral), fiber tracts: **alv**: alveus, **dhc**: dorsal hippocampal commissure, **ec**: external capsule.

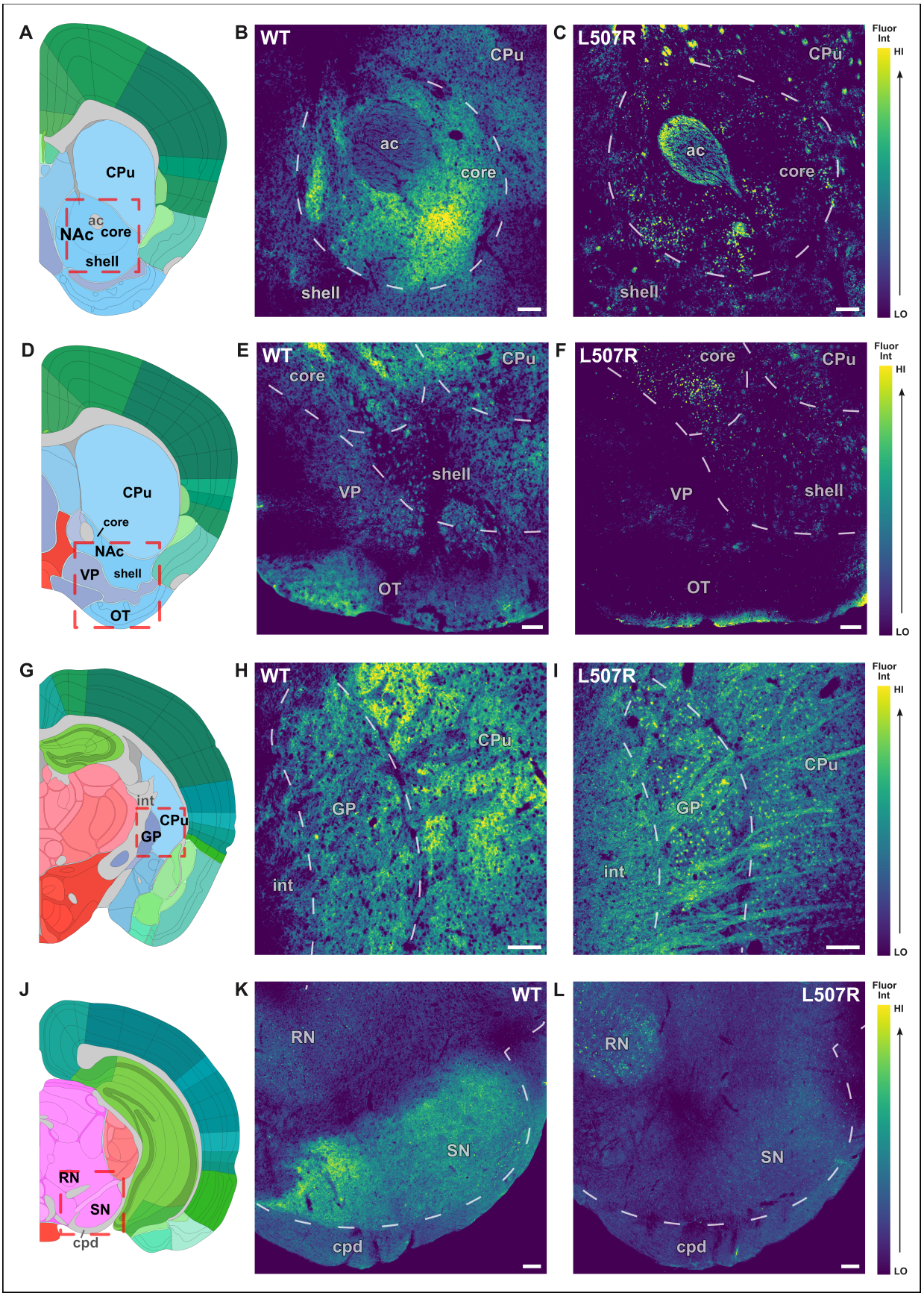

A
CPu
ac
NAc
core
shell
B
WT
CPu
ac
core
shell
C
L507R
CPu
ac
core
shell
Fluor Int
HI
LO
D
CPu
core
NAc
VP
shell
OT
E
WT
core
CPu
shell
VP
OT
F
L507R
core
CPu
VP
shell
OT
Fluor Int
HI
LO
G
int
CPu
GP
H
WT
CPu
GP
int
I
L507R
CPu
GP
int
Fluor Int
HI
LO
J
RN
SN
cpd
K
WT
RN
SN
cpd
L
L507R
RN
SN
cpd
Fluor Int
HI
LO

Figure 14: RGS14 immunoreactivity is variable across the basal ganglia. Relative fluorescence intensity in RGS14-immunostained tissue sections from wild type (WT) and L507R-reporter mice. Anatomical annotations (left; **A,D,G,J**) from the Allen Mouse Brain Reference Atlas (atlas.brain-map.org) aligned with confocal images of RGS14 immunoreactivity in LR reporter (middle; **B,E,H,K**) and WT mice (right; **C,F,I,L**). Red dashed box in atlas images indicates approximate anatomical location of tissue cross-sections in each row; black text indicates nuclei and subnuclei, gray text indicates fiber tracts. Scale bar = 100 μm. Abbreviations: **CPu**: caudoputamen, **GP**: globus pallidus, **NAc**: nucleus accumbens, **OT**: olfactory tubercle, **RN**: red nucleus, **SI**: substantia innominata, **SN**: substantia nigra, **VP**: ventral pallidum; fiber tracts: **ac**: anterior commissure, **cpd**: cerebral peduncle, **int**: internal capsule.

Table 2: Summary of RGS14 immunoreactivity in adult mouse brain: limbic system, basal ganglia, and midbrain. Relative expression determined from immunofluorescence heat atlas.

	BRAIN REGION		RGS14 EXPRESSION	
	STRUCTURE	**ABBV.**	**LEVEL**	**NUCLEAR**
SEPTAL REGIONS	Septofimbrial nucleus	**SF**		✓
	Subfornical organ	**SFO**		✓
	Lateral septal nucleus	**LS**		✓
	Triangular nucleus of septum	**TRS**		✗
	Septohippocampal nucleus	**SH**		✓
	Nucleus of the diagonal band	**NDB**		✗
AMYGDALOID COMPLEX	Central amygdala, lateral	**CeL**		✓
	Basolateral amygdala, posterior	**BLAp**		✓
	Cortical amygdalar area, posterior, medial zone	**COApm**		✓
	Basolateral amygdala, anterior	**BLAa**		✓
	Central amygdala, capsular	**CeC**		✓
	Central amygdala, medial	**CeM**		✓
	Lateral amygdala	**LA**		✓
	Medial amygdala, posterodorsal	**MeApd**		✓
EXTENDED AMYGDALA	Bed nucleus of stria terminalis, juxtacapsular	**BNSTju**		✓
	Bed nucleus of stria terminalis, oval	**BNSTov**		✓
	Substantia innominata	**SI**		✗
HIPPOCAMPAL FORMATION	Fasciola cinerea	**FC**		✓
	Field CA2	**CA2**		✓
	Induseum griseum	**IG**		✓
	Field CA1	**CA1**		✓
	Entorhinal cortex	**ENT**		✓
	Subiculum, ventral	**SUBv**		✓
	Dentate gyrus	**DG**		✓
	Postsubiculum	**POST**		✓
	Subiculum, dorsal	**SUBd**		✗
BASAL GANGLIA & MIDBRAIN	Nucleus accumbens, core	**NAcC**		✓
	Caudoputamen	**CPu**		✓
	Nucleus accumbens, shell	**NAcS**		✓
	Olfactory tubercle	**OT**		✗
	Substantia nigra	**SN**		✗
	Ventral pallidum	**VP**		✗
	Globus pallidus	**GP**		✓
	Red nucleus	**RN**		✗

Table 3: Summary of RGS14 immunoreactivity in adult mouse brain: fiber tracts. Relative expression determined from immunofluorescence heat atlas.

FIBER TRACT	ABBV.	RGS14 LEVEL
Fimbria	fi	
Stria terminalis	st	
Ventrohippocampal commissure	vhc	
Dorsal fornix	df	
Lateral olfactory tract	lot	
Alveus	alv	
Anterior commissure	ac	
Columns of the fornix	fx	
External capsule	ec	
Stria medullaris	sm	
Cerebral peduncle	cpd	
Dorsal hippocampal commissure	dhc	
Internal capsule	int	
Optic tract	opt	

3.8 Discussion

RGS14 is a multifunctional signaling protein that serves as a natural suppressor of synaptic signaling and plasticity. Our results present a comprehensive characterization of the distribution of RGS14 protein immunoreactivity throughout the adult mouse brain. The use of the RGS14 reporter mouse line (RGS14-LR) permitted us to positively identify RGS14 in regions that had previously escaped detection due to low or diffuse protein expression, and comparisons between LR and WT mice provided insight into key questions about the cellular origin and axonal expression of RGS14 in the brain. Overall, RGS14 immunoreactivity is found to varying degrees in cell bodies and neuropil in a variety of brain nuclei across the full extent of forebrain and midbrain regions in adult mice. The most intense levels are seen in the hippocampus proper, septum, NAcC subregion of the striatum, CeL subregion of the amygdala, and oval and juxtacapsular subregions of the BNST. It is also apparently trafficked along several major fiber tracts that involve cortico-limbic-basal ganglia connections that are central to emotional processing (Ingram, 2005; Willis & Haines, 2018). These results reaffirm and expand upon our previous knowledge of adult mouse brain RGS14 protein (Evans et al., 2014; Foster et al., 2021). Among the new discoveries are strong RGS14 immunoreactivity in discrete nuclei in the BNST and throughout nuclei and fiber tracts in the septum, and light immunoreactivity in isocortex that had previously escaped detection in adult mice.

Our data show that the expression profile of RGS14 protein in the murine brain largely aligns with our previous results from human and nonhuman primates with a few notable distinctions (Harbin et al., 2021; Montanez-Miranda et al., 2023; Squires et al., 2018). For one RGS14 is differently distributed among the constituent subregions of the amygdala and the striatum. In the amygdala, both species show RGS14 hotspots in CeL, but species differences in labeling intensity

between CeL and other amygdala nuclei are noticeable. In mice, the RGS14 signal in BLA is significantly lower than in CeL and the labeling in the basomedial amygdala signal is very low if not undetectable (Fig. 11E), while staining in primate basomedial amygdala and BLA is just as strong as in CeL (Squires et al., 2018). Additionally, our findings show light signal in the mice LA, while this nucleus is devoid of staining in macaques. At the striatal level, the murine RGS14 labeling in the NAcC is higher than in the CPu, while the reverse is was found in primates (Squires et al., 2018). Another difference is seen in the pattern of labeling in the GP such that RGS14 in murine GP is localized in both cell bodies and terminal-like profiles (Fig. 14H,I), while the labeling in the primate GP is confined to postsynaptic neuronal perikarya and dendritic processes (Squires et al., 2018).

Some notable features of its protein distribution profile hint to new roles for RGS14 in brain and behavior. RGS14 is known to suppress long-term potentiation and is required for long-term depression in hippocampal field CA2 (Evans et al., 2018b; Lee et al., 2010; Samadi et al., 2023). Our group has also recently shown that RGS14 protein expression can be markedly upregulated in the hippocampus as a protective mechanism in response to seizure-induced hyperactivity (Harbin et al., 2023). Considering that many RGS14-containing regions identified in this report are known to be conditionally plastic, it is possible that RGS14 functions as a tunable regulator of synaptic plasticity throughout many functionally related parts of the rodent brain. Here we will explore this possibility by highlighting several of the most noteworthy results and discussing the potential implications of regional RGS14 action on cognition, behavior, and human disease.

3.8.1 RGS14 in the hippocampal formation, septal regions, and basolateral amygdala

RGS14 is abundant throughout the hippocampal formation in regions that mediate various components of learning and memory (Bett et al., 2013; Dimsdale-Zucker et al., 2018; Garcia &

Buffalo, 2020; Hartopp et al., 2019; Jonas & Lisman, 2014; Park et al., 2022; Tzakis & Holahan, 2019). The implications of RGS14 in hippocampus proper have been previously discussed at length by our group and so will not be discussed here (Evans et al., 2014; Harbin et al., 2021; Montanez-Miranda et al., 2023). Regarding retrohippocampal regions, RGS14 is most abundant in ENT (Fig. 13H,I), which is critical for formation and recall of declarative memories due to its extensive relay between the cortex and the rest of the hippocampal formation (Canto et al., 2008; Garcia & Buffalo, 2020; Lee et al., 2021; Schultz et al., 2015). RGS14 is seen equally in medial ENT, which processes spatial memory and navigation, and lateral ENT, which processes associative learning of external stimuli (Fig. 7E,F) (Lee et al., 2021). Previous studies have demonstrated that RGS14 suppresses medial ENT-dependent functions by showing that loss of RGS14 enhances spatial memory in the Morris water maze (Lee et al., 2010), as well as lateral ENT-dependent functions by showing that RGS14 loss enhances cued fear memory in female mice (G. M. Alexander et al., 2019). RGS14 is also abundant in SUB (Fig. 13E,F), which mediates episodic memory retrieval through connections with ENT and receives synapses from CA1 that undergo both long-term potentiation and long-term depression (Behr et al., 2009; Matsumoto et al., 2019; O'Mara et al., 2000; Roy et al., 2017)

RGS14 is found in limbic regions involved in processing both positively- and negatively-valenced emotions (Fadok et al., 2018; Pignatelli & Beyeler, 2019; Rizzi-Wise & Wang, 2021). It is found at high levels in LS (Fig. 5F,G & Fig. 10E,H), which mediates social and emotional aspects of motivation, including integrating social cues and contextual information to influence behaviors related to social interactions (Clemens et al., 2020; Ishida et al., 2012; Shin et al., 2018) The LS sits between field CA3 and the ventral tegmental area (VTA) in a tri-synaptic circuit that activates VTA dopamine neurons and drives the association of context with reward, and activation

of CA2 inputs to LS were shown to disinhibit social aggression (Jiang et al., 2018; Leroy et al., 2018) .

The BLA integrates incoming sensory and valuation inputs from temporal and prefrontal cortical regions, respectively, with previously-learned information about a given stimulus from the hippocampus to assign emotional salience to said stimulus (Fudge & Emiliano, 2003; Hintiryan et al., 2021). Valence-coded BLA neuronal populations drive appetitive or aversive behaviors through their outputs to other regions; for example, BLA-NAc projections are generally appetitive while BLA-CeA projections are generally aversive (Beyeler et al., 2016). Long-term potentiation of synapses onto BLA principal neurons has been shown to underlie emotion-driven associative learning and behaviors (Goosens & Maren, 2002; Li & Rainnie, 2014; Rogan et al., 1997). Thus, it seems likely that RGS14 in emotional processing regions like the LS and BLA may limit the impact of emotional information on learning/memory and shaping behavior. As mentioned previously, RGS14 protein levels in murine BLA are low, but are much higher in primates (Squires et al., 2018). The reason for this species disparity is unknown, but could be related to the relative complexity of information conveyed by cortical inputs onto the primate BLA compared to rodents (McDonald, 1998).

The SFO is functionally and neurochemically distinct from the neighboring lateral septal complex. It is a hypothalamic circumventricular organ that exists beyond the highly selective blood-brain barrier making it sensitive and highly responsive to circulating signals such as hormones and osmotic changes. Intense RGS14 signal is expressed in select populations of SFO neurons (Fig. 10H,I), suggesting that it plays a role in interoception, or the cognitive perception of the internal physiological state. Given previous findings our group showing that RGS14 is required for microglia recruitment in response to seizure activity in the hippocampus (Harbin et al., 2023;

Winter et al., 2022), it is possible that RGS14 in SFO regulates neuroimmune functions of microglia sensing protein in response to injury-induced fear or other insults. To further understand the role of RGS14 in SFO, future studies to identify the specific cell populations in the SFO that express RGS14 must be carried out.

3.8.2 RGS14 in the extended amygdala

The extended amygdala is a key mediator of stress and threat responses, and is involved in certain types of emotional processing, particularly of negatively-valenced emotions such as fear and anxiety (Fox & Shackman, 2019). RGS14 is found throughout the extended amygdala, but distinct hotspots are observed in CeL, BNSTov, and BNSTju.

Information about fearful stimuli processed by the basolateral amygdala complex is transmitted to the brainstem and hypothalamic regions as well as the BNST via the CeL (Fig. 11E) and other subnuclei of the central amygdala complex to engage autonomic and neuroendocrine stress responses (Pitkänen et al., 1997; Sah et al., 2003). The CeL sends long-range projections externally to the periaqueductal gray, which processes pain and defensive and aversive behaviors, and to the paraventricular nucleus of the thalamus, considered a critical node in the brain anxiety network (Kirouac, 2021; Penzo et al., 2014). Synaptic plasticity at local and long-range projection neurons in CeL is essential for fear learning, fear memory recall, and behavioral fear responses (Li et al., 2013; Penzo et al., 2014). Despite their many similarities in processing fearful stimuli, studies suggest that the central amygdala mediates the phasic emotional state that defines fear while the BNST mediates a sustained, lower-intensity fear response characteristic of anxiety (Ueda et al., 2021; D. L. Walker et al., 2009). Evidence exists for RGS14 involvement in both fear and anxiety behaviors based on fear conditioning and open field test studies (Alexander et al., 2019; Foster et al., 2021; Parker et al., 2012). The mutation used in these mouse studies was a global genetic

deletion of RGS14 and as such the effects could not be definitively localized to specific brain regions, though one study found elevated c-Fos and pERK in CeA, CA1, and CA2 in RGS14-null mice following high-dose cocaine and novelty stress (Foster et al., 2021).

The BNSTov where RGS14 is expressed (Fig, 11B) is tied to the development of maladaptive behaviors in response to chronic and early life stress (Hu et al., 2020a; Hu et al., 2020b). Importantly, CeL and BNSTov neurons produce the highest amounts of the stress hormone CRF in the rodent brain outside of the hypothalamus (Hammack et al., 2021), and both regions exhibit strong postsynaptic RGS14 expression (Fig. 11B,E). Neuropeptides such as CRF are capable of profound changes in the brain due to their prolonged duration of action and wide field of influence (Mantsch, 2022). It is possible that maintaining high basal levels of RGS14 in CeL and BNSTov occurs as a preventative measure against over-recruitment of CRF systems. In theory, RGS14 localization in putative CRF-producing neurons in these regions renders them resistant to plasticity induced by stressful conditions, blunting their reactivity to subsequent stressful events. In addition to the likely effects of RGS14 in CRF-producing neurons, we also found RGS14 expression in neurons of highly CRF-receptive brain regions, including the ACC (Fig. 8E), CeA (Fig. 11E), and hippocampus (Fig. 12). These regions strongly express the CRF type I receptor (CRFR1) (Rissman et al., 2012; Yoshida et al., 2018), which couples with Gi/o under conditions of concentrated local CRF (i.e. stressful conditions) (Berger et al., 2006; Beyermann et al., 2007). On top of any effects on plasticity, we anticipate that the GTPase-activating functionality of RGS14 also limits CRFR1-Gi/o signaling, which is essential to many of the effects of acute and chronic stress alike (Klump & Fowler, 2020; Stern et al., 2011; Wang et al., 2011). Future studies should examine co-localization of RGS14 with CRF in CeL and BNSTov, and with CRFR1 throughout the brain.

In contrast with BNSTov, the neighboring BNSTju is relatively under-studied, but is also highly enriched with RGS14 (Fig. 11B,C). The BNSTju has unique connections with the amygdala compared to other lateral BNST nuclei, including little to no innervation from CeA, dense glutamatergic innervation from BLA, and robust inhibitory projections to CeM (Dong et al., 2000; Dong et al., 2001). High-frequency stimulation of the stria terminalis causes BNSTju neurons to undergo long-term potentiation of intrinsic excitability (LTP-IE), which describes a form of non-synaptic plasticity characterized by a protracted decrease in firing threshold and increase in firing probability (Francesconi et al., 2009a; Francesconi et al., 2009b). LTP-IE is impaired during protracted withdrawal from drugs of abuse but is restored by CRFR1 antagonism. RGS14 is packed extraordinarily densely into the miniscule BNSTju, though it is unknown what purpose this extreme expression is serving. Presumably RGS14 is affecting plasticity in the region, possibly canonically by disrupting H-Ras/ERK and Ca^{++}/CaM/CaMKII signaling to suppress synaptic potentiation onto BNSTju (Evans et al., 2018a; Shu et al., 2010; Willard et al., 2009), and/or possibly by maintaining the capacity for LTP-IE through limiting CRFR1-Gi/o signaling. In both hypothetical scenarios, RGS14 in BNSTju neurons would serve to normalize aberrant plasticity resulting from administration of drugs of abuse by mitigating either over-potentiation of synapses from limbic and cortical projections following drug intake or under-potentiation of BNSTju neuron intrinsic excitability during drug withdrawal. Future studies should explore RGS14 function in BNSTju, including the intriguing possible relationship between RGS14 and LTP-IE in BNSTju neurons.

3.8.3 RGS14 in the basal ganglia

The striatum is a large subcortical structure involved in processing goal-directed behavior and reward (De Groote & de Kerchove d'Exaerde, 2021). It serves as a nexus for the integration of

signals from the cortex, limbic system, and brainstem into a unified signal that travels outward through the pallidum and/or midbrain en route to the thalamus (Young et al., 2024). The striatum is anatomically divided into ventral (NAcC and NAcS) and dorsal (CPu) regions, which process reward/aversion and conscious motor behaviors, respectively. The striatum and midbrain send reciprocal projections, forming hierarchical loops that shift the locus of control over behavior from NAcS → NAcC → CPu as a behavior transitions from volitional to habitual (Belin & Everitt, 2008; Haber et al., 2000). The densest striatal RGS14 signal is seen in the NAcC (Fig. 5D & Fig. 14B,C), a principal function of which is forming associations between stimuli and rewarding or punishing outcomes (Ambroggi et al., 2011; Cerri et al., 2014; Hamel et al., 2017; Ma et al., 2020; West & Carelli, 2016). RGS14 levels are more modest in NAcS, but are highest in the lateral portion which mediates reward seeking (Plasse et al., 2012; Smedley et al., 2019). The expression of RGS14 in the dorsal striatum is also appreciable, most notably in the ventrolateral CPu (Fig. 5C-G), a striatal region that receives sensorimotor cortical inputs and is uniquely connected to AgI, which is critically involved in salience processing (Gogolla, 2017; Hintiryan et al., 2016). As a whole, this protein distribution pattern points to a role of RGS14 in reward-related behavior. It has the capacity to impact multiple points of processing reward-based learning/memory in the basal ganglia alone, potentially disrupting aspects of emotional, procedural, and motor learning needed for goal-directed behavior and habit formation.

3.8.4 Caveats and limitations

Immunofluorescent staining of brain tissue sections has some drawbacks mostly related to non-specific fluorescence, including issues with residual fluorescence near immunoreactivity hotspots, and autofluorescence generated by light scatter throughout tissue structural elements. Issues with autofluorescence were particularly problematic in sections of thalamus and hypothalamus,

rendering the data from these regions inconclusive. We suspect that RGS14 is present to some extent in these regions, particularly in the arcuate nucleus of the hypothalamus, but further investigation is needed. Also, fluorescence contamination from neuropil RGS14 reduces the resolution of immunofluorescence staining in WT mice, obscuring ultrastructural features such as cell bodies. This is a limitation that we partially address using the LR reporter mouse, in which RGS14 is sequestered into cell nuclei and out of neuropil, dramatically increasing resolution specifically of RGS14-expressing cell bodies. Immunohistochemical approaches in general are vulnerable to non-specific edge stain artifacts, which are especially problematic for proteins localized to superficial cortical layers like RGS14. Conveniently, the LR reporter mice address this problem as well by 1) positively identifying RGS14-expressing nuclei in superficially-projecting cortical layers, and 2) serving as a secondary, pseudo-negative control for WT neuropil and cell body elements.

The use of the LR reporters as a substitute for an RGS14-KO negative control permitted us to reduce the total number of animals required for the study, but with the caveat that tissue expression of RGS14 is not truly absent. Additionally, it appears to be the case that nuclear capture in LR mice is incomplete, as non-nuclear RGS14 signal is seen in several LR tissue images. Regardless, non-nuclear RGS14 signal is nearly universally much lighter in LR tissue than WT tissue, permitting LR tissue to retain value as a pseudo-KO control. While we did not expect to see non-nuclear RGS14 signal in LR tissue, this result is not entirely surprising. Our group previously revealed that the regulatory protein 14-3-3γ associates with RGS14 in murine hippocampal neurons, and that phosphorylation-independent binding of RGS14 by 14-3-3γ interferes with RGS14 nuclear import and nucleocytoplasmic shuttling (Gerber et al., 2018). While most RGS14 protein re-enters the nucleus for additional modifications shortly after translation, there is an apparent portion that is

precluded from nuclear re-entry, likely through interactions with regulatory proteins such as 14-3-3γ.

Another limitation of our approach stems from the semi-quantitative nature of relative fluorescence intensity as a measure of protein level, which is an approximation and limits the types of observations that can be made. This is further limited by the fact that atlas images could only be pseudo-standardized based on features like autofluorescence intensity in common tissue features, which is less reliable than, say, staining for an additional protein marker with established tissue protein levels to standardize to. An important caveat of our approach relates to the drawing of regional boundaries in microscopy images. Boundaries were manually drawn largely based on subjective matching of tissue structural features and fluorescence patterns to atlas images. While they are informed approximations of anatomical boundaries, they are inherently subjective and vulnerable to bias.

3.8.5 Conclusions

In summary, our findings here demonstrate the broad expression profile of RGS14 in adult mouse brain and open new avenues for future studies to explore RGS14 actions in these interconnected brain circuits.

Chapter 4: Endogenous RGS14 suppresses cocaine-induced emotionally motivated behaviors in female mice

RGS14 is expressed in limbic and basal ganglia regions known to undergo psychostimulant-induced plasticity. RGS14 may protect against developing addiction by serving as a natural suppressor of synaptic plasticity in emotion and motivation processing circuits. We assessed cocaine-driven changes in locomotor activity and place preference in RGS14-KO and WT mice and performed immunostaining of striatal tissue to assess RGS14 levels in cocaine-treated mice and to localize RGS14 to D1R and D2R-expressing cells.

4.1 RGS14 localizes to D1R- and D2R-expressing cells in the nucleus accumbens

In the mouse ventral striatum, both D1- and D2-MSNs project along direct and indirect pathways through the basal ganglia (Kupchik & Kalivas, 2017), and work in concert in the NAcC to process motivated learning and adaptive behavior (Flanigan & Leclair, 2017; Gingrich & Caron, 1993; Urs et al., 2011; Verharen et al., 2019; Zachry et al., 2024). RGS14 immunoreactivity is abundant in the striatum, particularly within NAcC (Fig. 5D). Using an RGS14 reporter mouse that targets RGS14 to the nuclei of cells where it is expressed (Squires et al., 2020), we verified intrinsic RGS14 protein expression in NAc neurons (Fig. 14C,F). To assess RGS14 abundance in D1R- vs D2R-exressing NAc neurons, we immunostained for RGS14 in striatal tissue sections from *Drd1-tdTomato* (Fig. 15A) and *Drd2-EGFP* (Fig. 15B) mice and evaluated colocalization. There was extensive colocalization of RGS14 with both tdTomato and EGFP in NAc core, and to a lesser extent in NAc shell and ventromedial CPu. RGS14 signal was apparent in both cell bodies and neuropil.

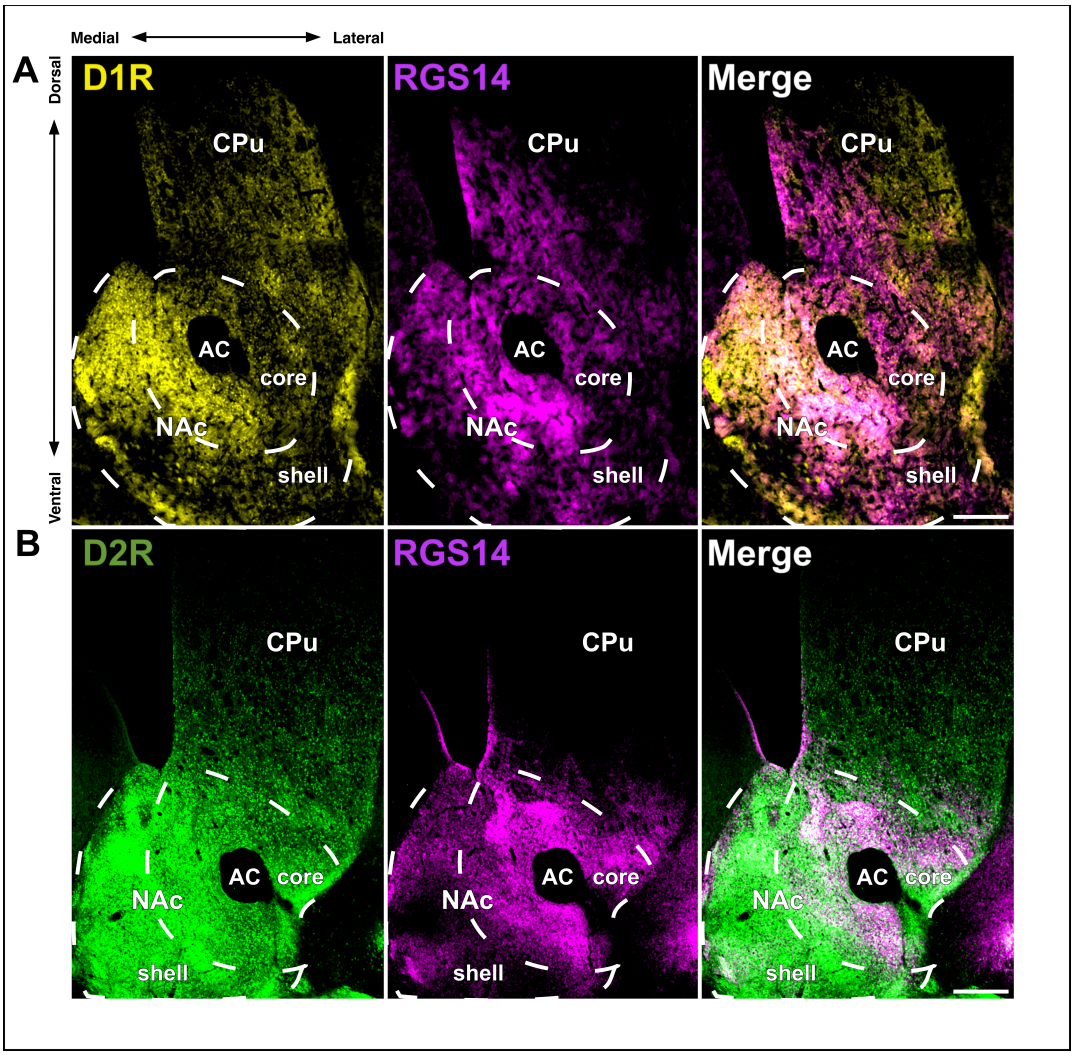


Figure 15. RGS14 localizes to D1R and D2R-expressing cells in the nucleus accumbens. Immunofluorescence detection of RGS14 with D1R and D2R in RGS14-immunostained striatal tissue from *Drd1-tdTomato* and *Drd2-EGFP* reporter mice. **A.** *Drd1-tdTomato* tissue immunoreactivity; panels:: yellow (left): D1R-tdTomato, magenta (middle): RGS14, white (right): overlap. **B.** *Drd2-EGFP* tissue immunoreactivity:: green (left): D2R-EGFP, magenta (middle): RGS14, white (right): overlap. Fluorophores were sequentially scanned in separate channels and computationally merged. Approximate borders of NAc core and shell outlined in white dashes. Scale bar = 250 µM. Anatomical abbreviations:: **CPu**: caudoputamen, **NAc(C,S)**: nucleus accumbens- (core, shell).

4.2 RGS14 is upregulated following cocaine challenge in the nucleus accumbens of mice with a chronic cocaine history

Our group recently reported that RGS14 is upregulated in the hippocampus by hyperexcitability during status epilepticus (Harbin et al., 2023). This raises the possibility that RGS14 could also be induced elsewhere to mitigate signaling hyperactivation, such as in the NAc when overactivated by psychostimulants. To determine whether cocaine challenge alters RGS14 induction in mice with a history of cocaine exposure, we quantified RGS14 immunofluorescence intensity 2 h after cocaine challenge (5 mg/kg, i.p.) in subjects 10 days after chronic cocaine administration (5 mg/kg/d, i.p. for 5 days) or saline. We did not find any significant differences in the BNST, CeA, or BLA (data not shown), but RGS14 levels were significantly higher in both the NAc core ($t(5.50) = 3.48$, $p = .015$) and shell ($t(4.07) = 5.48$, $p = .005$) in subjects chronically treated with cocaine compared to saline (Fig. 16).

4.3 Enhanced locomotor sensitization to cocaine in RGS14-KO mice

The operational definition of sensitization is a magnitude of response in a subsequent exposure to a stimulus that surpasses that elicited by its initial exposure. It is well-established that locomotor activation sensitizes to repeated cocaine treatment in rodents, an adaptation marked by neuroplastic changes in mesocorticolimbic pathways (Thomas et al., 2008; Vélez-Hernández et al., 2013) including increased spine density specifically in NAc core (Li et al., 2004). RGS14 inhibits spine enlargement following two-photon glutamate uncaging in CA2 dendrites (Evans, Parra-Bueno, et al., 2018), leading us to suspect that it can also act in the NAc core, through this and/or additional mechanisms, to suppress cocaine-induced plasticity underlying locomotor sensitization. To test the

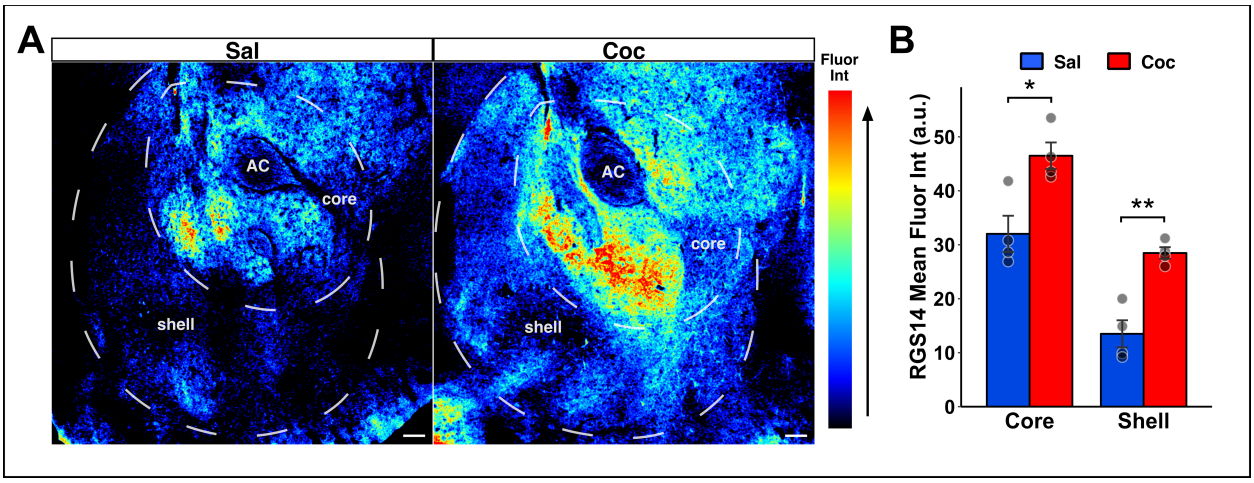


Figure 16: RGS14 is upregulated in nucleus accumbens core and shell 2 hours after cocaine challenge in cocaine-experienced mice. Immunofluorescence detection and relative quantification of RGS14 protein in NAc 2 hours after Coc challenge (i.p.) in naïve and Coc-experienced WT mice. A. Representative images of RGS14-immunostained NAc tissue from naive (left) and Coc-experienced (right) mice, pseudocolored to show relative fluorescence intensity. B. Mean fluorescence intensity (arbitrary units) in NAc core and shell of RGS14-immunostained tissue. Analyzed by Welch's t-test. Error bars represent mean ± SEM. Symbols: †p < .10, *p < .05, **p < .01, ***p < .001. Scale bar = 100 µm. Anatomical abbreviations:: AC: anterior commissure, NAc(C,S): nucleus accumbens- (core, shell).

hypothesis that RGS14 loss increases susceptibility to the behaviorally sensitizing effects of cocaine, we performed the locomotor sensitization experiment diagrammed in Fig. 17A with female RGS14-KO mice and WT littermate controls (n = 48). Briefly, after 3 days of habituation with saline, WT and RGS14-KO mice were treated with either saline or cocaine every day for 5 days (induction of sensitization), withdrawn for 10 days, then given a challenge dose of cocaine (expression of sensitization). Locomotor activity was measured for 60 min following each treatment. We selected a low dose of cocaine (5 mg/kg) (1) to minimize genotype differences in the baseline response to drug in naïve animals, according to our previously published dose response curve (Foster et al., 2021), and (2) because we predicted that RGS14 KO mice would have enhanced sensitization and wanted to avoid a ceiling effect. For a complete lists of statistical tests, see Tables 4 & 5.

Locomotor activity on each day of the paradigm during the first 30 min following cocaine or saline treatment is shown in Fig. 17B. We first assessed the effects of RGS14 loss on induction of locomotor sensitization to cocaine, and a linear mixed model analysis revealed a significant genotype × treatment × day interaction ($F(1, 188) = 4.64$, $p = .032$). Analysis of locomotor activity on the first and last days of the induction period (Fig. 17C, paired t-tests) showed that chronic cocaine induced significant locomotor sensitization only in RGS14-KO mice (RGS14KO+Coc: $t(11) = 2.54$, $p = .028$); cocaine-induced locomotor activation did not significantly change between the first and final induction phase cocaine treatment in WT controls (WT+Coc: $t(11) = 1.63$, $p = .131$). Saline-treated controls of both genotypes became hypoactive as they habituated, as expected (WT+Sal: $t(11) = -4.15$, $p = .004$; RGS14KO+Sal: $t(11) = -4.33$, $p = .003$),

We analyzed group interactions across the induction phase using linear mixed models followed by pairwise comparisons of estimated marginal means. There was a significant treatment × day

interaction effect within the WT group (Fig. 17D; $F(1, 94) = 11.56$, $p < .001$), but no significant differences in locomotor activity between cocaine- and saline-treated mice on any individual induction day were detected. We observed a trend for cocaine-induced locomotor activation starting on induction day 3, but it never reached significance (Ind3: $t(38.1) = 2.34$, $p = .094$; Ind4: $t(38.1) = 2.45$, $p = .094$; Ind5: $t(38.1) = 2.39$, $p = .094$). This result is not entirely surprising, as we were using a low dose of cocaine (5 mg/kg) that is below the typical threshold for sensitization in rodents (Smith et al., 2016; Walker et al., 2001). There was a significant treatment × day interaction within the RGS14-KO group (Fig. 17E; $F(1, 94) = 25.41$, $p < .001$). A trend for increased locomotor activity in cocaine-treated mice was evident on induction day 1 (Ind1: $t(27.8) = 1.79$, $p = .085$), and the difference reached statistical significance on induction day 2 (Ind2: $t(27.8) = 3.03$, $p = .010$), after which cocaine consistently elicited significant locomotor activation for the rest of the induction phase (Ind3: $t(27.8) = 3.88$, $p = .002$; Ind4: $t(27.8) = 3.80$, $p = .002$; Ind5: $t(27.8) = 4.41$, $p < .001$).

Within cocaine-treated mice (Fig. 17G), we found a significant genotype × day interaction effect over induction ($F(1, 94) = 6.75$, $p = .022$). Post-hoc analysis confirmed that locomotor activation by acute cocaine was not significantly different between drug-naïve WT and RGS14-KO mice (Ind3: $t(28.7) = 1.21$, $p = .236$), but revealed a trend for enhanced locomotor activation in RGS14-KO mice by the third cocaine exposure (Ind3: $t(28.7) = 2.37$, $p = .100$) that reached statistical significance on the final day of induction (Ind5: $t(28.7) = 2.80$, $p = .045$). Together, these data indicate that loss of RSG14 promotes the induction of sensitization by cocaine.

4.4 RGS14 loss increases the expression of cocaine-induced locomotor sensitization

To determine whether RGS14 loss affects the persistent expression of cocaine sensitization, all groups were challenged with cocaine (5 mg/kg, i.p.) 10 d after the last induction day. Locomotor

activity was recorded for 60 min. A two-way ANOVA revealed a significant genotype × treatment interaction ($F(1, 44) = 4.63$, $p = .037$) (Fig. 4B, shaded box). Tukey tests revealed that the locomotor response to cocaine challenge was enhanced by chronic cocaine only in RGS14-KO mice (Fig. 4E, shaded box; $t(44) = 3.41$, $p = .008$); locomotor activity in WT mice did not differ by drug history (Fig. 4D, shaded box; $t(44) = 0.71$, $p = .894$). Additionally, the locomotor response was significantly larger in RGS14-KO mice previously given chronic cocaine than in WT mice with the same drug history (Fig. 4F, shaded box; $t(44) = 3.34$, $p = .009$). These data indicate that the augmenting effect of RGS14 loss on the sensitized response to cocaine persists after a period of withdrawal.

4.5 RGS14 loss alters the temporal dynamics of cocaine-induced locomotor activation

Proper cellular function requires precise control of both the intensity and duration of signaling events (Dolmetsch, 2003; Mariathasan et al., 2001; Sacks, 2006). To assess the effects of RGS14 loss on the temporal dynamics of cocaine-induced locomotor activation, we analyzed locomotor activity over time during cocaine challenge (Fig. 17H) using linear mixed models. No significant group differences were detected during the 90 min habituation period, though there was a trend for a treatment × time interaction ($F(1, 406) = 3.54$, $p = .061$) in RGS14-KO mice that is apparently driven by sustained elevated locomotor activity in the chronic cocaine treatment group in the time leading up to challenge (Fig. 17J). A significant genotype × treatment × time interaction effect ($F(1, 513) = 5.24$, $p < .001$) was found over the 60 min period following cocaine treatment. Further analysis revealed significant treatment × time interactions within both WT ($F(1, 240) = 17.19$, $p < .001$) and RGS14-KO genotype groups ($F(1, 262) = 61.43$, $p < .001$), and a significant genotype × time interaction within the chronic cocaine treatment group ($F(1, 262) = 23.81$, $p < .001$).

To further investigate significant two-way interactions, we ran pairwise comparisons of estimated marginal means at each time point after cocaine treatment. We found that, during the first 10 minutes of challenge, cocaine-induced locomotor activation is significantly enhanced in both WT (Fig. 17I) and RGS14-KO (Fig. 17J) mice previously given chronic cocaine (WT+95 min: $t(81.1) = 3.33$, $p = .015$; WT+100 min: $t(81.1) = 3.17$, $p = .023$, RGS14KO+95 min: $t(49.2) = 5.68$, $p < .001$; RGS14KO+100 min: $t(49.2) = 4.25$, $p = .001$), plus a trend for higher activity for 10 additional minutes in RGS14-KO mice (105 min: $t(49.2) = 2.64$, $p = .099$; 110 min: $t(49.2) = 2.82$, $p = .070$). Analysis of the chronic cocaine group reveals that locomotor activity is enhanced in RGS14-KO mice over WT mice with the same drug history for a full 30 min after injection (Fig. 17L; 95 min: $t(57.1) = 4.31$, $p < .001$); 100 min: $t(57.1) = 4.08$, $p = .002$; 105 min: $t(57.1) = 3.26$, $p = .019$; 110 min: $t(57.1) = 2.63$, $p = .076$; 115 min: $t(57.1) = 2.99$, $p = .037$; 120 min: $t(57.1) = 2.89$, $p = .044$). Examined together, the challenge time course data indicate that RGS14 loss extends the duration of locomotor activation by low-dose cocaine irrespective of prior cocaine exposure, while the interaction of RGS14 loss and chronic cocaine history is required to augment the magnitude of response to this dose. This suggests dissociable mechanisms for RGS14 regulation of the magnitude and duration of cocaine-induced locomotor activation, which will be discussed further below.

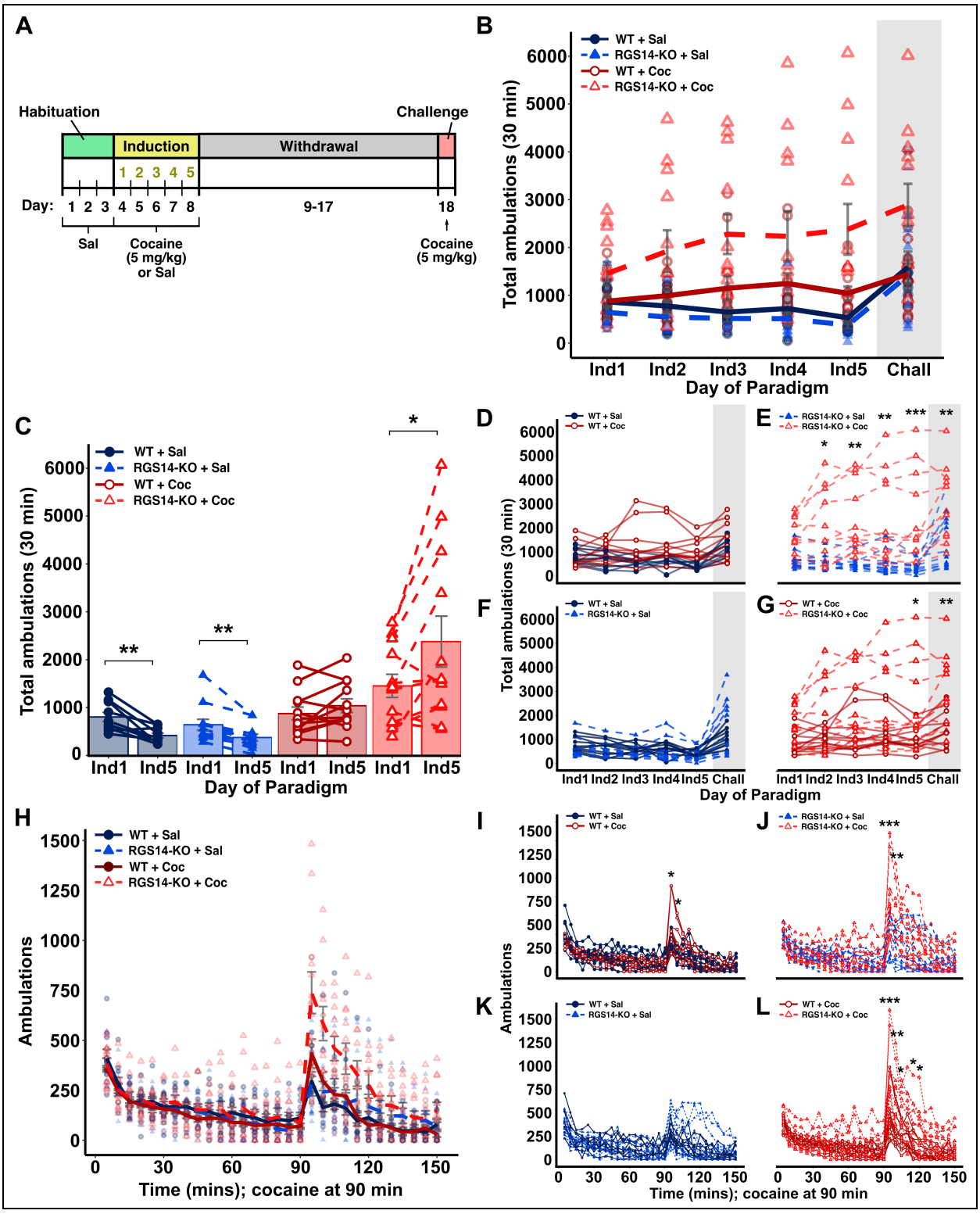


Figure 17. Locomotor sensitization to cocaine is enhanced in RGS14-KO mice. A. Diagram of cocaine sensitization protocol (n = 48); cocaine (5mg/kg) or saline administered by i.p. injection. **(B-G)** Total ambulatory

activity (beam breaks/30 min) each day of induction and challenge. **B.** Total ambulatory activity (error bars: ± S.E.M.) each day for all groups. There is a significant genotype × treatment × day interaction effect over induction (LMM) and a significant genotype × treatment interaction effect during cocaine challenge (Two-way ANOVA). **C.** Within-subjects changes in ambulatory activity from the first to the last day of induction (Ind1 to Ind5). Locomotor activity was decreased in Sal-treated controls as expected from habituation. Locomotor activity was significantly increased only in the RGS14KO+Coc group (paired pairwise t-tests^).**D.** In WT mice, there is a significant treatment × day interaction effect over induction (LMM), but no significant differences between WT+Coc and WT+Sal group locomotor activity were detected on any individual day (pairwise t-tests^). **E.** In RGS14-KO mice, there is a highly significant treatment × day interaction effect over induction (LMM). Locomotor activity is significantly elevated in the RGS14KO+Coc group over RGS14KO+Sal controls at Ind2-Ind5 (pairwise t-tests^) and challenge (Tukey HSD test). **F.** No significant genotype × day interaction in the Sal treatment group (LMM). **G.** In the cocaine treatment group, there is a significant genotype × day interaction effect over induction (LMM). Locomotor activity is significantly elevated in the RGS14KO+Coc group over WT+Coc controls at Ind5 (pairwise t-tests^) and challenge (Tukey HSD test). **(H-L)** Ambulatory activity (bream breaks/5 min) over time during cocaine challenge. **H.** Ambulatory activity (error bars: ± S.E.M.) over time for all groups. There is a highly significant genotype × treatment × time interaction effect over the 60 min following cocaine treatment (LMM). **I.** In the WT group, there is a significant treatment × time interaction effect in the 60 min following cocaine injection (LMM). Locomotor activity is significantly elevated in the WT+Coc group over WT+Sal controls during the first 10 minutes after injection (pairwise t-tests^). **J.** In RGS14-KO mice, there is a significant treatment × time interaction effect over the 60 min following cocaine injection (LMM). Locomotor activity is significantly elevated in the RGS14KO+Coc group over RGS14KO+Sal controls during the first 10 minutes after injection (pairwise t-tests^). **K.** No significant genotype × time interaction effects in Sal group (LMM). **L.** In the Coc treatment group, there is a significant genotype × time interaction effect over the 60 min following cocaine injection (LMM). Locomotor activity is significantly elevated in the RGS14KO+Coc group over WT+Coc controls during the first 30 minutes after injection (pairwise t-tests^). Asterisks (*) denote significant difference between groups (*$p < .05$, **$p < .01$, ***$p < .001$). Carat (^) indicates Holm correction.

Table 4. Locomotor sensitization statistics: induction. Carat (^) indicates Holm correction.

Fig	Statistical test	Day(s)	Factors	Effect or Groups	df	Statistic	Value	Pval	Sig
4B	Linear Mixed-Effects models	Induction	Geno, Trtmt, Day	Geno	1, 51.33	F	0.90	.348	
				Trtmt	1, 51.33	F	4.99	.030	*
				Day	1, 188	F	4.86	.029	*
				Geno × Trtmt	1, 51.33	F	3.43	.070	†
				Geno × Day	1, 188	F	6.78	.010	**
				Trtmt × Day	1, 188	F	36.95	< .001	***
				Geno × Trtmt × Day	1, 188	F	4.64	.032	*
4C	Paired pairwise t-tests^	Ind1 vs. Ind5		WT+Sal	11	t	4.15	.004	**
				RGS14KO+Sal	11	t	4.33	.003	**
				WT+CC	11	t	-1.63	.131	
				RGS14KO+CC	11	t	-2.54	.028	*
4D	Linear Mixed-Effects models	Induction	Trtmt, Day (WT)	Trtmt	1, 29.99	F	0.21	> .999	
				Day	1, 94	F	0.12	> .999	
				Trtmt × Day	1, 94	F	11.56	< .001	***
4E			Trtmt, Day (RGS14-KO)	Trtmt	1, 24.88	F	5.03	.068	†
				Day	1, 94	F	8.67	.008	**
				Trtmt × Day	1, 94	F	25.41	< .001	***
4F			Geno, Day (Sal)	Geno	1, 29.43	F	2.34	.274	
				Day	1, 94	F	23.29	< .001	***
				Geno × Day	1, 94	F	0.31	> .999	
4G			Geno, Day (Coc)	Geno	1, 25.34	F	2.14	.310	
				Day	1, 94	F	20.45	< .001	***
				Geno × Day	1, 94	F	6.75	.022	*
4D	Pairwise t-tests^	Ind1		WT+Coc vs. WT+Sal	38.1	t	0.07	.947	
		Ind2			38.1	t	1.02	.633	
		Ind3			38.1	t	2.34	.094	†
		Ind4			38.1	t	2.45	.094	†
		Ind5			38.1	t	2.39	.094	†
4E		Ind1		RGS14KO+Coc vs. RGS14KO+Sal	27.8	t	1.79	.085	†
		Ind2			27.8	t	3.03	.010	*
		Ind3			27.8	t	3.88	.002	**
		Ind4			27.8	t	3.80	.002	**
		Ind5			27.8	t	4.41	< .001	***
4G		Ind1		RGS14KO+Coc vs. WT+Coc	28.7	t	1.21	.236	
		Ind2			28.7	t	1.95	.144	
		Ind3			28.7	t	2.37	.100	†
		Ind4			28.7	t	2.07	.144	
		Ind5			28.7	t	2.80	.045	*

Table 5. Locomotor sensitization statistics: challenge. Carat (^) indicates Holm correction.

Fig	Statistical test	Day(s)	Factors	Effect or Groups	df	Statistic	Value	Pval	Sig
4B	Two-Way ANOVA	Chall	Geno, Trtmt	Geno	1, 44	F	4.98	.031	*
				Trtmt	1, 44	F	5.38	.025	*
				Geno × Trtmt	1, 44	F	4.63	.037	*
4D	Tukey HSD test	Chall		WT+Coc vs. WT+Sal	44	t	0.71	.894	
4E				RGS14KO+Coc vs. RGS14KO+Sal	44	t	3.41	.008	**
4F				RGS14KO+Sal vs. WT+Sal	44	t	0.64	.918	
4G				RGS14KO+Coc vs. WT+Coc	44	t	3.34	.009	**
4H	Linear Mixed-Effects models	Chall	Geno, Trtmt, Time	Geno	1, 418.62	F	14.35	< .001	***
				Trtmt	1, 418.62	F	55.34	< .001	***
				Time	1, 513	F	496.2	< .001	***
				Geno × Trtmt	1, 418.62	F	24.67	< .001	***
				Geno × Time	1, 513	F	8.65	.003	**
				Trtmt × Time	1, 513	F	55.52	< .001	***
				Geno × Trtmt × Time	1, 513	F	5.24	< .001	***
4I	Linear Mixed-Effects models	Chall (Habituation)	Trtmt, Time (WT)	Trtmt	1, 33.33	F	1.07	.309	
				Time	1, 389	F	435.97	< .001	***
				Trtmt × Time	1, 389	F	0.02	.879	
4J			Trtmt, Time (RGS14-KO)	Trtmt	1, 27.09	F	0.01	.927	
				Time	1, 406	F	413.84	< .001	***
				Trtmt × Time	1, 406	F	3.54	.061	†
4K			Geno, Time (Sal)	Geno	1, 28.92	F	0.07	.787	
				Time	1, 389	F	438.79	< .001	***
				Geno × Time	1, 389	F	0.88	.350	
4L			Geno, Time (Coc)	Geno	1, 28.22	F	0.41	.530	
				Time	1, 406	F	408.08	< .001	***
				Geno × Time	1, 406	F	1.25	.264	
4I		Chall (Post-Coc)	Trtmt, Time (WT)	Trtmt	1, 256.49	F	17.95	< .001	***
				Time	1, 240	F	233.21	< .001	***
				Trtmt × Time	1, 240	F	17.19	< .001	***
4J			Trtmt, Time (RGS14-KO)	Trtmt	1, 184.89	F	61.05	< .001	***
				Time	1, 262	F	267.08	< .001	***
				Trtmt × Time	1, 262	F	61.43	< .001	***
4K			Geno, Time (Sal)	Geno	1, 170.03	F	0.53	.469	
				Time	1, 240	F	132.30	< .001	***
				Geno × Time	1, 240	F	0.04	.846	
4L			Geno, Time (Coc)	Geno	1, 228.52	F	32.60	< .001	***
				Time	1, 262	F	365.82	< .001	***
				Geno × Time	1, 262	F	23.81	< .001	***
4I	Pairwise t-tests^	Chall	WT+Coc vs. WT+Sal	t = 95 min	81.1	t	3.33	.015	*
				t = 100 min	81.1	t	3.17	.023	*
				t = 105 min	81.1	t	1.14	> .999	
				t = 110 min	81.1	t	1.47	> .999	
				t = 115 min	81.1	t	0.45	> .999	
				t = 120 min	81.1	t	-0.92	> .999	
				t = 125 min	81.1	t	-0.02	> .999	
				t = 130 min	81.1	t	-0.02	> .999	
				t = 135 min	81.1	t	-0.15	> .999	
				t = 140 min	81.1	t	-0.07	> .999	
				t = 145 min	81.1	t	0.46	> .999	
				t = 150 min	81.1	t	1.17	> .999	
4J			RGS14KO+Coc vs. RGS14KO+Sal	t = 95 min	49.2	t	5.68	< .001	***
				t = 100 min	49.2	t	4.25	.001	**
				t = 105 min	49.2	t	2.64	.099	†
				t = 110 min	49.2	t	2.82	.070	†
				t = 115 min	49.2	t	1.54	> .999	
				t = 120 min	49.2	t	1.37	> .999	
				t = 125 min	49.2	t	0.42	> .999	
				t = 130 min	49.2	t	0.64	> .999	
				t = 135 min	49.2	t	0.37	> .999	
				t = 140 min	49.2	t	0.25	> .999	
				t = 145 min	49.2	t	0.12	> .999	
				t = 150 min	49.2	t	1.01	> .999	
4L			RGS14KO+Coc vs. WT+Coc	t = 95 min	57.1	t	4.31	< .001	***
				t = 100 min	57.1	t	4.08	.002	**
				t = 105 min	57.1	t	3.26	.019	*
				t = 110 min	57.1	t	2.63	.076	†
				t = 115 min	57.1	t	2.99	.037	*
				t = 120 min	57.1	t	2.89	.044	*
				t = 125 min	57.1	t	1.42	.578	
				t = 130 min	57.1	t	1.58	.578	
				t = 135 min	57.1	t	1.60	.578	
				t = 140 min	57.1	t	0.93	.712	
				t = 145 min	57.1	t	0.69	.712	
				t = 150 min	57.1	t	1.70	.571	

4.6 RGS14 loss augments the magnitude and duration of cocaine conditioned place preference

We and others showed previously that RGS14 loss enhances spatial learning in mice (Lee et al., 2010) and fear conditioning specifically in female mice (Alexander et al., 2019). Based on these studies and the brain expression profile of RGS14, we anticipated that reward learning would be enhanced in female RGS14-KO mice. We tested this hypothesis using a canonical biased cocaine conditioned place preference (CPP) paradigm, except that rather than a single posttest the day after the final conditioning day, we conducted two additional posttests at 10 d intervals thereafter to assess the persistence of the cocaine-association context memory (Figure 18A). We also examined the change in distance traveled on the cocaine-paired side as a measure of conditioned locomotor activation. Refer to Table 6 for full statistical analyses.

CPP results are shown in Figure 18B. When examining all post-tests by three-way repeated measures ANOVA, the main effects for treatment and post-test were significant (Treatment: $F(1, 28) = 59.24$, $p < .001$; Post-test: $F(1.54, 43.24) = 11.10$, $p < .001$), and there was a trend for a main effect of genotype ($F(1, 28) = 2.99$, $p = .095$). The genotype × treatment × post-test interaction effect was not significant ($F(1.54, 43.24) = 1.24$, $p = .353$), but the treatment × post-test interaction was significant ($F(1.54, 43.24) = 10.78$, $p < .001$) and there was a trend for a genotype × treatment interaction ($F(1, 28) = 3.08$, $p = .090$). Two-way ANOVAs at each post-test revealed a significant genotype × treatment interaction effect at Post1 ($F(1, 28) = 4.57$, $p = .042$), a trend for an interaction at Post2 ($F(1, 28) = 3.26$, $p = .082$), and no significant interaction at Post3 ($F(1, 28) = 0.81$, $p = .377$). Main effect of treatment was significant at each post-test (Post1: $F(1, 28) = 63.88$, $p < .001$; Post2: $F(1, 28) = 74.40$, $p < .001$; Post3: $F(1, 28) = 20.45$, $p < .001$).

Analysis of planned comparisons at Post1 revealed that time spent on the cocaine-paired side was significantly enhanced in the cocaine-treated WT ($t(28) = 4.14$, $p = .002$) and RGS14-KO

groups ($t(28) = 7.16$, $p < .001$) compared to controls that received saline on both sides, indicating that cocaine induced a place preference in both genotypes. Additionally, there was a trend for a CPP of greater magnitude in RGS14-KO mice ($t(28) = 2.47$, $p = .087$). CPP persisted when measured at Post2 in both WT ($t(28) = 4.82$, $p < .001$) and RGS14-KO groups ($t(28) = 7.38$, $p < .001$), and the initial trend for a greater effect in the RGS14-KO group reached significance at this time point ($t(28) = 2.88$, $p = .036$). By Post3, a full 3 weeks after the final conditioning session, preference for the cocaine-paired side in the WT group had been reduced to a trend ($t(28) = 2.56$, $p = .072$) but remained significant in the RGS14-KO group (Post3: $t(28) = 3.26$, $p = .004$). Together, these data indicate that RGS14 loss increases the magnitude and persistence of cocaine-CPP.

4.7 RGS14 loss augments the magnitude and duration of cocaine-conditioned locomotor hyperactivity

Environmental context has been shown to modulate cocaine-induced structural plasticity in NAc core and subsequent psychomotor sensitization (Badiani & Robinson, 2004; Li et al., 2004). Furthermore, cocaine-associated environments can elicit conditioned locomotor hyperactivity in the absence of the acute pharmacological effects of the drug itself (Barr et al., 1983; Cervo & Samanin, 1996; Di Ciano et al., 1998; Stewart et al., 1984). Conditioned locomotor hyperactivity may therefore be an indicator of the modulatory effect of a given environment on cocaine-induced plasticity in the NAc and/or NAc-projecting regions. We examined locomotor activity/distance traveled in the cocaine-paired context during CPP post-tests to assess how RGS14 impacts cocaine-conditioned locomotor activation.

Locomotor activity results are shown in Figure 18C. We initially analyzed data from all post-tests using three-way repeated measures ANOVA on ranks. We found no significant genotype ×

treatment × post-test interaction effect ($F(1.67, 46.86) = 0.45$, $p = .604$), but a trend for a genotype × post-test interaction ($F(1.67, 46.86) = 3.17$, $p = .060$) and a significant main effect of treatment ($F(1, 28) = 13.11$, $p = .001$). Two-way ANOVAs at each post-test showed no significant genotype × treatment interaction effects, but a trend for an interaction at Post1 ($F(1, 28) = 3.08$, $p = .090$). Main effect of treatment was significant at each post-test (Post1: $F(1, 28) = 29.45$, $p < .001$; Post2: $F(1, 28) = 6.96$, $p = .013$; Post3: $F(1, 28) = 4.46$, $p = .044$), and there was a significant main effect of genotype at Post1 ($F(1, 28) = 5.05$, $p = .033$) and a trend at Post2 ($F(1, 28) = 3.04$, $p = .092$).

Analysis of planned comparisons at Post1 revealed that distance traveled on the cocaine-paired side was significantly increased in the cocaine-treated RGS14-KO group ($t(28) = 5.08$, $p < .001$) compared to RGS14-KO controls that received saline on both sides, but there was only a trend for an increase in the cocaine-treated WT group ($t(28) = 2.60$, $p = .067$). Within the cocaine treatment group, locomotor hyperactivity was significantly greater in RGS14-KO mice ($t(28) = 2.83$, $p = .040$) than WTs. At Post2, locomotor activity remained significantly elevated in the cocaine-treated RGS14-KO group compared to saline-treated controls ($t(28) = 2.74$, $p = .049$). By Post3, no significant differences in locomotor activity were observed between any of the groups. To ensure that observed increases in locomotor activity were specifically elicited by the cocaine-paired context and were not the result of general locomotor hyperactivity, we examined the change in total distance traveled in all compartments and found no significant differences between groups (Table 6). Together, these data indicate that RGS14 loss enhances the magnitude and duration of conditioned locomotor hyperactivity in a cocaine-paired context. This suggests that RGS14 suppresses environment-based enhancement of cocaine-induced plasticity in the NAc and/or connected regions.

4.8 RGS14 regulates cocaine-conditioned place preference and cocaine-conditioned locomotor activation through dissociable mechanisms

The mechanisms that process emotional valence and behavioral engagement are distinct, but overlap in their governance of motivated behavior. Having determined that RGS14 loss enhances both cocaine-CPP and cocaine-conditioned locomotor hyperactivity, we next asked whether these metaplastic behavioral effects of RGS14 loss were mechanistically intertwined by analyzing the correlation (Pearson's test) between the change in time and the change in distance on the cocaine-paired side during Post1, when these measures were enhanced in both cocaine-treated WT and RGS14-KO groups (Fig. 18D). We observed a trend for a positive correlation in the WT group ($r(6) = .69$, $p = .059$) but no relationship in the RGS14-KO group ($r(6) = .32$, $p = .439$), suggesting that RGS14 regulates cocaine-CPP and cocaine-conditioned locomotor activation through dissociable mechanisms. This interpretation is further supported by the distinct temporal profiles of cocaine-CPP and cocaine-conditioned locomotor hyperactivity in the RGS14-KO group when compared across post-tests: CPP persists for at least 3 weeks, while hyperactivity decays more rapidly.

4.9 Cocaine conditioning overcomes stronger inherent place aversion in RGS14-KO mice

While reward is typically associated with inducing positive emotional states, relief from negative emotional states is also rewarding in and of itself; certain anxiolytic drugs like benzodiazepines and the type-1 cannabinoid receptor agonist arachidonylcyclopropylamide support a CPP in rodents (Tokutake et al., 2022; Wilks & File, 2008). The compartments of the CPP chambers used in this study were designed to be emotionally neutral, but one side features a semi-reflective white floor that somewhat augments ambient illumination, potentially making the compartment mildly aversive to rodents (Bourin & Hascoët, 2003). Indeed, nearly all subjects

preferred the black-floored compartment at baseline. Based on prior studies showing that RGS14-KO mice are prone to anxiety-like behaviors and may have heightened aversion sensitivity (Alexander et al., 2019; Foster et al., 2021; Lee et al., 2010), we predicted that RGS14-KO would enhance baseline aversion to the white-floored compartment in experimental mice. Analysis by Welch's t-test revealed that RGS14-KO mice spend significantly less time in the white-floored compartment during pre-test than WT controls (Fig. 18E, $t(28.82) = -3.79$, $p < .001$), supporting the notion that RGS14 loss increases sensitivity to aversive stimuli and augments avoidance behavior. Furthermore, time spent in the white-floored compartment post-cocaine pairing was at least as high in the RGS14-KO group as WT (Fig. 18F; $t(9.28) = 1.33$, $p = .214$), indicating that enhanced cocaine-CPP in RGS14-KO mice may be driven, at least in part, by overcoming stronger inherent place aversion.

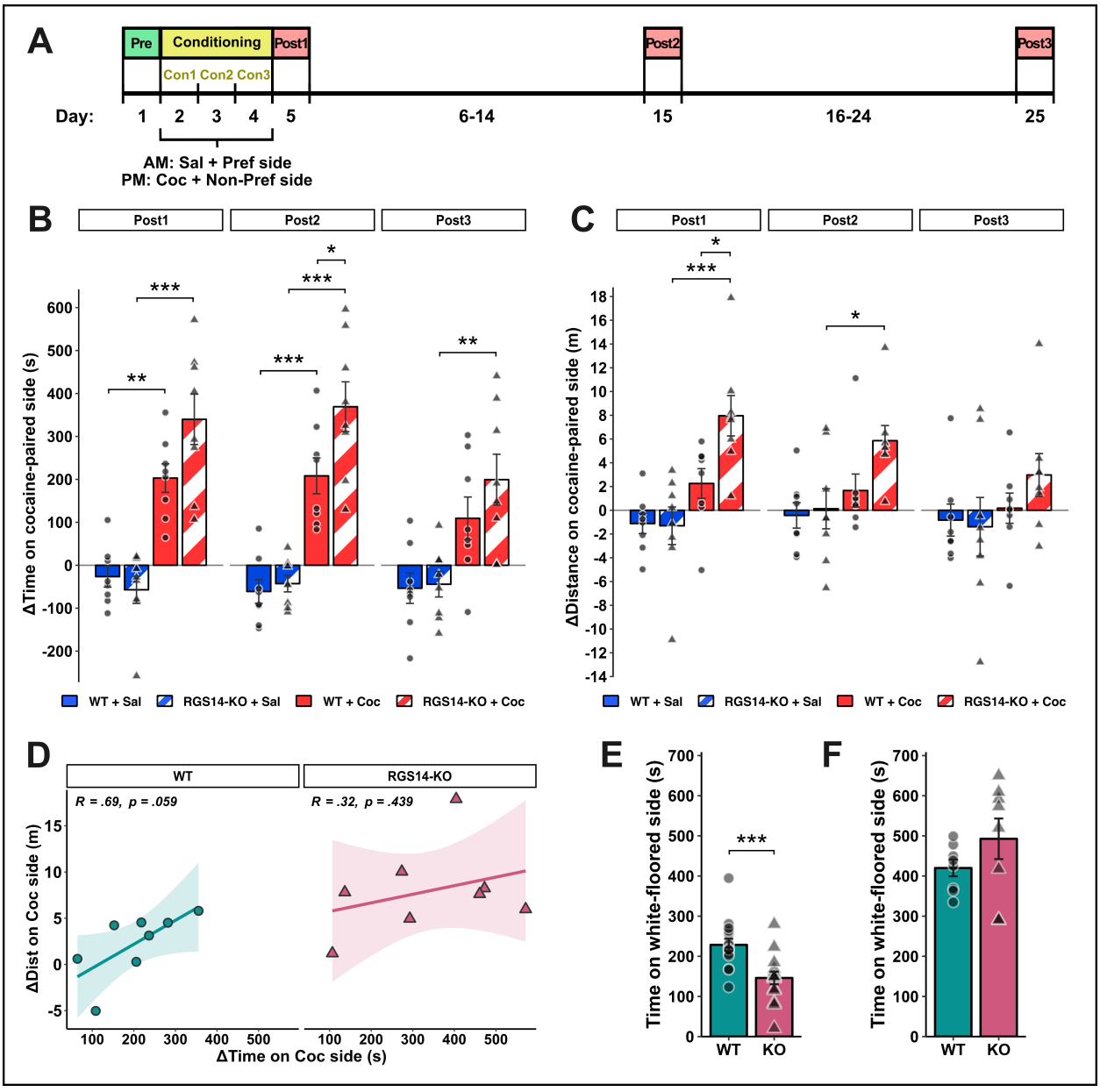


Figure 18. RGS14 loss enhances cocaine-conditioned place preference and locomotor hyperactivity. A. Diagram of cocaine-conditioned place preference (CPP) protocol (n = 32); cocaine (5 mg/kg) or saline administered by i.p. injection. **B.** *Increased magnitude and duration of cocaine-conditioned place preference in RGS14-KO mice.* Time spent on the cocaine-paired side (i.e. preference, Δpre-test) was significantly enhanced in WT and RGS14-KO groups at Post1 and Post2, an effect that is significant only in RGS14-KO mice at Post3. Preference was significantly enhanced in RGS14-KO mice over WT controls at Post2 (Tukey HSD test^). **C.** *Increased magnitude and duration of cocaine-conditioned locomotor hyperactivity in RGS14-KO mice.* Distance traveled on the cocaine-paired side (Δpre-test) was significantly enhanced exclusively in RGS14-KO mice at Post1 and Post2. ΔDistance was significantly

enhanced in RGS14-KO mice over WT controls at Post1 (Tukey HSD test^). **D.** Correlation plots of cocaine-conditioned place preference (Δtime) and locomotor hyperactivation (Δdistance) at Post1 (shaded area: 95% confidence interval). There is a trend for a positive correlation in WT mice that is absent in RGS14-KO mice (Pearson's test). **E.** RGS14-KO mice spend significantly less total time in the aversive white-floored compartment during pre-test (n = 32, Welch Two Sample t-test). **F.** *Association with cocaine overcomes stronger inherent place aversion in RGS14-KO mice.* No significant difference between WT and RGS14-KO groups in total time in the white-floored compartment once paired with cocaine (Post1, n = 16, Welch Two Sample t-test). All error bars represent mean ± SEM. Symbols: †p < .10, *p < .05, **p < .01, ***p < .001. Carat (^) indicates Bonferroni correction.

Table 6. Conditioned place preference statistics. Carat (^) indicates Bonferroni correction.

Fig	Statistical test	Day(s)	Outcome measure	Factors (ANOVA)	Effect or Groups	df	Statistic	Value	Pval	Sig
5B	Three-way ANOVA		Time on Coc side (ΔPre-Test)	Geno, Trtmt, Stage	Geno	1, 28	F	2.99	.095	†
					Trtmt	1, 28	F	59.24	< .001	***
					Stage	1.54, 43.24	F	11.10	< .001	***
					Geno × Trtmt	1, 28	F	3.08	.090	†
					Geno × Stage	1.54, 43.24	F	1.00	.358	
					Trtmt × Stage	1.54, 43.24	F	10.78	< .001	***
					Geno × Trtmt × Stage	1.54, 43.24	F	1.02	.353	
	Two-way ANOVA	Post1	Time on Coc side (ΔPre-Test)	Geno, Trtmt	Geno	1, 28	F	1.84	.186	
					Trtmt	1, 28	F	63.88	< .001	***
					Geno × Trtmt	1, 28	F	4.57	.041	*
		Post2		Geno, Trtmt	Geno	1, 28	F	5.16	.031	*
					Trtmt	1, 28	F	74.40	< .001	***
					Geno × Trtmt	1, 28	F	3.26	.082	†
		Post3		Geno, Trtmt	Geno	1, 28	F	1.22	.278	
					Trtmt	1, 28	F	20.45	< .001	***
					Geno × Trtmt	1, 28	F	0.81	.377	
	Tukey HSD test^	Post1	Time on Coc side (ΔPre-Test)		KO+Sal vs. WT+Sal	28	t	-0.55	.945	
					WT+Coc vs. WT+Sal	28	t	4.14	.002	**
					KO+Coc vs. KO+Sal	28	t	7.16	< .001	***
					KO+Coc vs. WT+Coc	28	t	2.47	.087	†
		Post2			KO+Sal vs. WT+Sal	28	t	0.33	.988	
					WT+Coc vs. WT+Sal	28	t	4.82	< .001	***
					KO+Coc vs. KO+Sal	28	t	7.38	< .001	***
					KO+Coc vs. WT+Coc	28	t	2.88	.036	*
		Post3			KO+Sal vs. WT+Sal	28	t	0.15	.999	
					WT+Coc vs. WT+Sal	28	t	2.56	.072	†
					KO+Coc vs. KO+Sal	28	t	3.83	.004	**
					KO+Coc vs. WT+Coc	28	t	1.42	.499	
5C	Three-way ANOVA		Dist on Coc side (ΔPre-Test) (ranked)	Geno, Trtmt, Stage	Geno	1, 28	F	2.89	.100	
					Trtmt	1, 28	F	13.11	.001	**
					Stage	1.67, 46.86	F	0.00	> .999	
					Geno × Trtmt	1, 28	F	1.64	.211	
					Geno × Stage	1.67, 46.86	F	0.89	.402	
					Trtmt × Stage	1.67, 46.86	F	3.17	.060	†
					Geno × Trtmt × Stage	1.67, 46.86	F	0.45	.604	
	Two-way ANOVA	Post1	Dist on Coc side (ΔPre-Test) (ranked)	Geno, Trtmt	Geno	1, 28	F	5.05	.033	*
					Trtmt	1, 28	F	29.45	< .001	***
					Geno × Trtmt	1, 28	F	3.08	.090	†
		Post2		Geno, Trtmt	Geno	1, 28	F	3.04	.092	†
					Trtmt	1, 28	F	6.96	.013	*
					Geno × Trtmt	1, 28	F	1.52	.227	
		Post3		Geno, Trtmt	Geno	1, 28	F	0.55	.464	
					Trtmt	1, 28	F	4.46	.044	*
					Geno × Trtmt	1, 28	F	0.34	.562	
	Tukey HSD test^	Post1	Dist on Coc side (ΔPre-Test) (ranked)		KO+Sal vs. WT+Sal	28	t	0.35	.985	
					WT+Coc vs. WT+Sal	28	t	2.60	.067	†
					KO+Coc vs. KO+Sal	28	t	5.08	< .001	***
					KO+Coc vs. WT+Coc	28	t	2.83	.040	*
		Post2			KO+Sal vs. WT+Sal	28	t	0.36	.984	
					WT+Coc vs. WT+Sal	28	t	0.99	.755	
					KO+Coc vs. KO+Sal	28	t	2.74	.049	*
					KO+Coc vs. WT+Coc	28	t	2.11	.176	
		Post3			KO+Sal vs. WT+Sal	28	t	0.11	> .999	
					WT+Coc vs. WT+Sal	28	t	1.08	.706	
					KO+Coc vs. KO+Sal	28	t	1.91	.248	
					KO+Coc vs. WT+Coc	28	t	0.94	.784	
N/A	Three-way ANOVA		Total dist (ΔPre-Test) (ranked)	Geno, Trtmt, Stage	Geno	1, 28	F	1.94	.175	
					Trtmt	1, 28	F	0.09	.762	
					Stage	1.73, 48.53	F	0.00	> .999	
					Geno × Trtmt	1, 28	F	0.47	.497	
					Geno × Stage	1.73, 48.53	F	5.33	.011	*
					Trtmt × Stage	1.73, 48.53	F	5.54	.009	**
					Geno × Trtmt × Stage	1.73, 48.53	F	0.87	.411	
	Two-way ANOVA	Post1	Total dist (ΔPre-Test) (ranked)	Geno, Trtmt	Geno	1, 28	F	4.70	.039	*
					Trtmt	1, 28	F	2.09	.159	
					Geno × Trtmt	1, 28	F	0.41	.526	
		Post2		Geno, Trtmt	Geno	1, 28	F	4.38	.046	*
					Trtmt	1, 28	F	2.83	.104	
					Geno × Trtmt	1, 28	F	1.51	.229	
		Post3		Geno, Trtmt	Geno	1, 28	F	0.26	.617	
					Trtmt	1, 28	F	0.29	.592	
					Geno × Trtmt	1, 28	F	0.00	.971	
	Tukey HSD test^	Post1	Total dist (ΔPre-Test) (ranked)		KO+Sal vs. WT+Sal	28	t	1.08	.705	
					WT+Coc vs. WT+Sal	28	t	0.57	.941	
					KO+Coc vs. KO+Sal	28	t	1.48	.464	
					KO+Coc vs. WT+Coc	28	t	1.99	.217	
		Post2			KO+Sal vs. WT+Sal	28	t	0.61	.928	
					WT+Coc vs. WT+Sal	28	t	-2.06	.191	
					KO+Coc vs. KO+Sal	28	t	-0.32	.989	
					KO+Coc vs. WT+Coc	28	t	2.35	.111	
		Post3			KO+Sal vs. WT+Sal	28	t	-0.33	.987	
					WT+Coc vs. WT+Sal	28	t	-0.36	.984	
					KO+Coc vs. KO+Sal	28	t	-0.41	.976	
					KO+Coc vs. WT+Coc	28	t	-0.38	.980	
5D	Pearson's correlation	Post1	ΔTime vs. ΔDist correlation		WT	6	t	2.32	.059	†
							R	0.69		
					KO	6	t	0.83	.439	
							R	0.32		
5E	Welch Two Sample t-test	Pre-Test	Time on white-floored side		KO vs. WT	28.82	t	-3.79	< .001	***
5F	Welch Two Sample t-test	Post1	Time on white-floored side	(Coc group)	KO vs. WT	9.28	t	1.33	.214	

4.10 RGS14 and pERK colocalize in distinct neurons in the nucleus accumbens and extended amygdala following cocaine

Dynamic ERK regulation is a major mechanistic underpinning of the neuroplastic changes underlying learning and memory in brain regions like the hippocampus and striatum. Certain extracellular signals of excitation and/or growth launch intracellular signaling cascades that lead to activating phosphorylation of ERK (pERK) and synaptic strengthening. Timing matters: transient ERK activation (< 1 hour) drives early-phase LTP-related adaptations in dendrites and spines, while sustained elevated ERK activity triggers late-phase LTP via ERK nuclear translocation and induction of LTP-stabilizing genes (Lidke et al., 2010; Liu et al., 2023; Ying et al., 2002; Zhu et al., 2002). As discussed earlier, RGS14 is known to suppress ERK signaling in the hippocampus by sequestering upstream effectors and may also affect ERK subcellular localization.

RGS14 suppression of the ERK pathway underlies its modulation of hippocampal-based LTP (Lee et al., 2010) and likely LTD as well (Samadi et al., 2023). It has been reported that addictive drugs, and only addictive drugs, share a signature profile of strong ERK activation in the NAc, CeA, and dorsolateral BNST, all regions exhibiting patches of exceptionally dense RGS14 immunoreactivity. We previously identified that RGS14 loss increases activated ERK immunoreactivity in the hippocampus and CeA following acute cocaine treatment (Foster et al., 2021). Additionally, inhibition of ERK signaling suppresses locomotor sensitization to cocaine (Pierce et al., 1999; Valjent et al., 2005) a behavioral change found herein to be enhanced by RGS14 loss. We assessed double-immunolabeled tissue sections from WT mice collected 2 hours after cocaine challenge using confocal microscopy and found distinct patterns of overlapping RGS14 and pERK1/2 immunoreactivity in the NAc, BNST, and CeA. Collections of notable

microscopy images for each region are shown in Figures 19-21, and observations are discussed in the following text.

4.10.1 RGS14 and pERK colocalize in patches in nucleus accumbens core and shell

Figure 19 details RGS14 and pERK1/2 immunoreactivity and colocalization in the NAc 2 hours post-cocaine challenge. The major anatomical subdivisions of the NAc are the core and shell (Fig. 19A), which respectively process learning Pavlovian stimulus-outcome associations and the emotional components of motivated behavior (Cacciapaglia et al., 2012; Saddoris & Carelli, 2014; Shiflett & Balleine, 2010). In Figure 19B, patchy RGS14 and pERK overlap is observed throughout the striatum, with the densest patches of colocalization seen in ventromedial NAc core and, to a lesser extent ventromedial shell.

In Figure 19C, we can see that RGS14 immunoreactivity appears to be thick at the border with the corpus callosum (yellow dashed circle) and appears to some extent to radiate outward from the anterior commissure. It may be the case that the patchy pattern of RGS14 protein in NAc core relates to the intersection of the output fields from these two major fiber tracts. Except near the corpus callosum, RGS14 and pERK immunoreactivity are mutually exclusive in this sample, likely because RGS14 fully suppresses cocaine-induced ERK activation in several neuronal populations shown here. In contrast, the tissue in Figure 19D shows patchy colocalization of RGS14 and pERK in ventromedial NAc core and shell. Of note, we see an almost linear trail of dense colocalization stretching between the ventromedial border of the anterior commissure and a diffuse patch of colocalization in ventrolateral core. We decided to focus in on the colocalization "trail" and its borders to learn more.

When viewing the dorsomedial portion of the colocalization "trail", nearest to the anterior commissure, at 40x magnification (Fig. 19E), we see abundant RGS14 signal in cell bodies and

neuropil elements. Immunoreactivity for pERK is also seen in cell bodies and neuropil, though the number of pERK-containing cell bodies appears fewer than those containing RGS14. Cell body colocalization is semi-obscured by noisy neuropil signal, but cell bodies appear to be mostly either RGS14- or pERK-exclusive throughout this subregion aside from a few cell bodies located on the outskirts that show definitive colocalization (Fig. 19E, yellow arrows), and colocalization is mostly localized to neuropil. Analysis of the ventrolateral "trail" portion (Fig. 19F) shows multiple co-labeled cell bodies (yellow arrows), with strong colocalization seen in neuropil elements running dorsomedially from them along the "trail" and light neuropil colocalization seen in a diffuse pattern laterally. Where not obscured by neuropil noise, it can be observed in co-labeled cell bodies that pERK signal is localized to both soma and nuclei while RGS14 signal is found perinuclearly, a localization pattern that continues through all regions examined.

We can glean a few interesting things from this data. For one, RGS14 appears to modulate the interactions between NAc core neurons and neurons connected to NAc core via projections traveling along the anterior commissure and/or corpus callosum. While speculative, controlling RGS14 at the interface between the output fields of the two major fiber tracts could be an innate mechanism for regulating NAc core-based associative learning. Additionally, the fact that pERK signal appears still slightly elevated specifically where it most densely colocalizes with RGS14 (Fig. 19D, yellow boxes) suggests incomplete suppression of cocaine-induced ERK activation by RGS14, which supports a role for RGS14 as a natural but surmountable barrier to NAc plasticity.

4.10.2 RGS14 and pERK colocalize in dorsal BNSTov and BNSTju

Like the CeA, the BNST is a major extended amygdala structure involved in motivated behavior. While both regions process fearful stimuli, evidence suggests that the CeA mediates the high-intensity, phasic emotional state of fear while the BNST mediates the low-intensity, sustained

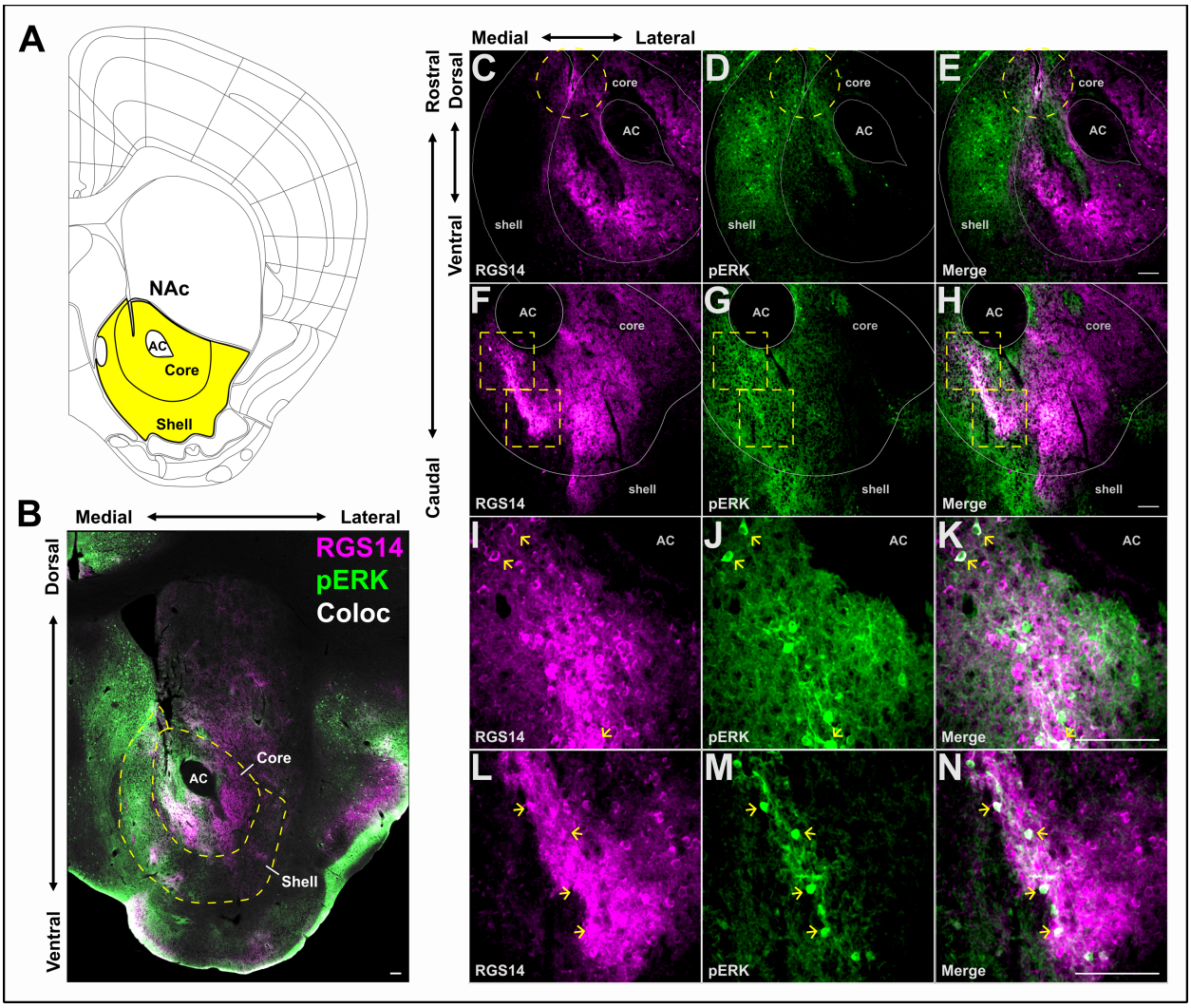


Figure 19. RGS14 colocalizes with pERK in ventromedial NAc following cocaine. Immunofluorescence detection of RGS14 with pERK1/2 in NAc 2 hours after cocaine. **A.** Anatomical annotations from the Allen Mouse Brain Reference Atlas (atlas.brain-map.org) highlighting the location of NAc. **B.** Composite tile-scan image of RGS14 and pERK1/2 immunoreactivity in striatum and surrounding tissue. **C-N.** Magnified images of RGS14 (**C,F,I,L**; magenta) and pERK1/2 (**D,G,J,M**; green) immunoreactivity, and overlap (**E,H,K,N**; white). Magnifications: **C-H**: 10x, **I-N**: 40x. **I-N** are magnifications of regions outlined in yellow dashed boxes in **F-H**. (dorsal box: **I-K**; ventral box: **L-N**). Yellow arrows in **I-N** indicate cells with signal overlap in soma. Scale bar = 100 µm. Abbreviations: **AC**: anterior commissure, **NAc**: nucleus accumbens.

emotional state of anxiety. RGS14 is intensely and exclusively expressed in the BNSTov and BNSTju, both in which altered synaptic plasticity has been observed during withdrawal from addictive drugs (Francesconi, Berton, Repunte-Canonigo, et al., 2009; Krawczyk et al., 2014). Additionally, the BNSTov is critically important to stress reactivity and modulation of stress responses, including stress responses tied to drug withdrawal. Figure 20 showcases RGS14 and pERK co-immunoreactivity following cocaine in BNST. The BNSTov and BNSTju are distinct subsections of dorsolateral BNST (Fig. 20A). Figure 20B reaffirms strong RGS14 expression in BNSTov and BNSTju and shows intense overlap with cocaine-induced pERK in dorsal BNSTov.

In 40x magnification shown Figure 20C, we see strong RGS14 immunoreactivity in the soma of more ventrolaterally-positioned cells and in lateral neuropil, and lighter but still substantial signal in dorsomedial neuropil. pERK immunoreactivity is dispersed throughout the region in both cell bodies and neuropil, with the most intense and widespread signal seen dorsally, including a particularly dense cluster in the dorsomedial portion. A large pERK-immunoreactive neuron with divergent branched processes extending dorsomedially and dorsolaterally from a ventrally localized cell body is conspicuously seen. Comparison of its morphology with other BNST neurons suggests it is a medium spiny projection neuron pictured with a branching dendritic process. Its bifurcating process appears to innervate separate, but possibly overlapping neuron populations. Merging the channels shows definitive colocalization in select cell bodies near the lateral BNSTov border and in the neuropil running along the dorsolateral border, and light colocalization in more ventral neuropil. Conversely, more ventrally-located cell bodies are largely exclusive for RGS14 or pERK signal, including the large presumed projection neuron that is exclusively pERK-immunoreactive. Notably, the divergent cell populations innervated by the bifurcated projections from this neuron appear to also differ in RGS14 immunoreactivity; projections from the

dorsolaterally-extending branch likely innervate more RGS14-containing cells than the dorsomedial branch. This suggests that RGS14 is used to selectively modify integrated signals in BNSTov, and likely other regions as well based on its broad expression profile in regions that process associative learning. Furthermore, colocalization within and near the fiber tract running dorsolaterally along the BNST border suggests that RGS14 intercepts signals traveling via the stria terminalis that are incoming to and/or outgoing from dorsal BNSTov, which includes communications with several important limbic regions. Altogether, this suggests that RGS14 selectively modifies integrated signals that are incoming and/or outgoing via the stria terminalis to the dorsal BNSTov, which includes communications with several important limbic regions.

In Figure 20D, RGS14 and pERK immunoreactivity are seen scattered throughout dorsal BNSTov, in cell bodies and neuropil. Colocalization is similarly scattered, and there is a somewhat even mix of RGS14-exclusive, pERK-exclusive, and colocalized immunoreactivity in dorsal BNST, which becomes RGS14-dominant in more ventral portions. The data show us a few notable things. For one, there are pERK-immunoreactive pyramidal-shaped neurons (solid yellow arrow) in BNSTov that, unlike the ones observed in CeL in the next section, do not colocalize with RGS14 after cocaine. While anecdotal, we did not see evidence of RGS14 expression in pyramidal cells in any of the BNST tissue assessed. Morphologically, all RGS14-containing cell bodies in BNST appeared have round-shaped soma, suggesting either interneurons or medium spiny neurons. Other notable cells are those with strong RGS14 but weak pERK immunoreactivity (dashed yellow arrows), which may indicate that RGS14 is suppressing ERK activation incompletely.

Data shown in Figures 20E&F show that signal for both RGS14 and pERK is intense after cocaine in BNSTju and, unsurprisingly, overlap is extensive. We see abundant RGS14-exclusive and colocalized signal in cell bodies and neuropil in this region but almost no pERK-exclusive

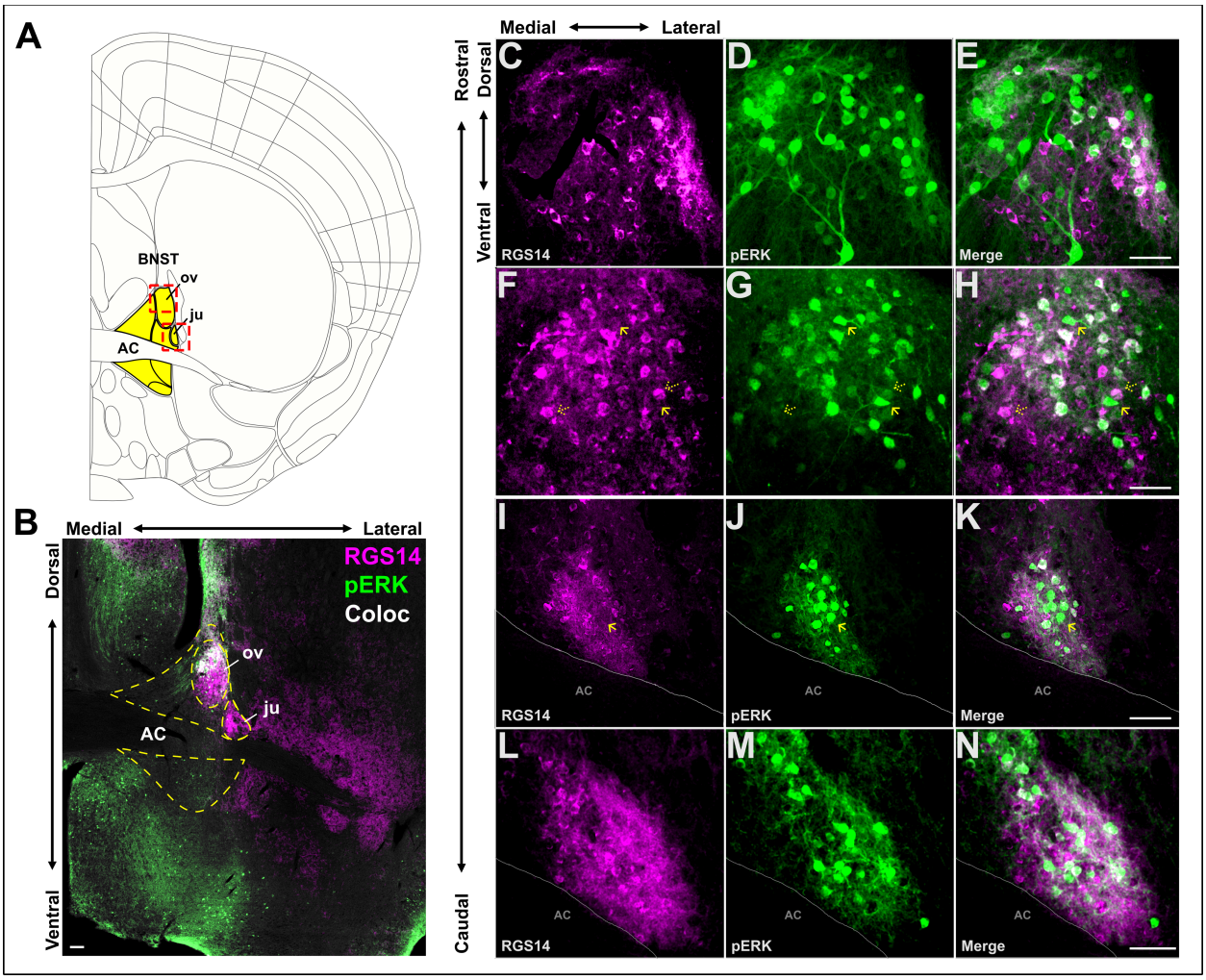


Figure 20. RGS14 colocalizes with pERK in dorsal BNSTov and BNSTju following cocaine. Immunofluorescence detection of RGS14 with pERK1/2 in BNST 2 hours after cocaine. **A.** Anatomical annotations from the Allen Mouse Brain Reference Atlas (atlas.brain-map.org) highlighting the location of BNST. Red dashed boxes indicate approximate tissue locations of images in **C-N** (dorsal box: **C-H**; ventral box: **I-N**). **B.** Composite tile-scan image of RGS14 and pERK1/2 immunoreactivity in BNST and surrounding tissue; approximate borders of BNST whole and ov and ju subnuclei outlined in yellow dashes. **C.** Magnified images (40x) of RGS14 (**C,F,I,L**; magenta) and pERK1/2 (**D,G,J,M**; green) immunoreactivity, and overlap (**E,H,K,N**; white) in BNSTov (**C-H**) & BNSTju (**I-N**). Scale bar = 100 µm. Abbreviations: **AC**: anterior commissure, **BNST(ju,ov)**: bed nucleus of the stria terminalis- (juxtacapsular, oval).

immunoreactivity, with the exception of a pocket of pERK-exclusive nuclei seemingly nestled into the center of rostral BNSTju (Fig. 20E, yellow arrow). The BNSTju is an under-studied region, and uncovering the role of RGS14 in it will require further research. This is a promising future direction, as strong baseline RGS14 expression in this region hints that it is likely to be biologically meaningful.

4.10.3 RGS14 and pERK colocalize in the lateral-capsular central amygdala

The CeA is the major output nucleus of the amygdala, known for its roles in modifying incentive salience and initiating physiological and defensive responses to stress. Plasticity in the CeA is well-documented to be critical for fear learning. Evidence suggests that dysregulation of functions controlled by the CeA and BNST, the other major extended amygdala nucleus, underlie the aversive motivational components of addictive drug withdrawal (Koob & Le Moal, 2008; Koob & Volkow, 2016). Studies show that ERK signaling specifically is involved, as stimulation of CeA ERK activation increases cocaine seeking during withdrawal (Lu et al., 2005). We examined overlap of RGS14 with cocaine-induced ERK activation in in CeA (Fig. 21). The CeA is anatomically divided into the medial (CeM), lateral (CeL), and capsular (CeC) subnuclei (Fig. 21A). The flow of information through the CeA follows a general structure in which projections from the BLA communicating emotional valence are received in CeL, which projects to CeM either directly or through CeC for subsequent extra-amygdalar output. This information flow structure explains why especially CeL and CeC are rich with GABAergic interneurons, which permit the fine-tuning of signals exiting the amygdala. Figure 21B shows intense and specific RGS14 and pERK signal overlap in lateral-most CeA, which encompasses components of both CeL and CeC.

To view more detailed characteristics of the cell types affected by RGS14 regulation of post-cocaine ERK activity, we imaged the CeA centered on CeL at 20x magnification (Fig. 21C&D). The most intense RGS14 immunoreactivity is seen encompassing the border between CeL and CeC, where the bulk of pERK immunoreactivity is also found. Merging the two channels shows abundant colocalization in cell bodies and neuropil in the CeL/C border region. When examining protein exclusivity, we find that RGS14 signal extends medially past ERK signal, and that signal in CeC neuropil just outside the CeL/C border region is largely pERK-dominant. Regarding the specific cell types featuring RGS14 and pERK overlap, in Figure 21C we see colocalization perinuclearly in cells with fusiform or rounded fusiform soma (solid yellow arrow), probably indicative of local interneurons, and at the apical point in cells with pyramidal-like soma (dashed yellow arrow), suggestive of projection neurons.

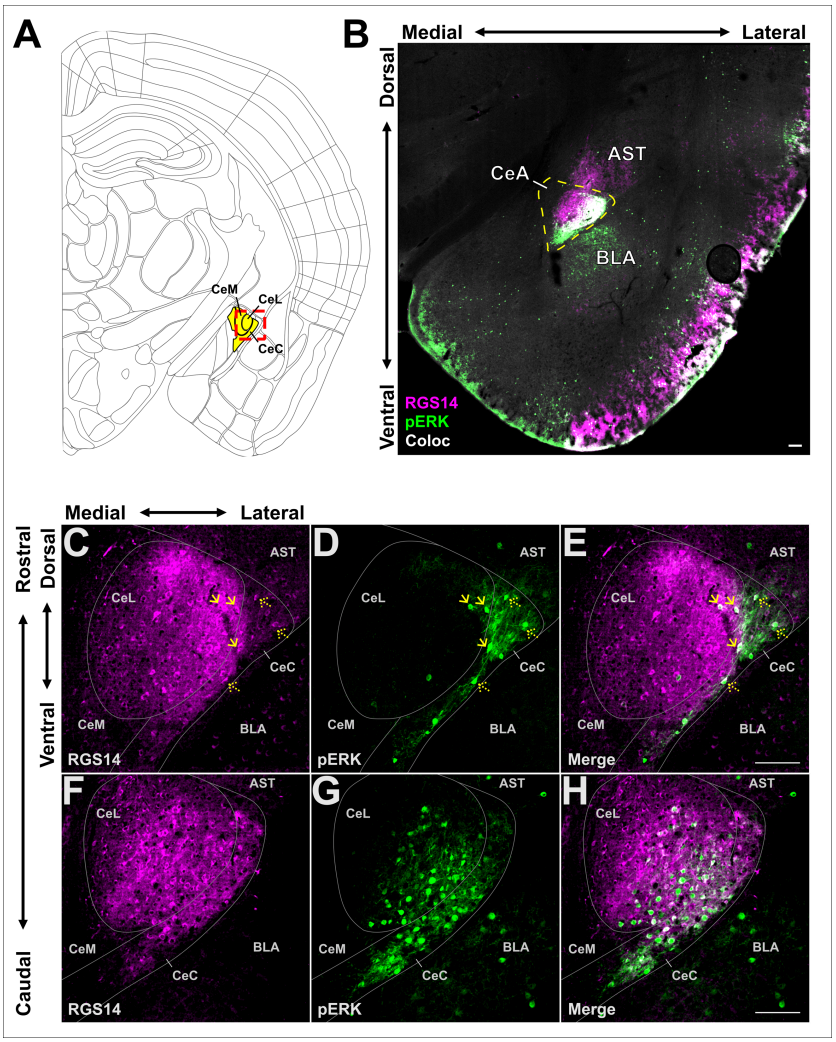


Figure 21. RGS14 colocalizes with pERK in lateral-capsular central amygdala following cocaine. Immunofluorescence detection of RGS14 with pERK1/2 in amygdala 2 hours after Coc challenge (i.p.) in Coc-experienced WT mice. **A.** Anatomical annotations from the Allen Mouse Brain Reference Atlas (atlas.brain-map.org) highlighting the location of CeA. Red dashed box indicates approximate tissue location of images in **C-H**. **B.** Composite tile-scan image of RGS14 and pERK1/2 immunoreactivity in amygdala and surrounding tissue. **C-H.** Magnified images (20x) of RGS14 (**C,F,I,L**; magenta) and pERK1/2 (**D,G,J,M**; green) immunoreactivity, and overlap (**E,H,K,N**; white). Scale bar = 100 µm. Abbreviations: **AST**: amygdalostriatal transition area, **BLA:** basolateral amygdala, **CeA**: central amygdala, **Ce(C,L,M)**: central amygdala- (capsular, lateral, medial).

4.11 DISCUSSION

In the present studies, we used behavioral assays and immunohistochemical analyses of genetically modified RGS14-null mice to investigate the role of RGS14 in cocaine-induced behavioral plasticity in emotional-motivational circuits. We observed strong RGS14 immunoreactivity in distinct, subregion-specific patterns in the NAc, dorsolateral BNST, and CeA. We revealed RGS14 immunoreactivity in D1R- and D2R-containing cells in the NAc, where we also found upregulated RGS14 two hours after cocaine challenge in WT mice with a history of chronic cocaine. Lastly, we found that loss of RGS14 augments the magnitude and duration of several behavioral indicators of cocaine-induced psychomotor sensitization and reward learning, including locomotor sensitization, CPP, and conditioned locomotor activation. Together, these findings suggest that RGS14 is a natural and possibly inducible suppressor of cocaine-induced potentiation in emotional-motivational circuits.

4.11.1 RGS14 actions in the nucleus accumbens and regulation of locomotor activity

In the previous chapter, we demonstrated RGS14 expression in postsynaptic striatal neurons using the LR reporter mouse line (Fig. 14C,F). Here, we found overlap of RGS14 immunoreactivity with D1R- and D2R-expressing neurons in the striatum (Fig. 15), strongly suggesting that RGS14 is present in both direct and indirect pathway MSNs. Striatal MSNs project through the basal ganglia to drive motor behavior (Alexander et al., 1986). Cocaine elicits motor hyperactivity by simultaneously stimulating motor-activating D1-MSNs via D1R-Gs/olf and inhibiting motor-inhibiting D2-MSNs via D2R-Gi/o (Kravitz et al., 2010). RGS14-KO mice show increased sensitivity to acute cocaine-induced locomotor activation at a high dose of cocaine (20 mg/kg) (Foster et al., 2021), presumably because RGS14 acts as a GAP in D2-MSNs to terminate D2R-Gi/o signaling and relieve cocaine-induced suppression of immobility pathways. Unlike in

D2-MSNs, it is unlikely that RGS14 modulates cocaine-induced dopamine signaling directly in D1-MSNs due to GAP incompatibility with D1R-Gs/olf. RGS14 is, however, capable of modifying cocaine-induced plasticity in D1-MSNs via binding active H-Ras and/or Ca2+/calmodulin to suppress ERK and/or Ca2+ pathway signaling (Evans et al., 2018a; Evans et al., 2018b; Lee et al., 2010; Shu et al., 2010; Vellano et al., 2013). We identified perinuclear overlap of RGS14 and pERK1/2 in the NAc 2 hours after cocaine (Fig. 19K,N), a sustained ERK signaling time point associated with enhanced ERK nuclear translocation (Lidke et al., 2010). The locomotor response to the low dose of cocaine used in this study (5 mg/kg) does not significantly differ between drug-naive WT and RGS14-KO mice, but becomes elevated in the RGS14-KO group following repeated cocaine exposure (Fig. 17G), suggesting enhanced NAc-based cocaine-induced plasticity RGS14-KO mice.

The effects of RGS14 loss on the temporal dynamics of the locomotor response to cocaine may be indicative of the mechanisms at play. The challenge time course data indicate that RGS14-KO mice exhibit a longer duration of cocaine-induced locomotor activation independent of drug history, and that chronic cocaine treatment only sensitizes the initial response magnitude in RGS14-KO mice (Fig. 17J-L). These results suggest dissociable mechanisms for RGS14 regulation of the magnitude and duration of cocaine-induced locomotor activation, in which response duration is primarily susceptible to RGS14 governance of acute neuronal excitability and response magnitude is more vulnerable to RGS14 regulation of neuroplasticity. A framework of differential actions of RGS14 in NAc D1- and D2-MSNs is consistent with the observed phenomenon. RGS14 GAP activity negatively modulates GPCR-Gi/o signaling by speeding up termination of signaling rather than affecting any aspect of signaling activation, therefore it is logical that RGS14 loss would not impact total cocaine-induced activation of D2R-Gi/o signaling

in D2-MSNs, but rather it would extend the duration of signaling events. On the other hand, cocaine-induced plasticity in the NAc is specific to D1-MSNs, and it has been shown that D1-MSNs in the RGS14-enriched NAc core communicate the magnitude of stimulus intensity (Lobo & Nestler, 2011; Zachry et al., 2024). RGS14 presumably has little impact on acute cocaine-induced excitability in D1-MSNs at the non-anxiogenic dose of cocaine used in the studies herein, but it is readily equipped to suppress ERK and Ca^{2+} signaling critical to NAc D1-MSN plasticity and behavioral sensitization to cocaine (Ceglia et al., 2017; Gore & Zweifel, 2013; Lafragette et al., 2017; Robison et al., 2013).

4.11.2 RGS14 actions in the extended amygdala and regulation of emotional drive

We also observed dense RGS14 immunoreactivity in discrete subnuclei of the extended amygdala, namely the oval and juxtacapsular nuclei of the BNST (Fig. 11B), and CeL (Fig. 11E). The extended amygdala connects extensively with brainstem nuclei and the basal ganglia to coordinate physiological and behavioral responses to stress, including evoking the emotional states of fear and anxiety (Etkin & Wager, 2007; Nader et al., 2001). Interestingly, the CeL and BNST oval nucleus specifically contain the largest populations of extrahypothalamic neurons that produce the stress neuropeptide corticotropin-releasing factor (CRF) in the rodent brain (Cassell et al., 1986; Hammack et al., 2021). Neuropeptides such as CRF can induce significant changes in brain and behavior due to their capacities for prolonged and wide-reaching signaling events (Mantsch, 2022). Evidence shows that dysregulation of CRF and other stress systems by chronic and early life stress underlies vulnerability to anxiety and depressive-like symptoms in adulthood (Lee et al., 2005; Tyrka et al., 2009).

We found that drug-naïve RGS14-KO mice were significantly more avoidant of the mildly aversive white-floored CPP compartment (Fig. 18E), suggesting that RGS14 suppresses anxiety-

like responses to stressful stimuli. Given that RGS14 inhibits the response to an acute and inherent stressor, RGS14 is likely modifying transient neuronal excitability by negatively modulating receptor-Gi/o signaling. A likely candidate for RGS14 GAP modulation under conditions of stress is CRF type I receptor (CRFR1), which couples with Gi/o when ambient CRF levels are high (Berger et al., 2006; Beyermann et al., 2007). CRFR1 is widely expressed in the brain, including high local expression in CRF-releasing extended amygdala subnuclei (Hunt et al., 2018; Weera et al., 2021; Zhang et al., 2024). In fact, CRFR1 overactivation in the BNST oval nucleus during stress was found to mediate female-specific effects of anxiety-like and avoidance behaviors (Zhang et al., 2024), underscoring the importance of proper CRFR1 regulation in evoking appropriate emotionally-driven responses under stress (Koob, 2010) particularly in females. For this reason and for other reasons discussed below, conditions impairing RGS14 function could be a greater risk factor for developing anxiety disorders in women than men.

Interestingly, we found that association of the white-floored compartment with cocaine reward during conditioning fully abolished stronger avoidance of that compartment by the RGS14-KO group (Fig. 18F). While the exact cell populations and mechanisms driving this shift are unclear, this result has broader implications regarding RGS14 dysfunction creating conditions that precipitate specific vulnerabilities to psychostimulant addiction. Our data shows that RGS14 loss exacerbates inherent avoidant and anxiety-like responses to an aversive context, but also facilitates reversing those responses by permitting stronger association of context with cocaine reward. If these results translate to humans, it suggests that RGS14 dysfunction could underlie a vulnerability to developing psychostimulant addiction through attempted self-medication for anxiety disorders Additionally, increased aversion sensitivity and stress system dysregulation resulting from impaired RGS14 function could heighten vulnerability to the negative affective motivational

components of drug withdrawal that drive relapse (Koob & Le Moal, 2008; Koob & Volkow, 2016).

4.11.3 Dissociation of RGS14 actions on cocaine-induced limbic and motor system adaptations

Another illuminating finding from these data is that RGS14 regulates learning/memory in emotional- and motor-processing circuits in a dissociable manner. Both CPP and conditioned locomotor hyperactivation elicited by cocaine were enhanced by RGS14 loss (Fig. 18B-C), but were not correlated in RGS14-KO mice (Fig. 18D) and decayed on separate time scales. That is, CPP persisted for longer than conditioned locomotor hyperactivation. This suggests that RGS14 effectively inhibits the capacity of cocaine to rewire behavior by suppressing cocaine-induced associative learning based in limbic regions and basal ganglia separately, and that consequences of RGS14 loss on cocaine-induced plasticity in limbic regions controlling emotional associations are likely the most profound. We propose that RGS14 is working in separate populations of neurons to prevent hijacking of the emotional and motor components of goal-directed behavior by cocaine, and is especially critical for regulating emotional drive.

4.11.4 RGS14 in addiction and anxiety in women and girls

While this study did not expressly examine sex effects, the results suggest that RGS14 dysfunction may increase susceptibility to cocaine-induced plasticity in females, and to cocaine addiction in women and girls. The female RGS14-KO mice used in this study demonstrate exaggerated avoidance of the mildly aversive white-floored CPP compartment during pre-test, but pairing the compartment with cocaine reward reverses place preference. Anxiety disorders are more prevalent in women (Grenier et al., 2018), and it has been reported that women are more likely to consume drugs of abuse to self-medicate for anxiety (Becker et al., 2007; Usman et al.,

2019; Wu & Howard, 2007). Additionally, women are more likely to report stress and negative emotions prior to relapse (Hendianti & Uthis, 2018). RGS14 dysfunction may exacerbate female-specific hypersensitivity to negatively reinforcing stimuli, compounding vulnerability to self-medicating and relapse.

It is only possible to speculate based on the available data, but the observable results are consistent with variable impact of RGS14 loss on cocaine-induced plasticity across the estrous cycle. It has been shown that estrogen enhances locomotor sensitization to cocaine, and that sensitization that occurs during periods of high estrogen levels remains when estrogen levels subsequently drop (Hu & Becker, 2003). The effect of enhanced sensitization in female RGS14-KO mice is driven by a subset of hyper-responding subjects that amount to a third of the sample group. Assuming random distribution of estrous cycle stage among subjects, approximately the same number of subjects would have been in late diestrus or proestrus at the start of induction (Wall et al., 2023; Zhu et al., 2015), and would have had moderate-to-high levels of circulating estradiol when receiving cocaine for the first time. It may be the case that while neither RGS14 loss nor elevated estradiol alone sufficiently lower the threshold for inducing sensitization to 5 mg/kg cocaine, they are sufficient in combination to achieve this. It would benefit future studies to examine the impact of estrous cycle on female-specific behavioral effects observed in RGS14-KO mice, including effects on anxiety- and addiction-related behaviors. A useful future study could also explicitly test for sex differences in RGS14-KO mice using balanced cohorts of male and female subjects.

The present study points to several intriguing implications for RGS14 in addiction pathology in humans. As mentioned previously, RGS14 loss is associated with increased fearful and anxiety-like behavior, especially in females (Alexander et al., 2019; Foster et al., 2021; Lee et al., 2010).

This is further supported herein by exaggerated avoidance of an inherently aversive context by female RGS14-KO mice, though, importantly, we also show that associating this context with cocaine switches aversion to preference. Anxiety disorders and substance use disorders are highly comorbid, in part because substance use disorders often develop from attempted self-medication of anxiety disorders (Grant et al., 2004; Kessler et al., 2005; Vorspan et al., 2015). Absent or impaired RGS14 functionality could conceivably be a major risk factor for developing comorbid anxiety and substance use disorders, particularly in women (Wallis et al., 2022). The results presented herein suggests that RGS14 is predominantly a protective factor against psychostimulant addiction by suppressing maladaptive learning caused by drug-induced overactivation of plasticity mechanisms.

4.11.5 Caveats and limitations

Several of our studies here have limitations that open up opportunities for future exploration. For example, our findings of behavioral sensitization were used as a proxy for plasticity in emotional-motivational circuits. While behavioral sensitization is typically a reliable indicator of synaptic plasticity (Alcantara et al., 2010) and we have directly shown that RGS14 loss increases LTP in hippocampal area CA2 (Lee et al., 2010), synaptic strength itself could be measured in future studies to rule out other mechanisms at play. Locomotor sensitization is commonly used as a reliable measure of psychomotor sensitization though other psychomotor behaviors also sensitize as well (e.g. head movements, stereotypy) (Aliane et al., 2009; Gaval-Cruz et al., 2012; Ünal et al., 2009) and these could be explored to expand this story. Since these studies were performed with global RGS14 knock outs, other factors could be contributing to the behaviors such as altered basal ganglia function, or RGS14 actions in the periphery such as in the kidney and intestines (Harbin et al., 2021) altering cocaine metabolism, and/or possibly additional

mechanisms. Targeted knock-out of RGS14 in brain sub-regions would be informative. Based on preliminary studies, we focused our studies on female mice and did not test males for differences in sex effects. Thus, the female-specific conclusions we can draw from the data are limited without further studies. Future studies should assess the contribution of RGS14 to cocaine-taking behavior (e.g. self-administration) and include region- and cell type-specific manipulations to disentangle how RGS14 modulates motor and emotional circuits.

4.11.6 Conclusions

RGS14 opposes long-term potentiation in hippocampal area CA2 and suppresses hippocampal-based learning and memory. Our study shows that RGS14 is strongly expressed in discrete subnuclei of the NAc and extended amygdala, is found in D1R- and D2R-containing cells in the NAc and is upregulated in the NAc in WT mice with a history of chronic cocaine. Behaviorally, loss of RGS14 increases cocaine-induced locomotor sensitization, CPP, and conditioned locomotor hyperactivity. Together, these findings point to a role for RGS14 as a natural barrier to plasticity in emotional and motivational brain circuits, and as a potentially protective factor against harmful cocaine-induced neuroadaptations leading to addiction.

Chapter 5: Final discussion, conclusions, and future directions

5.1 Overview of brain RGS14 expression and possible functional implications

An updated anatomo-functional neurocircuitry diagram of RGS14-expressing brain regions is shown in Figure 22. The expression profile of RGS14 in the brain points to a possible role in governing aspects of several core cognitive functions: sensory perception, emotion, memory, motivation, and execution of actions. It is also in or just upstream of regions that process stress, which can have profound effects on cognitive functions (Marin et al., 2011). It seems that RGS14 may be particularly important to associative learning, which serves as a thread to tie many of these functions together. RGS14 is found in regions that form associations between concurrent stimuli (isocortex layer II), and between stimuli and context/content (ENT-hippocampus), social relationships (CA2), emotional states (BLA), responses (CPu), and outcomes (NAcC) (Beyeler et al., 2016; Cerri et al., 2014; Lee et al., 2021; Samadi et al., 2023; Stalnaker et al., 2010; Wang & Cui, 2018). It may be telling that the regions in which RGS14 is most abundant are also especially dopaminoceptive (Hall et al., 1994). Dopamine is a strong driver of experience-based neuroplasticity, and RGS14 likely works to keep its influence in check (Speranza et al., 2021). It is possible even that RGS14 is induced in response to dopamine-driven hyperexcitation, similar to that which is seen during status epilepticus (Harbin et al., 2023). In support of this, we observed stronger RGS14 immunoreactivity 2 hours after cocaine challenge in the NAc core and shell of WT mice with a history of chronic cocaine compared to drug-naïve WT mice (Fig. 16), suggesting that upregulating RGS14 in the NAc could serve as an endogenous mechanistic counterweight to oppose overactivation of plasticity mechanisms by chronic cocaine.

Complex organisms are receiving and processing a multitude of stimuli every moment they are conscious. RGS14-mediated suppression of intracellular plasticity pathways could help filter the signal from the noise to improve the fidelity of associative learning. Evidence for this is seen in impaired social discrimination in RGS14-KO mice (Samadi et al., 2023). And because RGS14-expressing regions are interconnected, RGS14 may contribute to setting an overall tone on the experience-to-action processing pipeline that underlies certain types of learned behaviors, particularly ones with a strong emotional component. Mutations that affect RGS14 function universally could have profound effects on attributes such as emotional resilience and emotional reactivity, compulsivity, impulsivity, and emotional memory. This is not just a hypothetical; the L507R mutation in the mice used in this study is a homolog of the naturally-occurring L505R genetic variant found in RGS14 of humans (Squires et al., 2020).

5.2 Possible differential regulation of signaling in nucleus accumbens D1- and D2-MSNs

From our current and previous immunohistological studies, we can conclude with reasonable confidence that RGS14 is expressed in both D1- and D2-MSNs in the striatum, including in the NAc and especially in NAc core. Cocaine drives hyperactivation of locomotor and other motor behaviors by simultaneously boosting excitability of striatal direct pathway-associated D1-MSNs and suppressing excitability of indirect pathway-associated D2-MSNs (Lobo & Nestler, 2011). RGS14-KO mice exhibit a hyperlocomotor response to acute high-dose cocaine (Foster et al., 2021), likely because there is no negative modulation of D2R-Gi/o signaling by RGS14 in D2-MSNs to relieve cocaine-imposed suppression of indirect/NO-GO pathway activity. On the other hand (or neuron), RGS14 is not equipped to regulate D1R-Gs/olf signaling directly, but can suppress D1R activation-enhanced Ca^{2+} and ERK signaling during coincident release of dopamine and glutamate that drives LTP in D1-MSNs (Cahill et al., 2014). Our proposed framework for

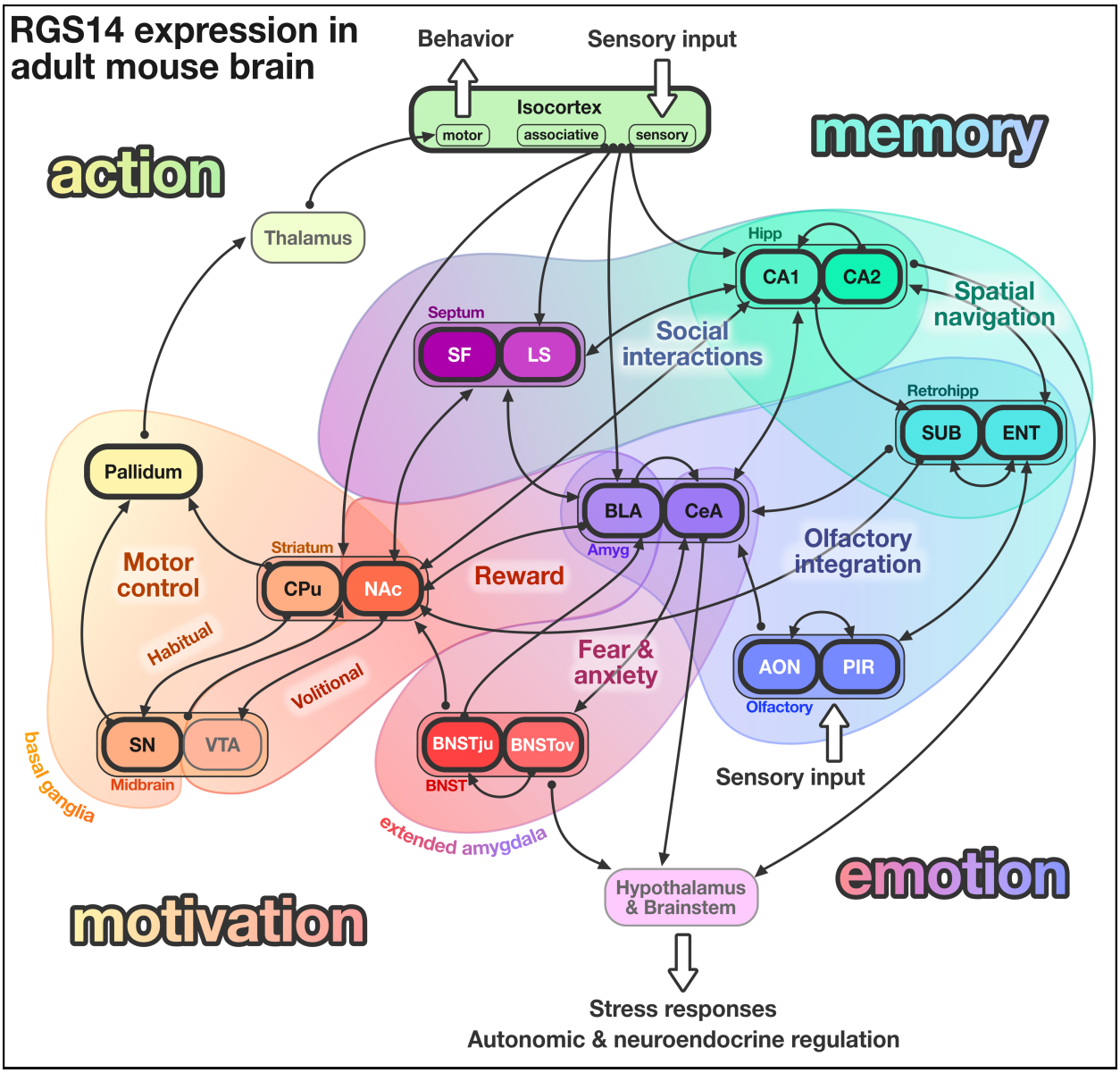


Figure 16: Simplified anatomo-functional neurocircuitry diagram of prominent RGS14-expressing regions in the adult mouse brain (updated model). Diagram is intended for conceptualization purposes and is not comprehensive. Individual brain regions are indicated by rounded rectangle with solid fill. Regions within shared anatomical structures are grouped within outer rounded rectangle as well as by shared color hue. Thick box borders with black or white text indicate RGS14+ regions. Thin box borders with gray text indicate RGS14- regions. Fill color intensity corresponds to relative intensity of RGS14 immunoreactivity within a given region. Oversized text with gradient fill indicates dimensions of function, and are generally located proximal to brain regions involved in their

processing. Bubbles with gradient fill encapsulate regions and connections involved in select functions. Gradient fills in oversized text and bubbles correspond with coded color hues of pertinent anatomical structures, and are intended to illustrate the overlapping functional nature of RGS14-expressing brain regions. Abbreviations: AON: anterior olfactory nucleus, BLA: basolateral amygdala, BNST(ju,ov): bed nucleus of the stria terminalis- (juxtacapsular, oval nucleus), CA(1,2): cornu ammonis (1,2), CeA: central amygdala, CPu: caudoputamen, ENT: entorhinal cortex, LS: lateral septal nucleus, NAc: nucleus accumbens, PIR: piriform cortex, SF: septofimbrial nucleus, SN: substantia nigra, SUB: subiculum, VTA: ventral tegmental area.

differential RGS14 regulation of dopamine signaling in D1- and D2-MSNS is shown in Figure 23. The current data support this model: RGS14-KO extends the duration of cocaine-induced locomotor activation regardless of drug history, probably because RGS14 accelerates termination of cocaine-activated D2R-Gi/o signaling in striatal D2-MSNs (Fig. 23B). In contrast, the initial magnitude of cocaine-induced locomotor activation was increased only in RGS14-KO mice previously given chronic cocaine, and not naïve RGS14-KO mice, strongly suggesting enhanced cocaine-induced plasticity in striatal D1-MSNs in the absence of RGS14 (Fig. 23A). Future studies should incorporate electrophysiological approaches to validate and expand upon the proposed framework of RGS14 regulation of signaling in D1- and D2-MSNs.

NAc D1- and D2-MSNs process different aspects of learning and adaptive behavior. While the current studies demonstrate RGS14 interference in reward learning and locomotor sensitization presumably in D1-MSNs, the role of RGS14 in regulating plasticity in D2-MSNs remains unexplored. Studies show involvement of NAc D2-MSNs in processing extinction learning and reward prediction error (Roberts-Wolfe et al., 2018; Zachry et al., 2024), and evidence suggests that D2-MSN plasticity is largely responsible for mediating the effects of stress on adaptive behavior (Fox et al., 2020; Francis et al., 2015; Pagliusi et al., 2022). The present data leads us to suspect that RGS14 is involved in regulating development of stress-related behaviors, and exploration of RGS14 regulation of stress-related signaling and plasticity in striatal D2-MSNs is a promising avenue of future investigation and would aid in painting a more complete picture of the role of RGS14 in governing emotional processing and behavioral flexibility.

5.3 Implications for RGS14 in human disease and future directions

The possible implications for RGS14 in human disease, especially psychiatric disease and behavioral disorders, are wide-ranging and multifaceted. Several RGS proteins have been linked

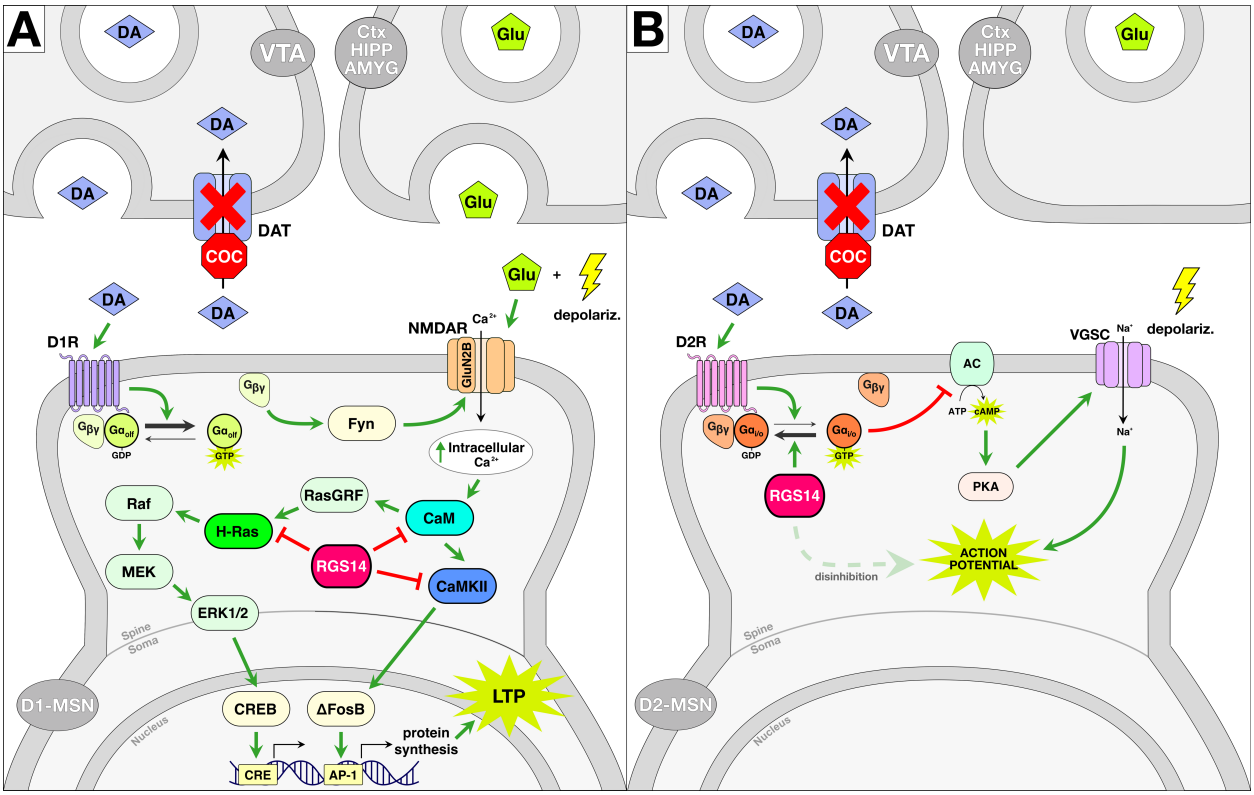


Figure 23. RGS14 may be regulating cocaine-induced dopamine signaling differently in striatal D1- and D2-MSNs. A. In D1-MSNs, RGS14 cannot directly modulate D1R-Gs/olf signaling, but can suppress D1R activation-enhanced Ca^{2+} and ERK signaling that drives LTP in the presence of coincident dopamine and glutamate release. **B.** In D2-MSNs, RGS14 can negatively modulate D2R-Gi/o signaling directly by accelerating inactivation of Gαi/o subunits, causing reassociation with Gβγ and re-coupling with D2R, terminating signaling. The resultant disinhibited cAMP/PKA pathway signaling restores D2-MSN excitability.

to neurological diseases including RGS4, RGS9-2, and RGSz (Hooks et al., 2008; Sakloth et al., 2020), and studies in rodents and primates alike suggest that RGS14 is a strong candidate to join this list in the future.

For example, in the hippocampus, RGS14 serves as a natural suppressor of synaptic plasticity and also acts to minimize neuronal damage following tissue insult or seizure induction. Consistent with this idea, CA2 hippocampus is protected against neuronal injury following seizure (Steve et al., 2014). We speculate that in the other limbic and basal ganglia regions where it has been found, RGS14 operates similarly as a suppressor of synaptic plasticity. Altogether, the brain regions that express RGS14 are associated with processing learning and memory (especially social memory), emotion, motivation, and movement. Though speculative at this point, RGS14 could be regulating any number of behaviors involving these functions or the interplay between them. For example, impaired RGS14 function could increase drug-seeking behavior when an addicted person feels the dysphoric effects of withdrawal, or it could impede the development of social relationships in a person with autism.

Due to its specific regional expression in area CA2 of the hippocampus, RGS14 may play a part in social disorders. Of particular interest is the possible role of RGS14 in autism spectrum disorder, a neurodevelopmental condition characterized by deficits in social behavior and communication that typically emerge in early childhood. Several genes linked to autism are downregulated in CA2 (Shen et al., 2012). The gradual increase of CA2 RGS14 expression throughout maturation into adulthood may underlie a closing developmental window for social behavior that could explain why early intervention in autism is most effective in improving outcomes (Evans et al., 2014). Consequently, manipulations or mutations that alter RGS14 levels or function may be relevant to autism development. Evidence for this comes from study which

showed that genetic knockout of the mineralocorticoid receptor leads to a dramatic loss of RGS14 expression as well as impairment of social discrimination (McCann et al., 2019). The gene for the mineralocorticoid receptor, *Nr3c2*, is listed by the Simons Foundation Autism Research Initiative as being mutated in some syndromic autism (Banerjee-Basu & Packer, 2010).

The gene encoding RGS14 has been identified as a risk gene in schizophrenia (Nguyen et al., 2017). Schizophrenia involves social impairments and is associated with a substantial loss of non-pyramidal neurons in CA2 (Benes et al., 1998). Compared with other hippocampal subregions that express much lower amounts of RGS14, CA2 is uniquely resistant to epileptic injury (Häussler et al., 2016). A recent study found that RGS14 protects against inflammatory damage in the kidneys, raising the possibility that it also mitigates insults in CA2 to prevent schizophrenia pathogenesis (Zhang et al., 2022). Parkinson's disease is a neurodegenerative disease caused the progressive destruction of midbrain dopamine neurons. Reduced levels of RGS14 in the putamen of Parkinson's disease patients may also be evident of a reduced capacity to regulate neuroinflammation in these patients (Lewis & Cookson, 2012). Further study is required.

Despite the conceivable therapeutic relevance of RGS14, investigation of its roles in human disease remains largely unexplored. Current animal studies of RGS14 have predominantly been performed in mice due to availability of an established RGS14-KO mouse line. Studies of RGS14 in mouse brain are valuable, but are in some aspects limited in human translatability because RGS14 is expressed at different levels in certain brain regions in rodents relative to primates (Fig. 3) (Harbin et al., 2021), and primate RGS14 is known to have additional splice variants (Squires et al., 2018) and a terminal PDZ binding domain (Fig. 1) (Friedman et al., 2022). While differential expression patterns are more difficult to address, differences in RGS14 protein homology between primates and rodents could be addressed by performing studies on “humanized” mice manipulated

to express human RGS14. Such studies would help to further elucidate roles for RGS14 at postsynaptic spines, in particular the role of RGS14 in regulating the various abundant and important PDZ regulatory proteins at the post-synaptic density.

Another issue to consider is that primates have more complex social structures and relationships than rodents, which may make certain types of studies of RGS14 effects on social behavior particularly difficult to translate from mouse models. While genetic manipulation of RGS14 in laboratory primates is currently not practicable, a more feasible approach would be to examine RGS14 genetic variants and expression levels post-mortem in primate brains that have been previously characterized for social behavior and social memory. It would also be useful to examine post-mortem brain tissue from humans diagnosed with autism, social anxiety disorders, and other social deficits. Lastly, the current gold standard for models of drug addiction is drug self-administration, which is generally not feasible to perform in mice due to the technical difficulty of implanting intravenous catheters at such a small scale. This could be addressed by genetically altering RGS14 expression using AAV or CRISPR/Cas9 techniques in rats, which are commonly used in self-administration studies.

In addition to these possible avenues for future RGS14 research, other studies are underway to examine novel roles for RGS14 in the brain. As discussed above, RGS14 contains both a nuclear localization sequence (NLS) and nuclear export sequence (NES) and is a nucleocytoplasmic shuttling protein. Related to this, splice variants of RGS14 have been reported to lack the RGS domain, and RGS14 has been observed in the nuclei of primate striatal neurons, suggesting non-canonical roles for RGS14 (Squires et al., 2018). To date though, RGS14 in the nucleus remains largely unexplored. The LR mice used in the current anatomical study contain a homolog of a human genetic variant of RGS14 that disrupts nuclear export (L505R) and localizes and

accumulates in the nuclei of neurons when introduced to cultured neurons or whole mice (Squires et al., 2020). This mouse model is continuing to be investigated to define the impact of constitutive RGS14 nuclear localization on neuronal function and animal behavior. This and other genetic variants of RGS14, as well as other RGS14 splice variants, are the subject of ongoing investigation.

REFERENCES

Aboitiz, F. (1999). Feature Article: Comparative Development of the Mammalian Isocortex and the Reptilian Dorsal Ventricular Ridge. Evolutionary Considerations. *Cerebral Cortex*, *9*(8), 783–791. https://doi.org/10.1093/cercor/9.8.783

Agudelo, L. Z., Ferreira, D. M. S., Cervenka, I., Bryzgalova, G., Dadvar, S., Jannig, P. R., Pettersson-Klein, A. T., Lakshmikanth, T., Sustarsic, E. G., Porsmyr-Palmertz, M., Correia, J. C., Izadi, M., Martínez-Redondo, V., Ueland, P. M., Midttun, Ø., Gerhart-Hines, Z., Brodin, P., Pereira, T., Berggren, P.-O., & Ruas, J. L. (2018). Kynurenic Acid and Gpr35 Regulate Adipose Tissue Energy Homeostasis and Inflammation. *Cell Metabolism*, *27*(2), 378-392.e5. https://doi.org/10.1016/j.cmet.2018.01.004

Alcantara, A. A., Lim, H. Y., Floyd, C. E., Garces, J., Mendenhall, J. M., Lyons, C. L., & Berlanga, M. L. (2010). Cocaine- and morphine-induced synaptic plasticity in the nucleus accumbens. *Synapse*, *65*(4). https://doi.org/10.1002/syn.20849

Alexander, G. E., DeLong, M. R., & Strick, P. L. (1986). Parallel organization of functionally segregated circuits linking basal ganglia and cortex. *Annual Review of Neuroscience*, *9*, 357–381. https://doi.org/10.1146/annurev.ne.09.030186.002041

Alexander, G. M., Riddick, N. V., McCann, K. E., Lustberg, D., Moy, S. S., & Dudek, S. M. (2019). Modulation of CA2 neuronal activity increases behavioral responses to fear conditioning in female mice. *Neurobiology of Learning and Memory*, *163*, 107044. https://doi.org/10.1016/j.nlm.2019.107044

Aliane, V., Pérez, S., Nieoullon, A., Deniau, J.-M., & Kemel, M. L. (2009). Cocaine-induced stereotypy is linked to an imbalance between the medial prefrontal and sensorimotor circuits of the basal ganglia. *European Journal of Neuroscience*, *30*(7). https://doi.org/10.1111/j.1460-9568.2009.06907.x

Allen Institute for Brain Science (2011). Allen Reference Atlas – Mouse Brain [Adult]. Available from atlas.brain-map.org.

Ambroggi, F., Ghazizadeh, A., Nicola, S. M., & Fields, H. L. (2011). Roles of Nucleus Accumbens Core and Shell in Incentive-Cue Responding and Behavioral Inhibition. *The Journal of Neuroscience*, *31*(18), 6820–6830. https://doi.org/10.1523/JNEUROSCI.6491-10.2011

Badiani, A., & Robinson, T. E. (2004). Drug-induced neurobehavioral plasticity: The role of environmental context. *Behavioural Pharmacology*, *15*(5), 327.

Banerjee-Basu, S., & Packer, A. (2010). SFARI Gene: An evolving database for the autism research community. *Disease Models & Mechanisms*, *3*(3–4), 133–135. https://doi.org/10.1242/dmm.005439

Barr, G. A., Sharpless, N. S., Cooper, S., Schiff, S. R., Paredes, W., & Bridger, W. H. (1983). Classical conditioning, decay and extinction of cocaine-induced hyperactivity and stereotypy. *Life Sciences*, *33*(14), 1341–1351. https://doi.org/10.1016/0024-3205(83)90817-2

Beaulieu, J. M., & Gainetdinov, R. R. (2011). The physiology, signaling, and pharmacology of dopamine receptors. *Pharmacological Reviews*, *63*(1), 182–217. https://doi.org/10.1124/pr.110.002642

Becker, W. C., Fiellin, D. A., & Desai, R. A. (2007). Non-medical use, abuse and dependence on sedatives and tranquilizers among U.S. adults: Psychiatric and socio-demographic correlates. *Drug and Alcohol Dependence*, *90*(2–3). https://doi.org/10.1016/j.drugalcdep.2007.04.009

Behr, J., Wozny, C., Fidzinski, P., & Schmitz, D. (2009). Synaptic plasticity in the subiculum. *Progress in Neurobiology*, *89*(4), 334–342. https://doi.org/10.1016/j.pneurobio.2009.09.002

Belin, D., & Everitt, B. J. (2008). Cocaine Seeking Habits Depend upon Dopamine-Dependent Serial Connectivity Linking the Ventral with the Dorsal Striatum. *Neuron*, *57*(3), 432–441. https://doi.org/10.1016/j.neuron.2007.12.019

Benes, F. M., Kwok, E. W., Vincent, S. L., & Todtenkopf, M. S. (1998). A reduction of nonpyramidal cells in sector CA2 of schizophrenics and manic depressives. *Biological Psychiatry*, *44*(2), 88–97. https://doi.org/10.1016/S0006-3223(98)00138-3

Berger, H., Heinrich, N., Wietfeld, D., Bienert, M., & Beyermann, M. (2006). Evidence that corticotropin-releasing factor receptor type 1 couples to Gs- and Gi-proteins through different conformations of its J-domain. *British Journal of Pharmacology*, *149*(7). https://doi.org/10.1038/sj.bjp.0706926

Berke, J. D., & Hyman, S. E. (2000). Addiction, dopamine, and the molecular mechanisms of memory. *Neuron*, *25*(3), 515–532. https://doi.org/10.1016/S0896-6273(00)81056-9

Bett, D., Stevenson, C. H., Shires, K. L., Smith, M. T., Martin, S. J., Dudchenko, P. A., & Wood, E. R. (2013). The Postsubiculum and Spatial Learning: The Role of Postsubicular Synaptic Activity and Synaptic Plasticity in Hippocampal Place Cell, Object, and Object-Location Memory. *Journal of Neuroscience*, *33*(16), 6928–6943. https://doi.org/10.1523/JNEUROSCI.5476-12.2013

Beyeler, A., Namburi, P., Glober, G. F., Simonnet, C., Calhoon, G. G., Conyers, G. F., Luck, R., Wildes, C. P., & Tye, K. M. (2016). Divergent Routing of Positive and Negative Information from the Amygdala during Memory Retrieval. *Neuron*, *90*(2), 348–361. https://doi.org/10.1016/j.neuron.2016.03.004

Beyermann, M., Heinrich, N., Fechner, K., Furkert, J., Zhang, W., Kraetke, O., Bienert, M., & Berger, H. (2007). Achieving signalling selectivity of ligands for the corticotropin-releasing factor type 1 receptor by modifying the agonist's signalling domain. *British Journal of Pharmacology*, *151*(6). https://doi.org/10.1038/sj.bjp.0707293

Bliss-Moreau, E., Bauman, M. D., & Amaral, D. G. (2011). Neonatal amygdala lesions result in globally blunted affect in adult rhesus macaques. *Behavioral Neuroscience*, *125*(6), 848–858. https://doi.org/10.1037/a0025757

Bourin, M., & Hascoët, M. (2003). The mouse light/dark box test. *European Journal of Pharmacology*, *463*(1), 55–65. https://doi.org/10.1016/S0014-2999(03)01274-3

Branch, M. R., & Hepler, J. R. (2017). Endogenous RGS14 is a cytoplasmic-nuclear shuttling protein that localizes to juxtanuclear membranes and chromatin-rich regions of the nucleus. *PLoS ONE*, *12*(9), 1–27. https://doi.org/10.1371/journal.pone.0184497

Brown, N. E., Lambert, N. A., & Hepler, J. R. (2016). RGS14 regulates the lifetime of Gα-GTP signaling but does not prolong Gβγ signaling following receptor activation in live cells. *Pharmacology Research & Perspectives*, *4*(5), e00249–e00249. https://doi.org/10.1002/prp2.249

Cacciapaglia, F., Saddoris, M. P., Wightman, R. M., & Carelli, R. M. (2012). Differential dopamine release dynamics in the nucleus accumbens core and shell track distinct aspects

of goal-directed behavior for sucrose. *Neuropharmacology*, *62*(5), 2050–2056. https://doi.org/10.1016/j.neuropharm.2011.12.027

Cahill, E., Salery, M., Vanhoutte, P., & Caboche, J. (2014). Convergence of dopamine and glutamate signaling onto striatal ERK activation in response to drugs of abuse. *Frontiers in Pharmacology*, *4 JAN*(January), 1–13. https://doi.org/10.3389/fphar.2013.00172

Callahan, L. B., Tschetter, K. E., & Ronan, P. J. (2013). Inhibition of corticotropin releasing factor expression in the central nucleus of the amygdala attenuates stress-induced behavioral and endocrine responses. *Frontiers in Neuroscience*, *7*. https://doi.org/10.3389/fnins.2013.00195

Canto, C. B., Wouterlood, F. G., & Witter, M. P. (2008). What Does the Anatomical Organization of the Entorhinal Cortex Tell Us? *Neural Plasticity*, *2008*, e381243. https://doi.org/10.1155/2008/381243

Cassell, M. D., Gray, T. S., & Kiss, J. Z. (1986). Neuronal architecture in the rat central nucleus of the amygdala: A cytological, hodological, and immunocytochemical study. *The Journal of Comparative Neurology*, *246*(4), 478–499. https://doi.org/10.1002/cne.902460406

Ceglia, I., Lee, K.-W., Cahill, M. E., Graves, S. M., Dietz, D., Surmeier, D. J., Nestler, E. J., Nairn, A. C., Greengard, P., & Kim, Y. (2017). WAVE1 in neurons expressing the D1 dopamine receptor regulates cellular and behavioral actions of cocaine. *Proceedings of the National Academy of Sciences*, *114*(6), 1395–1400. https://doi.org/10.1073/pnas.1621185114

Cerri, D. H., Saddoris, M. P., & Carelli, R. M. (2014). Nucleus Accumbens Core Neurons Encode Value-Independent Associations Necessary for Sensory Preconditioning. *Behavioral Neuroscience*, *128*(5), 567–578. https://doi.org/10.1037/a0037797

Cervo, L., & Samanin, R. (1996). Effects of dopaminergic and glutamatergic receptor antagonists on the establishment and expression of conditioned locomotion to cocaine in rats. *Brain Research*, *731*(1), 31–38. https://doi.org/10.1016/0006-8993(96)00455-6

Chiara, G. D., & Impérato, A. (1988). Drugs abused by humans preferentially increase synaptic dopamine concentrations in the mesolimbic system of freely moving rats. *Proceedings of the National Academy of Sciences*, *85*(14). https://doi.org/10.1073/pnas.85.14.5274

Cho, H., Kim, D.-U., & Kehrl, J. H. (2005). RGS14 Is a Centrosomal and Nuclear Cytoplasmic Shuttling Protein That Traffics to Promyelocytic Leukemia Nuclear Bodies Following Heat Shock *. *Journal of Biological Chemistry*, *280*(1), 805–814. https://doi.org/10.1074/jbc.M408163200

Ciocchi, S., Herry, C., Grenier, F., Wolff, S. B. E., Letzkus, J. J., Vlachos, I., Ehrlich, I., Sprengel, R., Deisseroth, K., Stadler, M. B., Müller, C., & Lüthi, A. (2010). Encoding of conditioned fear in central amygdala inhibitory circuits. *Nature*, *468*(7321), 277–282. https://doi.org/10.1038/nature09559

Clemens, A. M., Wang, H., & Brecht, M. (2020). The lateral septum mediates kinship behavior in the rat. *Nature Communications*, *11*(1). https://doi.org/10.1038/s41467-020-16489-x

Cui, Z., Gerfen, C. R., & Young 3rd, W. S. (2013). Hypothalamic and other connections with dorsal CA2 area of the mouse hippocampus. *Journal of Comparative Neurology*, *521*(8), 1844–1866. https://doi.org/10.1002/cne.23263

Cummings, S., Elde, R., Ells, J., & Lindall, A. (1983). Corticotropin-releasing factor immunoreactivity is widely distributed within the central nervous system of the rat: An

immunohistochemical study. *Journal of Neuroscience*, *3*(7), 1355–1368. https://doi.org/10.1523/JNEUROSCI.03-07-01355.1983

De Groote, A., & de Kerchove d'Exaerde, A. (2021). Thalamo-Nucleus Accumbens Projections in Motivated Behaviors and Addiction. *Frontiers in Systems Neuroscience*, *15*. https://doi.org/10.3389/fnsys.2021.711350

de Guglielmo, G., Kallupi, M., Pomrenze, M. B., Crawford, E., Simpson, S., Schweitzer, P., Koob, G. F., Messing, R. O., & George, O. (2019). Inactivation of a CRF-dependent amygdalofugal pathway reverses addiction-like behaviors in alcohol-dependent rats. *Nature Communications*, *10*(1), 1238. https://doi.org/10.1038/s41467-019-09183-0

Di Chiara, G., & Imperato, A. (1988). Drugs abused by humans preferentially increase synaptic dopamine concentrations in the mesolimbic system of freely moving rats. *Proceedings of the National Academy of Sciences of the United States of America*, *85*(14), 5274–5278. https://doi.org/10.1073/pnas.85.14.5274

Di Ciano, P., Blaha, C. D., & Phillips, A. G. (1998). The relation between dopamine oxidation currents in the nucleus accumbens and conditioned increases in motor activity in rats following repeated administration of d-amphetamine or cocaine. *European Journal of Neuroscience*, *10*(3), 1113–1120. https://doi.org/10.1046/j.1460-9568.1998.00124.x

Dimsdale-Zucker, H. R., Ritchey, M., Ekstrom, A. D., Yonelinas, A. P., & Ranganath, C. (2018). CA1 and CA3 differentially support spontaneous retrieval of episodic contexts within human hippocampal subfields. *Nature Communications*, *9*(1), 294. https://doi.org/10.1038/s41467-017-02752-1

Dolmetsch, R. (2003). Excitation-Transcription Coupling: Signaling by Ion Channels to the Nucleus. *Science's STKE*, *2003*(166), pe4–pe4. https://doi.org/10.1126/stke.2003.166.pe4

Dong, H., Petrovich, G. D., & Swanson, L. W. (2000). Organization of projections from the juxtacapsular nucleus of the BST: A PHAL study in the rat. *Brain Research*, *859*(1), 1–14. https://doi.org/10.1016/s0006-8993(99)02246-5

Dong, H. W., Petrovich, G. D., & Swanson, L. W. (2001). Topography of projections from amygdala to bed nuclei of the stria terminalis. *Brain Research. Brain Research Reviews*, *38*(1–2), 192–246. https://doi.org/10.1016/s0165-0173(01)00079-0

Etkin, A., & Wager, T. D. (2007). Functional Neuroimaging of Anxiety: A Meta-Analysis of Emotional Processing in PTSD, Social Anxiety Disorder, and Specific Phobia. *American Journal of Psychiatry*, *164*(10). https://doi.org/10.1176/appi.ajp.2007.07030504

Evans, P. R., Dudek, S. M., & Hepler, J. R. (2015). Regulator of G Protein Signaling 14: A Molecular Brake on Synaptic Plasticity Linked to Learning and Memory. In *Progress in Molecular Biology and Translational Science* (Vol. 133). Elsevier Inc. https://doi.org/10.1016/bs.pmbts.2015.03.006

Evans, P. R., Gerber, K. J., Dammer, E. B., Duong, D. M., Goswami, D., Lustberg, D. J., Zou, J., Yang, J. J., Dudek, S. M., Griffin, P. R., Seyfried, N. T., & Hepler, J. R. (2018). Interactome Analysis Reveals Regulator of G Protein Signaling 14 (RGS14) is a Novel Calcium/Calmodulin (Ca 2+ /CaM) and CaM Kinase II (CaMKII) Binding Partner. *Journal of Proteome Research*, *17*(4), 1700–1711. https://doi.org/10.1021/acs.jproteome.8b00027

Evans, P. R., Lee, S. E., Smith, Y., & Hepler, J. R. (2014). Postnatal developmental expression of regulator of G protein signaling 14 (RGS14) in the mouse brain. *Journal of Comparative Neurology*, *522*(1), 186–203. https://doi.org/10.1002/cne.23395

Evans, P. R., Parra-Bueno, P., Smirnov, M. S., Lustberg, D. J., Dudek, S. M., Hepler, J. R., & Yasuda, R. (2018). RGS14 restricts plasticity in hippocampal CA2 by limiting postsynaptic calcium signaling. *eNeuro*, *5*(3), 1–13. https://doi.org/10.1523/ENEURO.0353-17.2018

Everitt, B. J., & Robbins, T. W. (2016). Drug Addiction: Updating Actions to Habits to Compulsions Ten Years On. *Annual Review of Psychology*, *67*(Volume 67, 2016), 23–50. https://doi.org/10.1146/annurev-psych-122414-033457

Fadok, J. P., Markovic, M., Tovote, P., & Lüthi, A. (2018). New perspectives on central amygdala function. *Current Opinion in Neurobiology*, *49*, 141–147. https://doi.org/10.1016/j.conb.2018.02.009

Flanigan, M., & Leclair, K. (2017). Shared motivational functions of ventral striatum D1 and D2 medium spiny neurons. *Journal of Neuroscience*, *37*(26), 6177–6179. https://doi.org/10.1523/JNEUROSCI.0882-17.2017

Foster, S. L., Lustberg, D. J., Harbin, N. H., Bramlett, S. N., Hepler, J. R., & Weinshenker, D. (2021). RGS14 modulates locomotor behavior and ERK signaling induced by environmental novelty and cocaine within discrete limbic structures. *Psychopharmacology*, *238*(10), 2755–2773. https://doi.org/10.1007/s00213-021-05892-x

Fox, A. S., & Shackman, A. J. (2019). The central extended amygdala in fear and anxiety: Closing the gap between mechanistic and neuroimaging research. *Neuroscience Letters*, *693*, 58–67. https://doi.org/10.1016/j.neulet.2017.11.056

Fox, M. E., Chandra, R., Menken, M. S., Larkin, E. J., Nam, H., Engeln, M., Francis, T. C., & Lobo, M. K. (2020). Dendritic remodeling of D1 neurons by RhoA/Rho-kinase mediates depression-like behavior. *Molecular Psychiatry*, *25*(5), 1022–1034. https://doi.org/10.1038/s41380-018-0211-5

Francesconi, W., Berton, F., Koob, G. F., & Sanna, P. P. (2009). Intrinsic neuronal plasticity in the juxtacapsular nucleus of the bed nuclei of the stria terminalis (jcBNST). *Progress in Neuro-Psychopharmacology and Biological Psychiatry*, *33*(8), 1347–1355. https://doi.org/10.1016/j.pnpbp.2009.08.003

Francesconi, W., Berton, F., Repunte-Canonigo, V., Hagihara, K., Thurbon, D., Lekic, D., Specio, S. E., Greenwell, T. N., Chen, S. A., Rice, K. C., Richardson, H. N., O'Dell, L. E., Zorrilla, E. P., Morales, M., Koob, G. F., & Sanna, P. P. (2009). Protracted withdrawal from alcohol and drugs of abuse impairs long-term potentiation of intrinsic excitability in the juxtacapsular bed nucleus of the stria terminalis. *The Journal of Neuroscience: The Official Journal of the Society for Neuroscience*, *29*(17), 5389–5401. https://doi.org/10.1523/JNEUROSCI.5129-08.2009

Francis, T. C., Chandra, R., Friend, D. M., Finkel, E., Dayrit, G., Miranda, J., Brooks, J. M., Iñiguez, S. D., O'Donnell, P., Kravitz, A., & Lobo, M. K. (2015). Nucleus Accumbens Medium Spiny Neuron Subtypes Mediate Depression-Related Outcomes to Social Defeat Stress. *Biological Psychiatry*, *77*(3), 212–222. https://doi.org/10.1016/j.biopsych.2014.07.021

Friedman, P. A., Sneddon, W. B., Mamonova, T., Montanez-Miranda, C., Ramineni, S., Harbin, N. H., Squires, K. E., Gefter, J. V., Magyar, C. E., Emlet, D. R., & Hepler, J. R. (2022). RGS14 regulates PTH- and FGF23-sensitive NPT2A-mediated renal phosphate uptake via binding to the NHERF1 scaffolding protein. *The Journal of Biological Chemistry*, *298*(5), 101836. https://doi.org/10.1016/j.jbc.2022.101836

Fudge, J. L., & Emiliano, A. B. (2003). The Extended Amygdala and the Dopamine System: Another Piece of the Dopamine Puzzle. *The Journal of Neuropsychiatry and Clinical Neurosciences*, *15*(3), 306–316.

Garcia, A. D., & Buffalo, E. A. (2020). Anatomy and Function of the Primate Entorhinal Cortex. *Annual Review of Vision Science*, *6*(Volume 6, 2020), 411–432. https://doi.org/10.1146/annurev-vision-030320-041115

Gaval-Cruz, M., Liles, L. C., & Iuvone, P. M. (2012). Chronic Inhibition of Dopamine β-Hydroxylase Facilitates Behavioral Responses to Cocaine in Mice. *PLoS ONE*, *7*(11). https://doi.org/10.1371/journal.pone.0050583

Gerber, K. J., Squires, K. E., & Hepler, J. R. (2018). 14-3-3ɣ binds regulator of G protein signaling 14 (RGS14) at distinct sites to inhibit the RGS14:Gαi–AlF4−signaling complex and RGS14 nuclear localization. *Journal of Biological Chemistry*, *293*(38), 14616–14631. https://doi.org/10.1074/jbc.RA118.002816

Gingrich, J. A., & Caron, M. G. (1993). Recent advances in the molecular biology of dopamine receptors. *Annual Review of Neuroscience*, *16*, 299–321. https://doi.org/10.1146/annurev.ne.16.030193.001503

Glangetas, C., Girard, D., Groc, L., Marsicano, G., Chaouloff, F., & Georges, F. (2013). Stress Switches Cannabinoid Type-1 (CB1) Receptor-Dependent Plasticity from LTD to LTP in the Bed Nucleus of the Stria Terminalis. *Journal of Neuroscience*, *33*(50), 19657–19663. https://doi.org/10.1523/JNEUROSCI.3175-13.2013

Goebel-Goody, S. M., Baum, M., Paspalas, C. D., Fernandez, S. M., Carty, N. C., Kurup, P., & Lombroso, P. J. (2012). Therapeutic Implications for Striatal-Enriched Protein Tyrosine Phosphatase (STEP) in Neuropsychiatric Disorders. *Pharmacological Reviews*, *64*(1), 65–87. https://doi.org/10.1124/pr.110.003053

Gogolla, N. (2017). The insular cortex. *Current Biology*, *27*(12), R580–R586. https://doi.org/10.1016/j.cub.2017.05.010

Gong, S., Zheng, C., Doughty, M. L., Losos, K., Didkovsky, N., Schambra, U. B., Nowak, N. J., Joyner, A., Leblanc, G., Hatten, M. E., & Heintz, N. (2003). A gene expression atlas of the central nervous system based on bacterial artificial chromosomes. *Nature*, *425*(6961), 917–925. https://doi.org/10.1038/nature02033

Goosens, K. A., & Maren, S. (2002). Long-term potentiation as a substrate for memory: Evidence from studies of amygdaloid plasticity and Pavlovian fear conditioning. *Hippocampus*, *12*(5), 592–599. https://doi.org/10.1002/hipo.10099

Gore, B. B., & Zweifel, L. S. (2013). Genetic Reconstruction of Dopamine D1 Receptor Signaling in the Nucleus Accumbens Facilitates Natural and Drug Reward Responses. *Journal of Neuroscience*, *33*(20), 8640–8649. https://doi.org/10.1523/JNEUROSCI.5532-12.2013

Gorka, A. X., Torrisi, S., Shackman, A. J., Grillon, C., & Ernst, M. (2018). Intrinsic functional connectivity of the central nucleus of the amygdala and bed nucleus of the stria terminalis. *NeuroImage*, *168*, 392–402. https://doi.org/10.1016/j.neuroimage.2017.03.007

Grant, B. F., Stinson, F. S., Dawson, D. A., Chou, S. P., Dufour, M. C., Compton, W., Pickering, R. P., & Kaplan, K. (2004). Prevalence and co-occurrence of substance use disorders and independent mood and anxiety disorders: Results from the National Epidemiologic Survey on Alcohol and Related Conditions. *Archives of General Psychiatry*, *61*(8), 807–816. https://doi.org/10.1001/archpsyc.61.8.807

Grenier, S., Payette, M.-C., Günther, B., Askari, S., Desjardins, F., Raymond, B., & Berbiche, D. (2018). Association of age and gender with anxiety disorders in older adults: A systematic review and meta-analysis. *International Journal of Geriatric Psychiatry*, *34*(3). https://doi.org/10.1002/gps.5035

Haber, S. N., Fudge, J. L., & McFarland, N. R. (2000). Striatonigrostriatal Pathways in Primates Form an Ascending Spiral from the Shell to the Dorsolateral Striatum. *The Journal of Neuroscience*, *20*(6), 2369–2382. https://doi.org/10.1523/JNEUROSCI.20-06-02369.2000

Hall, H., Sedvall, G., Magnusson, O., Kopp, J., Halldin, C., & Farde, L. (1994). Distribution of D1- and D2-Dopamine Receptors, and Dopamine and Its Metabolites in the Human Brain. *Neuropsychopharmacology*, *11*(4), 245–256. https://doi.org/10.1038/sj.npp.1380111

Hamel, L., Thangarasa, T., Samadi, O., & Ito, R. (2017). Caudal Nucleus Accumbens Core Is Critical in the Regulation of Cue-Elicited Approach-Avoidance Decisions. *eNeuro*, *4*(1). https://doi.org/10.1523/ENEURO.0330-16.2017

Hammack, S. E., Braas, K. M., & May, V. (2021). Chemoarchitecture of the BNST: Neurophenotypic diversity and function. *Handbook of Clinical Neurology*, *179*, 385–402. https://doi.org/10.1016/B978-0-12-819975-6.00025-X

Harbin, N. H., Bramlett, S. N., Montanez-Miranda, C., Terzioglu, G., & Hepler, J. R. (2021). RGS14 Regulation of Post-Synaptic Signaling and Spine Plasticity in Brain. *International Journal of Molecular Sciences*, *22*(13). https://doi.org/10.3390/ijms22136823

Harbin, N. H., Lustberg, D. J., Hurst, C., Pare, J., Crotty, K. M., Waters, A. L., Yeligar, S. M., Smith, Y., Seyfried, N. T., Weinshenker, D., & Hepler, J. R. (2023). RGS14 limits seizure-induced mitochondrial oxidative stress and pathology in hippocampus. *Neurobiology of Disease*, *181*, 106128. https://doi.org/10.1016/j.nbd.2023.106128

Harris, N. A., & Winder, D. G. (2018). Synaptic Plasticity in the Bed Nucleus of the Stria Terminalis: Underlying Mechanisms and Potential Ramifications for Reinstatement of Drug- and Alcohol-Seeking Behaviors. *ACS Chemical Neuroscience*, *9*(9), 2173–2187. https://doi.org/10.1021/acschemneuro.8b00169

Hartopp, N., Wright, P., Ray, N. J., Evans, T. E., Metzler-Baddeley, C., Aggleton, J. P., & O'Sullivan, M. J. (2019). A Key Role for Subiculum-Fornix Connectivity in Recollection in Older Age. *Frontiers in Systems Neuroscience*, *12*. https://doi.org/10.3389/fnsys.2018.00070

Häussler, U., Rinas, K., Kilias, A., Egert, U., & Haas, C. A. (2016). Mossy fiber sprouting and pyramidal cell dispersion in the hippocampal CA2 region in a mouse model of temporal lobe epilepsy. *Hippocampus*, *26*(5), 577–588. https://doi.org/10.1002/hipo.22543

Hendianti, G. N., & Uthis, P. (2018). Factors related to methamphetamine relapse risk among clients in the substance rehabilitation center of National Narcotics Board in West Java, Indonesia. *Journal of Health Research*, *32*(4). https://doi.org/10.1108/jhr-05-2018-035

Hintiryan, H., Bowman, I., Johnson, D. L., Korobkova, L., Zhu, M., Khanjani, N., Gou, L., Gao, L., Yamashita, S., Bienkowski, M. S., Garcia, L., Foster, N. N., Benavidez, N. L., Song, M. Y., Lo, D., Cotter, K. R., Becerra, M., Aquino, S., Cao, C., … Dong, H.-W. (2021). Connectivity characterization of the mouse basolateral amygdalar complex. *Nature Communications*, *12*(1), 2859. https://doi.org/10.1038/s41467-021-22915-5

Hintiryan, H., Foster, N. N., Bowman, I., Bay, M., Song, M. Y., Gou, L., Yamashita, S., Bienkowski, M. S., Zingg, B., Zhu, M., Yang, X. W., Shih, J. C., Toga, A. W., & Dong, H.-W. (2016). The mouse cortico-striatal projectome. *Nature Neuroscience*, *19*(8), 1100–1114. https://doi.org/10.1038/nn.4332

Hitchcock, J., & Davis, M. (1986). Lesions of the amygdala, but not of the cerebellum or red nucleus, block conditioned fear as measured with the potentiated startle paradigm. *Behavioral Neuroscience*, *100*(1), 11–22. https://doi.org/10.1037/0735-7044.100.1.11

Hitti, F. L., & Siegelbaum, S. A. (2014). The hippocampal CA2 region is essential for social memory. *Nature*, *508*(7494), 88–92. https://doi.org/10.1038/nature13028

Hollinger, S., Taylor, J. B., Goldman, E. H., & Hepler, J. R. (2001). RGS14 is a bifunctional regulator of Gαi/o activity that exists in multiple populations in brain. *Journal of Neurochemistry*, *79*(5), 941–949. https://doi.org/10.1046/j.1471-4159.2001.00629.x

Homologene. Regulator of G-Protein Signaling 14. Available online: https://www.ncbi.nlm.nih.gov/homologene/4735 (accessed on 18 April 2021).

Hooks, S. B., Martemyanov, K., & Zachariou, V. (2008). A role of RGS proteins in drug addiction. *Biochemical Pharmacology*, *75*(1), 76–84. https://doi.org/10.1016/j.bcp.2007.07.045

Hu, H., & Gereau, R. W. (2003). ERK Integrates PKA and PKC Signaling in Superficial Dorsal Horn Neurons. II. Modulation of Neuronal Excitability. *Journal of Neurophysiology*, *90*(3). https://doi.org/10.1152/jn.00341.2003

Hu, M., & Becker, J. B. (2003). Effects of Sex and Estrogen on Behavioral Sensitization to Cocaine in Rats. *Journal of Neuroscience*, *23*(2), 693–699. https://doi.org/10.1523/JNEUROSCI.23-02-00693.2003

Hu, P., Liu, J., Maita, I., Kwok, C., Gu, E., Gergues, M. M., Kelada, F., Phan, M., Zhou, J.-N., Swaab, D. F., Pang, Z. P., Lucassen, P. J., Roepke, T. A., & Samuels, B. A. (2020). Chronic Stress Induces Maladaptive Behaviors by Activating Corticotropin-Releasing Hormone Signaling in the Mouse Oval Bed Nucleus of the Stria Terminalis. *Journal of Neuroscience*, *40*(12), 2519–2537. https://doi.org/10.1523/JNEUROSCI.2410-19.2020

Hu, P., Maita, I., Phan, M. L., Gu, E., Kwok, C., Dieterich, A., Gergues, M. M., Yohn, C. N., Wang, Y., Zhou, J.-N., Qi, X.-R., Swaab, D. F., Pang, Z. P., Lucassen, P. J., Roepke, T. A., & Samuels, B. A. (2020). Early-life stress alters affective behaviors in adult mice through persistent activation of CRH-BDNF signaling in the oval bed nucleus of the stria terminalis. *Translational Psychiatry*, *10*(1), 1–17. https://doi.org/10.1038/s41398-020-01070-3

Hummel, M., & Unterwald, E. M. (2002). D1 dopamine receptor: A putative neurochemical and behavioral link to cocaine action. *Journal of Cellular Physiology*, *191*(1), 17–27. https://doi.org/10.1002/jcp.10078

Hunnicutt, B. J., Jongbloets, B. C., Birdsong, W. T., Gertz, K. J., Zhong, H., & Mao, T. (2016). A comprehensive excitatory input map of the striatum reveals novel functional organization. *eLife*, *5*, e19103. https://doi.org/10.7554/eLife.19103

Hunt, A. J., Dasgupta, R., Rajamanickam, S., Jiang, Z., Beierlein, M., Chan, C. S., & Justice, N. J. (2018). Paraventricular hypothalamic and amygdalar CRF neurons synapse in the external globus pallidus. *Brain Structure and Function*, *223*(6). https://doi.org/10.1007/s00429-018-1652-y

Ingram, C. D. (2005). Chapter 4.11—Pathways transmitter interactions mediating an integrated stress response. In T. Steckler, N. H. Kalin, & J. M. H. M. Reul (Eds.), *Techniques in the*

Behavioral and Neural Sciences (Vol. 15, pp. 609–639). Elsevier. https://doi.org/10.1016/S0921-0709(05)80033-1

Ishida, H., Iwata, M., Shirayama, Y., & Muneoka, K. (2012). Neural Activation by Milnacipran and Memory Extinction. *Journal of Behavioral and Brain Science*, *02*(02). https://doi.org/10.4236/jbbs.2012.22016

Jiang, J.-X., Liu, H., Huang, Z.-Z., Cui, Y., Zhang, X.-Q., Zhang, X.-L., Cui, Y., & Xin, W.-J. (2018). The role of CA3-LS-VTA loop in the formation of conditioned place preference induced by context-associated reward memory for morphine. *Addiction Biology*, *23*(1), 41–54. https://doi.org/10.1111/adb.12468

Jiang, S. Z., Sweat, S., Dahlke, S. P., Loane, K., Drossel, G., Xu, W., Tejeda, H. A., Gerfen, C. R., & Eiden, L. E. (2021). Cocaine-Dependent Acquisition of Locomotor Sensitization and Conditioned Place Preference Requires D1 Dopaminergic Signaling through a Cyclic AMP, NCS-Rapgef2, ERK, and Egr-1/Zif268 Pathway. *The Journal of Neuroscience: The Official Journal of the Society for Neuroscience*, *41*(4), 711–725. https://doi.org/10.1523/JNEUROSCI.1497-20.2020

Jonas, P., & Lisman, J. (2014). Structure, function, and plasticity of hippocampal dentate gyrus microcircuits. *Frontiers in Neural Circuits*, *8*. https://doi.org/10.3389/fncir.2014.00107

Jones, J. D., Hall, F. S., Uhl, G. R., Rice, K., & Riley, A. L. (2009). Differential involvement of the norepinephrine, serotonin and dopamine reuptake transporter proteins in cocaine-induced taste aversion. *Pharmacology Biochemistry and Behavior*, *93*(1), 75–81. https://doi.org/10.1016/j.pbb.2009.04.009

Kalin, N. H., Shelton, S. E., & Davidson, R. J. (2004). The Role of the Central Nucleus of the Amygdala in Mediating Fear and Anxiety in the Primate. *The Journal of Neuroscience*, *24*(24), 5506–5515. https://doi.org/10.1523/JNEUROSCI.0292-04.2004

Kalivas, P. W. (2009). The glutamate homeostasis hypothesis of addiction. *Nature Reviews Neuroscience*, *10*(8), 561–572. https://doi.org/10.1038/nrn2515

Kalivas, P. W., & O'Brien, C. (2008). Drug Addiction as a Pathology of Staged Neuroplasticity. *Neuropsychopharmacology*, *33*(1), 166–180. https://doi.org/10.1038/sj.npp.1301564

Kardestuncer, T., Wu, H., Lim, A. L., & Neer, E. J. (1998). Cardiac myocytes express mRNA for ten RGS proteins: Changes in RGS mRNA expression in ventricular myocytes and cultured atria. *FEBS Letters*, *438*(3), 285–288. https://doi.org/10.1016/S0014-5793(98)01319-2

Kay, K., Sosa, M., Chung, J. E., Karlsson, M. P., Larkin, M. C., & Frank, L. M. (2016). A hippocampal network for spatial coding during immobility and sleep. *Nature*, *531*(7593), 185–190. https://doi.org/10.1038/nature17144

Kessler, R. C., Chiu, W. T., Demler, O., & Walters, E. E. (2005). Prevalence, Severity, and Comorbidity of Twelve-month DSM-IV Disorders in the National Comorbidity Survey Replication (NCS-R). *Archives of General Psychiatry*, *62*(6), 617–627. https://doi.org/10.1001/archpsyc.62.6.617

Kirouac, G. J. (2021). The Paraventricular Nucleus of the Thalamus as an Integrating and Relay Node in the Brain Anxiety Network. *Frontiers in Behavioral Neuroscience*, *15*. https://doi.org/10.3389/fnbeh.2021.627633

Klump, K. L., & Fowler, N. (2020). Faculty Opinions recommendation of Chronic stress increases susceptibility to food addiction by increasing the levels of DR2 and MOR in the nucleus accumbens. *Faculty Opinions – Post-Publication Peer Review of the Biomedical Literature*. https://doi.org/10.3410/f.735985359.793573086

Kochli, D. E., Keefer, S. E., Gyawali, U., & Calu, D. J. (2020). Basolateral Amygdala to Nucleus Accumbens Communication Differentially Mediates Devaluation Sensitivity of Sign- and Goal-Tracking Rats. *Frontiers in Behavioral Neuroscience*, *14*. https://doi.org/10.3389/fnbeh.2020.593645

Koob, G. F. (2010). The role of CRF and CRF-related peptides in the dark side of addiction. *Brain Research*, *1314*, 3–14. https://doi.org/10.1016/j.brainres.2009.11.008

Koob, G. F., & Le Moal, M. (2008). Addiction and the Brain Antireward System. *Annual Review of Psychology*, *59*(1), 29–53. https://doi.org/10.1146/annurev.psych.59.103006.093548

Koob, G. F., & Volkow, N. D. (2016). Neurobiology of addiction: A neurocircuitry analysis. *The Lancet Psychiatry*, *3*(8), 760–773. https://doi.org/10.1016/S2215-0366(16)00104-8

Kravitz, A. V., Freeze, B. S., Parker, P. R. L., Kay, K., Thwin, M. T., Deisseroth, K., & Kreitzer, A. C. (2010). Regulation of parkinsonian motor behaviors by optogenetic control of basal ganglia circuitry $watermark-text $watermark-text $watermark-text. *Nature*, *466*(7306), 622–626. https://doi.org/10.1038/nature09159

Krawczyk, M., deBacker, J., Mason, X., Jones, A. A., & Dumont, E. C. (2014). Dopamine decreases NMDA currents in the oval bed nucleus of the stria terminalis of cocaine self-administering rats. *Progress in Neuro-Psychopharmacology & Biological Psychiatry*, *51*, 83–88. https://doi.org/10.1016/j.pnpbp.2014.01.011

Kupchik, Y. M., Brown, R. M., Heinsbroek, J. A., Kay Lobo, M., Schwartz, D. J., Kalivas, P. W., & Neurosci, N. (2015). Coding the direct/indirect pathways by D1 and D2 receptors is not valid for accumbens projections. *Nat Neurosci*, *18*(9), 1230–1232. https://doi.org/10.1038/nn.4068

Kupchik, Y. M., & Kalivas, P. W. (2017). The Direct and Indirect Pathways of the Nucleus Accumbens are not What You Think. *Neuropsychopharmacology*, *42*(1), 369–370. https://doi.org/10.1038/npp.2016.160

Lafragette, A., Bardo, M. T., Lardeux, V., Solinas, M., & Thiriet, N. (2017). Reduction of Cocaine-Induced Locomotor Effects by Enriched Environment Is Associated with Cell-Specific Accumulation of ΔFosB in Striatal and Cortical Subregions. *International Journal of Neuropsychopharmacology*, *20*(3), 237–246. https://doi.org/10.1093/ijnp/pyw097

Laham, B. J., Diethorn, E. J., & Gould, E. (2021). Newborn mice form lasting CA2-dependent memories of their mothers. *Cell Reports*, *34*(4), 108668. https://doi.org/10.1016/j.celrep.2020.108668

Lanciego, J. L., Luquin, N., & Obeso, J. A. (2012). Functional neuroanatomy of the basal ganglia. *Cold Spring Harbor Perspectives in Medicine*, *2*(12), a009621–a009621. https://doi.org/10.1101/cshperspect.a009621

Lee, J. Y., Jun, H., Soma, S., Nakazono, T., Shiraiwa, K., Dasgupta, A., Nakagawa, T., Xie, J. L., Chavez, J., Romo, R., Yungblut, S., Hagihara, M., Murata, K., & Igarashi, K. M. (2021). Dopamine facilitates associative memory encoding in the entorhinal cortex. *Nature*, *598*(7880), 321–326. https://doi.org/10.1038/s41586-021-03948-8

Lee, R., Geracioti, T. D., Kasckow, J., & Coccaro, E. F. (2005). Childhood Trauma and Personality Disorder: Positive Correlation With Adult CSF Corticotropin-Releasing Factor Concentrations. *American Journal of Psychiatry*, *162*(5). https://doi.org/10.1176/appi.ajp.162.5.995

Lee, S. E., Simons, S. B., Heldt, S. A., Zhao, M., Schroeder, J. P., Vellano, C. P., Cowan, D. P., Ramineni, S., Yates, C. K., Feng, Y., Smith, Y., Sweatt, J. D., Weinshenker, D., Ressler,

K. J., Dudek, S. M., & Hepler, J. R. (2010). RGS14 is a natural suppressor of both synaptic plasticity in CA2 neurons and hippocampal-based learning and memory. *Proceedings of the National Academy of Sciences*, *107*(39), 16994–16998. https://doi.org/10.1073/pnas.1005362107

Leroy, F., Park, J., Asok, A., Brann, D. H., Meira, T., Boyle, L., Buss, E. W., Kandel, E. R., & Siegelbaum, S. A. (2018). A hippocampal CA2 to lateral septal circuit disinhibits social aggression. *Nature*, *564*(7735), 213–218. https://doi.org/10.1038/s41586-018-0772-0

Lewis, P. A., & Cookson, M. R. (2012). Gene expression in the Parkinson's disease brain. *Brain Research Bulletin*, *88*(4), 302–312. https://doi.org/10.1016/j.brainresbull.2011.11.016

Li, C., & Rainnie, D. G. (2014). Bidirectional regulation of synaptic plasticity in the basolateral amygdala induced by the D1-like family of dopamine receptors and group II metabotropic glutamate receptors. *The Journal of Physiology*, *592*(Pt 19), 4329–4351. https://doi.org/10.1113/jphysiol.2014.277715

Li, H., Penzo, M. A., Taniguchi, H., Kopec, C. D., Huang, Z. J., & Li, B. (2013). Experience-dependent modification of a central amygdala fear circuit. *Nature Neuroscience*, *16*(3), 332–339. https://doi.org/10.1038/nn.3322

Li, Y., Acerbo, M. J., & Robinson, T. E. (2004). The induction of behavioural sensitization is associated with cocaine-induced structural plasticity in the core (but not shell) of the nucleus accumbens. *European Journal of Neuroscience*, *20*(6), 1647–1654. https://doi.org/10.1111/j.1460-9568.2004.03612.x

Lidke, D. S., Huang, F., Post, J. N., Rieger, B., Wilsbacher, J. L., Thomas, J. L., Pouysségur, J., Jovin, T. M., & Lenormand, P. (2010). ERK Nuclear Translocation Is Dimerization-independent but Controlled by the Rate of Phosphorylation. *Journal of Biological Chemistry*, *285*(5). https://doi.org/10.1074/jbc.m109.064972

Liu, H., Acharya, S., Sudan, S. K., Hu, L., Wu, C., Cao, Y., Li, H., & Zhang, X. (2023). Comparative study of the molecular mechanisms underlying the G protein and β-arrestin-dependent pathways that lead to ERKs activation upon stimulation by dopamine D2 receptor. *The FEBS Journal*, *290*(21), 5204–5233. https://doi.org/10.1111/febs.16921

Liu, H. C., Chang, Y. F., Chi, C. W., Lee, C. R., Cheung, S. C., & Liu, T. Y. (1989). Analysis of monoamines in the cerebrospinal fluid of Chinese patients with neurological diseases. *Zhonghua Yi Xue Za Zhi = Chinese Medical Journal; Free China Ed*, *44*(1), 1–6.

Lobo, M. K., & Nestler, E. J. (2011). The striatal balancing act in drug addiction: Distinct roles of direct and indirect pathway medium spiny neurons. *Frontiers in Neuroanatomy*, *5*(JULY), 1–11. https://doi.org/10.3389/fnana.2011.00041

Lu, L., Hope, B. T., Dempsey, J., Liu, S. Y., Bossert, J. M., & Shaham, Y. (2005). Central amygdala ERK signaling pathway is critical to incubation of cocaine craving. *Nature Neuroscience*, *8*(2), 212–219. https://doi.org/10.1038/nn1383

Ma, L., Chen, W., Yu, D., & Han, Y. (2020). Brain-Wide Mapping of Afferent Inputs to Accumbens Nucleus Core Subdomains and Accumbens Nucleus Subnuclei. *Frontiers in Systems Neuroscience*, *14*. https://doi.org/10.3389/fnsys.2020.00015

Mankin, E. A., Diehl, G. W., Sparks, F. T., Leutgeb, S., & Leutgeb, J. K. (2015). Hippocampal CA2 Activity Patterns Change over Time to a Larger Extent than between Spatial Contexts. *Neuron*, *85*(1), 190–201. https://doi.org/10.1016/j.neuron.2014.12.001

Mantsch, J. R. (2022). Corticotropin releasing factor and drug seeking in substance use disorders: Preclinical evidence and translational limitations. *Addiction Neuroscience*, *4*, 100038. https://doi.org/10.1016/j.addicn.2022.100038

Mariathasan, S., Zakarian, A., Bouchard, D., Michie, A. M., Zúñiga-Pflücker, J. C., & Ohashi, P. S. (2001). Duration and Strength of Extracellular Signal-Regulated Kinase Signals Are Altered During Positive Versus Negative Thymocyte Selection1. *The Journal of Immunology*, *167*(9), 4966–4973. https://doi.org/10.4049/jimmunol.167.9.4966

Marin, M.-F., Lord, C., Andrews, J., Juster, R.-P., Sindi, S., Arsenault-Lapierre, G., Fiocco, A. J., & Lupien, S. J. (2011). Chronic stress, cognitive functioning and mental health. *Neurobiology of Learning and Memory*, *96*(4), 583–595. https://doi.org/10.1016/j.nlm.2011.02.016

Matsumoto, N., Kitanishi, T., & Mizuseki, K. (2019). The subiculum: Unique hippocampal hub and more. *Neuroscience Research*, *143*, 1–12. https://doi.org/10.1016/j.neures.2018.08.002

McCann, K. E., Lustberg, D. J., Shaughnessy, E. K., Carstens, K. E., Farris, S., Alexander, G. M., Radzicki, D., Zhao, M., & Dudek, S. M. (2019). Novel role for mineralocorticoid receptors in control of a neuronal phenotype. *Molecular Psychiatry*. https://doi.org/10.1038/s41380-019-0598-7

McDonald, A. J. (1998). Cortical pathways to the mammalian amygdala. *Progress in Neurobiology*, *55*(3), 257–332. https://doi.org/10.1016/S0301-0082(98)00003-3

Meira, T., Leroy, F., Buss, E. W., Oliva, A., Park, J., & Siegelbaum, S. A. (2018). A hippocampal circuit linking dorsal CA2 to ventral CA1 critical for social memory dynamics. *Nature Communications*, *9*(1), 4163. https://doi.org/10.1038/s41467-018-06501-w

Mogenson, G. J., & Calaresu, F. R. (1973). Cardiovascular responses to electrical stimulation of the amygdala in the rat. *Experimental Neurology*, *39*(1), 166–180. https://doi.org/10.1016/0014-4886(73)90049-6

Montanez-Miranda, C., Bramlett, S. N., & Hepler, J. R. (2023). RGS14 expression in CA2 hippocampus, amygdala, and basal ganglia: Implications for human brain physiology and disease. *Hippocampus*, *33*(3), 166–181. https://doi.org/10.1002/hipo.23492

Nader, K., Majidishad, P., Amorapanth, P., & LeDoux, J. E. (2001). Damage to the Lateral and Central, but Not Other, Amygdaloid Nuclei Prevents the Acquisition of Auditory Fear Conditioning. *Learning &Amp; Memory*, *8*(3). https://doi.org/10.1101/lm.38101

Nestler, E. J. (2005). Is there a common molecular pathway for addiction? *Nature Neuroscience*, *8*(11), 1445–1449. https://doi.org/10.1038/nn1578

Nguyen, H. T., Bryois, J., Kim, A., Dobbyn, A., Huckins, L. M., Munoz-Manchado, A. B., Ruderfer, D. M., Genovese, G., Fromer, M., Xu, X., Pinto, D., Linnarsson, S., Verhage, M., Smit, A. B., Hjerling-Leffler, J., Buxbaum, J. D., Hultman, C., Sklar, P., Purcell, S. M., … Stahl, E. A. (2017). Integrated Bayesian analysis of rare exonic variants to identify risk genes for schizophrenia and neurodevelopmental disorders. *Genome Medicine*, *9*(1), 114. https://doi.org/10.1186/s13073-017-0497-y

O'Mara, S. M., Commins, S., & Anderson, M. (2000). Synaptic plasticity in the hippocampal area CA1-subiculum projection: Implications for theories of memory. *Hippocampus*, *10*(4), 447–456. https://doi.org/10.1002/1098-1063(2000)10:4<447::AID-HIPO11>3.0.CO;2-2

Pagliusi, M., Franco, D., Cole, S., Morais-Silva, G., Chandra, R., Fox, M. E., Iñiguez, S. D., Sartori, C. R., & Lobo, M. K. (2022). The BDNF-TrkB Pathway Acts Through Nucleus Accumbens D2 Expressing Neurons to Mediate Stress Susceptible Outcomes. *Frontiers in Psychiatry*, *13*. https://doi.org/10.3389/fpsyt.2022.854494

Pan, B., Hillard, C. J., & Liu, Q. (2008). Endocannabinoid Signaling Mediates Cocaine-Induced Inhibitory Synaptic Plasticity in Midbrain Dopamine Neurons. *Journal of Neuroscience*, *28*(6), 1385–1397. https://doi.org/10.1523/JNEUROSCI.4033-07.2008

Park, S.-B., Lim, H.-Y., Lee, E.-Y., Yoo, S.-W., Jung, H.-S., Lee, E., Sun, W., & Lee, I. (2022). The fasciola cinereum subregion of the hippocampus is important for the acquisition of visual contextual memory. *Progress in Neurobiology*, *210*, 102217. https://doi.org/10.1016/j.pneurobio.2022.102217

Parker, C. C., Sokoloff, G., Cheng, R., & Palmer, A. A. (2012). Genome-Wide Association for Fear Conditioning in an Advanced Intercross Mouse Line. *Behavior Genetics*, *42*(3), 437–448. https://doi.org/10.1007/s10519-011-9524-8

Pascoli, V., Cahill, E., Bellivier, F., Caboche, J., & Vanhoutte, P. (2014). Extracellular signal-regulated protein kinases 1 and 2 activation by addictive drugs: A signal toward pathological adaptation. *Biological Psychiatry*, *76*(12), 917–926. https://doi.org/10.1016/j.biopsych.2014.04.005

Paxinos, G. and Franklin, K.B.J. (2001) The Mouse Brain in Stereotaxic Coordinates. 2nd Edition, Academic Press, San Diego.

Pêgo, J. M., Morgado, P., Pinto, L. G., Cerqueira, J. J., Almeida, O. F. X., & Sousa, N. (2008). Dissociation of the morphological correlates of stress-induced anxiety and fear. *European Journal of Neuroscience*, *27*(6), 1503–1516. https://doi.org/10.1111/j.1460-9568.2008.06112.x

Penzo, M. A., Robert, V., & Li, B. (2014). Fear Conditioning Potentiates Synaptic Transmission onto Long-Range Projection Neurons in the Lateral Subdivision of Central Amygdala. *Journal of Neuroscience*, *34*(7), 2432–2437. https://doi.org/10.1523/JNEUROSCI.4166-13.2014

Pierce, R. C., Pierce-Bancroft, A. F., & Prasad, B. M. (1999). Neurotrophin-3 contributes to the initiation of behavioral sensitization to cocaine by activating the Ras/Mitogen-activated protein kinase signal transduction cascade. *The Journal of Neuroscience: The Official Journal of the Society for Neuroscience*, *19*(19), 8685–8695. https://doi.org/10.1523/JNEUROSCI.19-19-08685.1999

Pignatelli, M., & Beyeler, A. (2019). Valence coding in amygdala circuits. *Current Opinion in Behavioral Sciences*, *26*, 97–106. https://doi.org/10.1016/j.cobeha.2018.10.010

Pitkänen, A., Savander, V., & LeDoux, J. E. (1997). Organization of intra-amygdaloid circuitries in the rat: An emerging framework for understanding functions of the amygdala. *Trends in Neurosciences*, *20*(11), 517–523. https://doi.org/10.1016/S0166-2236(97)01125-9

Plasse, G. van der, Schrama, R., Seters, S. P. van, Vanderschuren, L. J. M. J., & Westenberg, H. G. M. (2012). Deep Brain Stimulation Reveals a Dissociation of Consummatory and Motivated Behaviour in the Medial and Lateral Nucleus Accumbens Shell of the Rat. *PLOS ONE*, *7*(3), e33455. https://doi.org/10.1371/journal.pone.0033455

Rissman, R. A., Staup, M., Lee, A. R., Justice, N. J., Rice, K. C., Vale, W., & Sawchenko, P. E. (2012). Corticotropin-releasing factor receptor-dependent effects of repeated stress on tau phosphorylation, solubility, and aggregation. *Proceedings of the National Academy of Sciences*, *109*(16). https://doi.org/10.1073/pnas.1203140109

Rizzi-Wise, C. A., & Wang, D. V. (2021). Putting Together Pieces of the Lateral Septum: Multifaceted Functions and Its Neural Pathways. *eNeuro*, *8*(6), ENEURO.0315-21.2021. https://doi.org/10.1523/ENEURO.0315-21.2021

Roberts-Wolfe, D., Bobadilla, A.-C., Heinsbroek, J. A., Neuhofer, D., & Kalivas, P. W. (2018). Drug Refraining and Seeking Potentiate Synapses on Distinct Populations of Accumbens Medium Spiny Neurons. *The Journal of Neuroscience: The Official Journal of the Society for Neuroscience*, *38*(32), 7100–7107. https://doi.org/10.1523/JNEUROSCI.0791-18.2018

Robison, A. J., Vialou, V., Mazei-Robison, M., Feng, J., Kourrich, S., Collins, M., Wee, S., Koob, G., Turecki, G., Neve, R., Thomas, M., & Nestler, E. J. (2013). Behavioral and Structural Responses to Chronic Cocaine Require a Feedforward Loop Involving ΔFosB and Calcium/Calmodulin-Dependent Protein Kinase II in the Nucleus Accumbens Shell. *Journal of Neuroscience*, *33*(10), 4295–4307. https://doi.org/10.1523/JNEUROSCI.5192-12.2013

Rogan, M. T., Stäubli, U. V., & LeDoux, J. E. (1997). Fear conditioning induces associative long-term potentiation in the amygdala. *Nature*, *390*(6660), 604–607. https://doi.org/10.1038/37601

Roy, D. S., Kitamura, T., Okuyama, T., Ogawa, S. K., Sun, C., Obata, Y., Yoshiki, A., & Tonegawa, S. (2017). Distinct Neural Circuits for the Formation and Retrieval of Episodic Memories. *Cell*, *170*(5), 1000-1012.e19. https://doi.org/10.1016/j.cell.2017.07.013

Russo, S. J., Dietz, D. M., Dumitriu, D., Morrison, J. H., Malenka, R. C., & Nestler, E. J. (2010). The addicted synapse: Mechanisms of synaptic and structural plasticity in nucleus accumbens. *Trends in Neurosciences*, *33*(6), 267–276. https://doi.org/10.1016/j.tins.2010.02.002

Sacks, D. B. (2006). The role of scaffold proteins in MEK/ERK signalling. *Biochemical Society Transactions*, *34*(5), 833–836. https://doi.org/10.1042/BST0340833

Saddoris, M. P., & Carelli, R. M. (2014). Cocaine Self-Administration Abolishes Associative Neural Encoding in the Nucleus Accumbens Necessary for Higher-Order Learning. *Biological Psychiatry*, *75*(2), 156–164. https://doi.org/10.1016/j.biopsych.2013.07.037

Sah, P., Faber, E. S. L., Lopez De Armentia, M., & Power, J. (2003). The Amygdaloid Complex: Anatomy and Physiology. *Physiological Reviews*, *83*(3), 803–834. https://doi.org/10.1152/physrev.00002.2003

Sakloth, F., Polizu, C., Bertherat, F., & Zachariou, V. (2020). Regulators of G Protein Signaling in Analgesia and Addiction. *Molecular Pharmacology*, *98*(6), 739–750. https://doi.org/10.1124/mol.119.119206

Salamone, J. D. (1994). The involvement of nucleus accumbens dopamine in appetitive and aversive motivation. *Behavioural Brain Research*, *61*(2), 117–133. https://doi.org/10.1016/0166-4328(94)90153-8

Salamone, J. D., & Correa, M. (2012). The Mysterious Motivational Functions of Mesolimbic Dopamine. *Neuron*, *76*(3). https://doi.org/10.1016/j.neuron.2012.10.021

Samadi, M., Hales, C. A., Lustberg, D. J., Farris, S., Ross, M. R., Zhao, M., Hepler, J. R., Harbin, N. H., Robinson, E. S. J., Banks, P. J., Bashir, Z. I., & Dudek, S. M. (2023). Mechanisms of mGluR-dependent plasticity in hippocampal area CA2. *Hippocampus*, *33*(6), 730–744. https://doi.org/10.1002/hipo.23529

Schielzeth, H., Dingemanse, N. J., Nakagawa, S., Westneat, D. F., Allegue, H., Teplitsky, C., Réale, D., Dochtermann, N. A., Garamszegi, L. Z., & Araya-Ajoy, Y. G. (2020). Robustness of linear mixed-effects models to violations of distributional assumptions.

Methods in Ecology and Evolution, *11*(9), 1141–1152. https://doi.org/10.1111/2041-210X.13434

Schultz, H., Sommer, T., & Peters, J. (2015). The Role of the Human Entorhinal Cortex in a Representational Account of Memory. *Frontiers in Human Neuroscience*, *9*. https://doi.org/10.3389/fnhum.2015.00628

Shen, E. H., Overly, C. C., & Jones, A. R. (2012). The Allen Human Brain Atlas: Comprehensive gene expression mapping of the human brain. *Trends in Neurosciences*, *35*(12), 711–714. https://doi.org/10.1016/j.tins.2012.09.005

Shiflett, M. W., & Balleine, B. W. (2010). At the limbic–motor interface: Disconnection of basolateral amygdala from nucleus accumbens core and shell reveals dissociable components of incentive motivation. *European Journal of Neuroscience*, *32*(10), 1735–1743. https://doi.org/10.1111/j.1460-9568.2010.07439.x

Shin, S., Pribiag, H., Lilascharoen, V., Knowland, D., Wang, X. Y., & Lim, B. K. (2018). Drd3 Signaling in the Lateral Septum Mediates Early Life Stress-Induced Social Dysfunction. *Neuron*, *97*(1). https://doi.org/10.1016/j.neuron.2017.11.040

Shindo, Y., Iwamoto, K., Mouri, K., Hibino, K., Tomita, M., Kosako, H., Sako, Y., & Takahashi, K. (2016). Conversion of graded phosphorylation into switch-like nuclear translocation via autoregulatory mechanisms in ERK signalling. *Nature Communications*, *7*(1). https://doi.org/10.1038/ncomms10485

Shu, F., Ramineni, S., & Hepler, J. R. (2010). RGS14 is a multifunctional scaffold that integrates G protein and Ras/Raf MAPkinase signalling pathways. *Cellular Signalling*, *22*(3), 366–376. https://doi.org/10.1016/j.cellsig.2009.10.005

Shuen, J. A., Chen, M., Gloss, B., & Calakos, N. (2008). Drd1a-tdTomato BAC Transgenic Mice for Simultaneous Visualization of Medium Spiny Neurons in the Direct and Indirect Pathways of the Basal Ganglia. *The Journal of Neuroscience*, *28*(11), 2681–2685. https://doi.org/10.1523/JNEUROSCI.5492-07.2008

Sjögren, B. (2011). 10 - Regulator of G Protein Signaling Proteins as Drug Targets: Current State and Future Possibilities. In R. R. Neubig (Ed.), *Advances in Pharmacology* (Vol. 62, pp. 315–347). Academic Press. https://doi.org/10.1016/B978-0-12-385952-5.00002-6

Smedley, E. B., DiLeo, A., & Smith, K. S. (2019). Circuit directionality for motivation: Lateral accumbens-pallidum, but not pallidum-accumbens, connections regulate motivational attraction to reward cues. *Neurobiology of Learning and Memory*, *162*, 23–35. https://doi.org/10.1016/j.nlm.2019.05.001

Smith, A. S., Williams Avram, S. K., Cymerblit-Sabba, A., Song, J., & Young, W. S. (2016). Targeted activation of the hippocampal CA2 area strongly enhances social memory. *Molecular Psychiatry*, *21*(8), 1137–1144. https://doi.org/10.1038/mp.2015.189

Smith, L. N., Penrod, R. D., Taniguchi, M., & Cowan, C. W. (2016). Assessment of Cocaine-induced Behavioral Sensitization and Conditioned Place Preference in Mice. *Journal of Visualized Experiments : JoVE*, *108*, 53107. https://doi.org/10.3791/53107

Snow, B. E., Antonio, L., Suggs, S., Gutstein, H. B., & Siderovski, D. P. (1997). Molecular Cloning and Expression Analysis of Rat *Rgs12* and *Rgs14*. *Biochemical and Biophysical Research Communications*, *233*(3), 770–777. https://doi.org/10.1006/bbrc.1997.6537

Speranza, L., di Porzio, U., Viggiano, D., de Donato, A., & Volpicelli, F. (2021). Dopamine: The Neuromodulator of Long-Term Synaptic Plasticity, Reward and Movement Control. *Cells*, *10*(4), 735. https://doi.org/10.3390/cells10040735

Squires, K. E., Gerber, K. J., Pare, J.-F., Branch, M. R., Smith, Y., & Hepler, J. R. (2018). Regulator of G protein signaling 14 (RGS14) is expressed pre- and postsynaptically in neurons of hippocampus, basal ganglia, and amygdala of monkey and human brain. *Brain Structure and Function*, *223*(1), 233–253. https://doi.org/10.1007/s00429-017-1487-y

Squires, K. E., Gerber, K. J., Tillman, M. C., Lustberg, D. J., Montañez-Miranda, C., Zhao, M., Ramineni, S., Scharer, C. D., Saha, R. N., Shu, F.-J., Schroeder, J. P., Ortlund, E. A., Weinshenker, D., Dudek, S. M., & Hepler, J. R. (2020). Human genetic variants disrupt RGS14 nuclear shuttling and regulation of LTP in hippocampal neurons. *The Journal of Biological Chemistry*, *296*, 100024. https://doi.org/10.1074/jbc.RA120.016009

Stalnaker, T. A., Calhoon, G. G., Ogawa, M., Roesch, M. R., & Schoenbaum, G. (2010). Neural Correlates of Stimulus–Response and Response–Outcome Associations in Dorsolateral Versus Dorsomedial Striatum. *Frontiers in Integrative Neuroscience*, *4*, 12. https://doi.org/10.3389/fnint.2010.00012

Stern, C. M., Meitzen, J., & Mermelstein, P. (2011). Corticotropin-releasing factor and urocortin I activate CREB through functionally selective Gβγ signaling in hippocampal pyramidal neurons. *European Journal of Neuroscience*, *34*(5). https://doi.org/10.1111/j.1460-9568.2011.07812.x

Steve, T. A., Jirsch, J. D., & Gross, D. W. (2014). Quantification of subfield pathology in hippocampal sclerosis: A systematic review and meta-analysis. *Epilepsy Research*, *108*(8), 1279–1285. https://doi.org/10.1016/j.eplepsyres.2014.07.003

Stevenson, E. L., & Caldwell, H. K. (2014). Lesions to the CA2 region of the hippocampus impair social memory in mice. *The European Journal of Neuroscience*, *40*(9), 3294–3301. https://doi.org/10.1111/ejn.12689

Stewart, A., & Fisher, R. A. (2015). Chapter One - Introduction: G Protein-coupled Receptors and RGS Proteins. In R. A. Fisher (Ed.), *Progress in Molecular Biology and Translational Science* (Vol. 133, pp. 1–11). Academic Press. https://doi.org/10.1016/bs.pmbts.2015.03.002

Stewart, J., de Wit, H., & Eikelboom, R. (1984). Role of unconditioned and conditioned drug effects in the self-administration of opiates and stimulants. *Psychological Review*, *91*(2), 251–268. https://doi.org/10.1037/0033-295X.91.2.251

Stock, G., Schlör, K. H., Heidt, H., & Buss, J. (1978). Psychomotor behaviour and cardiovascular patterns during stimulation of the amygdala. *Pflügers Archiv*, *376*(2), 177–184. https://doi.org/10.1007/BF00581581

Stuber, G. D., Sparta, D. R., Stamatakis, A. M., van Leeuwen, W. A., Hardjoprajitno, J. E., Cho, S., Tye, K. M., Kempadoo, K. A., Zhang, F., Deisseroth, K., & Bonci, A. (2011). Excitatory transmission from the amygdala to nucleus accumbens facilitates reward seeking. *Nature*, *475*(7356), 377–380. https://doi.org/10.1038/nature10194

Sun, Y., Gooch, H., & Sah, P. (2020). *Fear conditioning and the basolateral amygdala* (9:53). F1000Research. https://doi.org/10.12688/f1000research.21201.1

Terburg, D., Scheggia, D., Rio, R. T. del, Klumpers, F., Ciobanu, A. C., Morgan, B., Montoya, E. R., Bos, P. A., Giobellina, G., Burg, E. H. van den, Gelder, B. de, Stein, D. J., Stoop, R., & Honk, J. van. (2018). The Basolateral Amygdala Is Essential for Rapid Escape: A Human and Rodent Study. *Cell*, *175*(3), 723-735.e16. https://doi.org/10.1016/j.cell.2018.09.028

Thomas, M. J., Kalivas, P. W., & Shaham, Y. (2008). Neuroplasticity in the mesolimbic dopamine system and cocaine addiction. *British Journal of Pharmacology*, *154*(2), 327–342. https://doi.org/10.1038/bjp.2008.77

Tokutake, T., Asano, T., Miyanishi, H., Nakaya, S., Izuo, N., & Nitta, A. (2022). Cannabinoid Type 1 Receptors in the Basolateral Amygdala Regulate ACPA-Induced Place Preference and Anxiolytic-Like Behaviors. *Neurochemical Research*, *47*(9), 2899–2908. https://doi.org/10.1007/s11064-022-03708-8

Tompkins, J. D., Clason, T. A., Hardwick, J. C., Girard, B. M., Merriam, L. A., May, V., & Parsons, R. L. (2016). Activation of MEK/ERK signaling contributes to the PACAP-induced increase in guinea pig cardiac neuron excitability. *American Journal of Physiology-Cell Physiology*, *311*(4). https://doi.org/10.1152/ajpcell.00164.2016

Tyrka, A. R., Price, L. H., Gelernter, J., Schepker, C., Anderson, G. M., & Carpenter, L. L. (2009). Interaction of Childhood Maltreatment with the Corticotropin-Releasing Hormone Receptor Gene: Effects on Hypothalamic-Pituitary-Adrenal Axis Reactivity. *Biological Psychiatry*, *66*(7). https://doi.org/10.1016/j.biopsych.2009.05.012

Tzakis, N., & Holahan, M. R. (2019). Social Memory and the Role of the Hippocampal CA2 Region. *Frontiers in Behavioral Neuroscience*, *13*. https://doi.org/10.3389/fnbeh.2019.00233

Ueda, S., Hosokawa, M., Arikawa, K., Takahashi, K., Fujiwara, M., Kakita, M., Fukada, T., Koyama, H., Horigane, S., Itoi, K., Kakeyama, M., Matsunaga, H., Takeyama, H., Bito, H., & Takemoto-Kimura, S. (2021). Distinctive Regulation of Emotional Behaviors and Fear-Related Gene Expression Responses in Two Extended Amygdala Subnuclei With Similar Molecular Profiles. *Frontiers in Molecular Neuroscience*, *14*, 741895. https://doi.org/10.3389/fnmol.2021.741895

Ünal, Ç. T., Beverley, J. A., Willuhn, I., & Steiner, H. (2009). Long-lasting dysregulation of gene expression in corticostriatal circuits after repeated cocaine treatment in adult rats: Effects on *zif 268* and *homer 1a*. *European Journal of Neuroscience*, *29*(8). https://doi.org/10.1111/j.1460-9568.2009.06691.x

Urs, N. M., Daigle, T. L., & Caron, M. G. (2011). A dopamine D1 receptor-dependent β-arrestin signaling complex potentially regulates morphine-induced psychomotor activation but not reward in mice. *Neuropsychopharmacology: Official Publication of the American College of Neuropsychopharmacology*, *36*(3), 551–558. https://doi.org/10.1038/npp.2010.186

Usman, D. M., Lawal, R. A., Jude, O., Lateef, O., Obadeji, A., & Ferdinand, K. (2019). Psychological Morbidity among Psychoactive Substance Users in a Rehabilitation Centre in Nigeria. *International Journal of TROPICAL DISEASE &Amp; Health*. https://doi.org/10.9734/ijtdh/2019/v39i330205

Valjent, E., Pagès, C., Hervé, D., Girault, J.-A., & Caboche, J. (2004). Addictive and non-addictive drugs induce distinct and specific patterns of ERK activation in mouse brain. *The European Journal of Neuroscience*, *19*(7), 1826–1836. https://doi.org/10.1111/j.1460-9568.2004.03278.x

Valjent, E., Pascoli, V., Svenningsson, P., Paul, S., Enslen, H., Corvol, J.-C., Stipanovich, A., Caboche, J., Lombroso, P. J., Nairn, A. C., Greengard, P., Hervé, D., & Girault, J.-A. (2005). Regulation of a protein phosphatase cascade allows convergent dopamine and glutamate signals to activate ERK in the striatum. *Proceedings of the National Academy of Sciences*, *102*(2), 491–496. https://doi.org/10.1073/pnas.0408305102

Vatner, D. E., Zhang, J., Oydanich, M., Guers, J., Katsyuba, E., Yan, L., Sinclair, D., Auwerx, J., & Vatner, S. F. (2018). Enhanced longevity and metabolism by brown adipose tissue with disruption of the regulator of G protein signaling 14. *Aging Cell*, *17*(4), e12751. https://doi.org/10.1111/acel.12751

Vélez-Hernández, M. E., Vázquez-Torres, R., Velasquez-Martinez, M. C., Jiménez, L., Báez, F., Sacktor, T. C., & Jiménez-Rivera, C. A. (2013). Inhibition of Protein kinase Mzeta (PKMζ) in the mesolimbic system alters cocaine sensitization in rats. *Journal of Drug and Alcohol Research*, *2*, 235669. https://doi.org/10.4303/jdar/235669

Vellano, C. P., Brown, N. E., Blumer, J. B., & Hepler, J. R. (2013). Assembly and function of the regulator of G protein signaling 14 (RGS14)·H-Ras signaling complex in live cells are regulated by Gαi1 and Gαi-linked G protein-coupled receptors. *The Journal of Biological Chemistry*, *288*(5), 3620–3631. https://doi.org/10.1074/jbc.M112.440057

Vellano, C. P., Maher, E. M., Hepler, J. R., & Blumer, J. B. (2011). G protein-coupled receptors and resistance to inhibitors of cholinesterase-8A (Ric-8A) both regulate the regulator of g protein signaling 14 RGS14·Gαi1 complex in live cells. *The Journal of Biological Chemistry*, *286*(44), 38659–38669. https://doi.org/10.1074/jbc.M111.274928

Verharen, J. P. H., Adan, R. A. H., & Vanderschuren, L. J. M. J. (2019). Differential contributions of striatal dopamine D1 and D2 receptors to component processes of value-based decision making. *Neuropsychopharmacology*, *44*(13). https://doi.org/10.1038/s41386-019-0454-0

Viviani, D., Charlet, A., van den Burg, E., Robinet, C., Hurni, N., Abatis, M., Magara, F., & Stoop, R. (2011). Oxytocin Selectively Gates Fear Responses Through Distinct Outputs from the Central Amygdala. *Science*, *333*(6038), 104–107. https://doi.org/10.1126/science.1201043

Volkow, N. D., Fowler, J. S., Wang, G.-J., Hitzemann, R., Logan, J., Schlyer, D. J., Dewey, S. L., & Wolf, A. P. (1993). Decreased dopamine D2 receptor availability is associated with reduced frontal metabolism in cocaine abusers. *Synapse*, *14*(2), 169–177. https://doi.org/10.1002/syn.890140210

Volkow, N. D., Wang, G.-J., Fowler, J. S., Logan, J., Hitzemann, R., Gatley, S. J., MacGregor, R. R., & Wolf, A. P. (1996). Cocaine Uptake Is Decreased in the Brain of Detoxified Cocaine Abusers. *Neuropsychopharmacology*, *14*(3), 159–168. https://doi.org/10.1016/0893-133X(95)00073-M

Volkow, N. D., Wang, G.-J., Telang, F., Fowler, J. S., Logan, J., Jayne, M., Ma, Y., Pradhan, K., & Wong, C. (2007). Profound Decreases in Dopamine Release in Striatum in Detoxified Alcoholics: Possible Orbitofrontal Involvement. *Journal of Neuroscience*, *27*(46), 12700–12706. https://doi.org/10.1523/JNEUROSCI.3371-07.2007

Vorspan, F., Mehtelli, W., Dupuy, G., Bloch, V., & Lépine, J.-P. (2015). Anxiety and Substance Use Disorders: Co-occurrence and Clinical Issues. *Current Psychiatry Reports*, *17*(2), 4. https://doi.org/10.1007/s11920-014-0544-y

Walker, D. L., Miles, L. A., & Davis, M. (2009). Selective Participation of the Bed Nucleus of the Stria Terminalis and CRF in Sustained Anxiety-Like versus Phasic Fear-Like Responses. *Progress in Neuro-Psychopharmacology & Biological Psychiatry*, *33*(8), 1291–1308. https://doi.org/10.1016/j.pnpbp.2009.06.022

Walker, Q. D., Cabassa, J., Kaplan, K. A., Li, S.-T., Haroon, J., Spohr, H. A., & Kuhn, C. M. (2001). Sex Differences in Cocaine-Stimulated Motor Behavior: Disparate Effects of

Gonadectomy. *Neuropsychopharmacology*, *25*(1), 118–130. https://doi.org/10.1016/S0893-133X(00)00248-7

Wall, E. G., Desai, R., Aung, Z. K., Yeo, S. H., Grattan, D. R., Handelsman, D. J., & Herbison, A. E. (2023). *Unexpected plasma gonadal steroid and reproductive hormone levels across the mouse estrous cycle*. Scite.Ai. https://doi.org/10.1101/2023.02.28.530435

Wallis, D., Coatsworth, J. D., Mennis, J., Riggs, N. R., Zaharakis, N., Russell, M. A., Brown, A. R., Rayburn, S., Radford, A., Hale, C., & Mason, M. J. (2022). Predicting Self-Medication with Cannabis in Young Adults with Hazardous Cannabis Use. *International Journal of Environmental Research and Public Health*, *19*(3), 1850. https://doi.org/10.3390/ijerph19031850

Wang, J.-H., & Cui, S. (2018). Associative memory cells and their working principle in the brain. *F1000Research*, *7*, 108. https://doi.org/10.12688/f1000research.13665.1

Wang, X.-D., Chen, Y., Wolf, M., Wagner, K. V., Liebl, C., Scharf, S. H., Harbich, D., Mayer, B., Wurst, W., Holsboer, F., Deussing, J. M., Baram, T. Z., Müller, M. B., & Schmidt, M. V. (2011). Forebrain CRHR1 deficiency attenuates chronic stress-induced cognitive deficits and dendritic remodeling. *Neurobiology of Disease*, *42*(3). https://doi.org/10.1016/j.nbd.2011.01.020

Wassum, K. M., & Izquierdo, A. (2015). The basolateral amygdala in reward learning and addiction. *Neuroscience & Biobehavioral Reviews*, *57*, 271–283. https://doi.org/10.1016/j.neubiorev.2015.08.017

Weera, M. M., Agoglia, A. E., Douglass, E., Jiang, Z., Rajamanikam, S., Shackett, R. S., Justice, N. J., Herman, M. A., & Gilpin, N. W. (2021). *Generation and validation of a CRF_1:Cre transgenic rat: The role of central amygdala CRF_1in nociception and anxiety-like behavior*. Scite.Ai. https://doi.org/10.1101/2021.02.23.432551

West, E. A., & Carelli, R. M. (2016). Nucleus Accumbens Core and Shell Differentially Encode Reward-Associated Cues after Reinforcer Devaluation. *Journal of Neuroscience*, *36*(4), 1128–1139. https://doi.org/10.1523/JNEUROSCI.2976-15.2016

Wilks, L. J., & File, S. E. (2008). Evidence for Simultaneous Anxiolytic and Aversive Effects Several Hours after Administration of Sodium Phenobarbitone to the Rat. *Neuropsychobiology*, *19*(2), 86–89. https://doi.org/10.1159/000118440

Willard, F. S., Willard, M. D., Kimple, A. J., Soundararajan, M., Oestreich, E. A., Li, X., Sowa, N. A., Kimple, R. J., Doyle, D. A., Der, C. J., Zylka, M. J., Snider, W. D., & Siderovski, D. P. (2009). Regulator of G-protein signaling 14 (RGS14) is a selective H-Ras effector. *PloS One*, *4*(3), e4884–e4884. https://doi.org/10.1371/journal.pone.0004884

Willis, M. A., & Haines, D. E. (2018). Chapter 31—The Limbic System. In D. E. Haines & G. A. Mihailoff (Eds.), *Fundamental Neuroscience for Basic and Clinical Applications (Fifth Edition)* (pp. 457-467.e1). Elsevier. https://doi.org/10.1016/B978-0-323-39632-5.00031-1

Winter, A. S., McMurray, K. M. J., Ahlbrand, R., Allgire, E., Shukla, S., Jones, J. W., & Sah, R. (2022). The subfornical organ regulates acidosis-evoked fear by engaging microglial acid-sensor TDAG8 and forebrain neurocircuits in male mice. *Journal of Neuroscience Research*, *100*(9). https://doi.org/10.1002/jnr.25059

Wu, L.-T., & Howard, M. O. (2007). Psychiatric disorders in inhalant users: Results from The National Epidemiologic Survey on Alcohol and Related Conditions. *Drug and Alcohol Dependence*, *88*(2–3). https://doi.org/10.1016/j.drugalcdep.2006.10.012

Ying, S.-W., Futter, M., Rosenblum, K., Webber, M. J., Hunt, S. P., Bliss, T. V. P., & Bramham, C. R. (2002). Brain-Derived Neurotrophic Factor Induces Long-Term Potentiation in

Intact Adult Hippocampus: Requirement for ERK Activation Coupled to CREB and Upregulation of Arc Synthesis. *Journal of Neuroscience*, *22*(5), 1532–1540. https://doi.org/10.1523/JNEUROSCI.22-05-01532.2002

Yoshida, S., Ohnishi, R., Tsuneoka, Y., Yamamoto-Mimura, Y., Muramatsu, R., Kato, T., Funato, H., & Kuroda, K. O. (2018). Corticotropin-Releasing Factor Receptor 1 in the Anterior Cingulate Cortex Mediates Maternal Absence-Induced Attenuation of Transport Response in Mouse Pups. *Frontiers in Cellular Neuroscience*, *12*. https://doi.org/10.3389/fncel.2018.00204

Young, C. B., Reddy, V., & Sonne, J. (2024). Neuroanatomy, Basal Ganglia. In *StatPearls*. StatPearls Publishing. http://www.ncbi.nlm.nih.gov/books/NBK537141/

Young, W. S., Li, J., Wersinger, S. R., & Palkovits, M. (2006). The vasopressin 1b receptor is prominent in the hippocampal area CA2 where it is unaffected by restraint stress or adrenalectomy. *Neuroscience*, *143*(4), 1031–1039. https://doi.org/10.1016/j.neuroscience.2006.08.040

Zachry, J. E., Kutlu, M. G., Yoon, H. J., Leonard, M. Z., Chevée, M., Patel, D. D., Gaidici, A., Kondev, V., Thibeault, K. C., Bethi, R., Tat, J., Melugin, P. R., Isiktas, A. U., Joffe, M. E., Cai, D. J., Conn, P. J., Grueter, B. A., & Calipari, E. S. (2024). D1 and D2 medium spiny neurons in the nucleus accumbens core have distinct and valence-independent roles in learning. *Neuron*, *112*(5), 835-849.e7. https://doi.org/10.1016/j.neuron.2023.11.023

Zhang, J., Ding, M., Liu, H., Shi, J., Wang, Z., Wen, P., Zhang, Y., Yan, B., Guo, D., Zhang, X., Tao, R., Yan, Z., Zhang, Y., Liu, Z., Guo, W., & Zhang, S. (2022). Regulator of G-protein signaling 14 protects the liver from ischemia–reperfusion injury by suppressing TGF-β-activated kinase 1 activation. *Hepatology (Baltimore, Md.)*, *75*(2), 338–352. https://doi.org/10.1002/hep.32133

Zhang, L., & Hernández, V. S. (2013). Synaptic innervation to rat hippocampus by vasopressin-immuno-positive fibres from the hypothalamic supraoptic and paraventricular nuclei. *Neuroscience*, *228*, 139–162. https://doi.org/10.1016/j.neuroscience.2012.10.010

Zhang, N., Zhao, S., Ma, Y., Xiao, Z., Xue, B., Dong, Y., Wang, Q., Xu, H., Zhang, X., & Wang, Y. (2024). Hyperexcitation of ovBNST CRF neurons during stress contributes to female-biased expression of anxiety-like avoidance behaviors. *Science Advances*, *10*(19), eadk7636. https://doi.org/10.1126/sciadv.adk7636

Zhu, J. J., Qin, Y., Zhao, M., Van Aelst, L., & Malinow, R. (2002). Ras and Rap control AMPA receptor trafficking during synaptic plasticity. *Cell*, *110*(4), 443–455. https://doi.org/10.1016/s0092-8674(02)00897-8

Zhu, J., Xu, X., Knight, G. E., He, C., Burnstock, G., & Xiang, Z. (2015). A subpopulation of gonadotropin-releasing hormone neurons in the adult mouse forebrain is γ-Aminobutyric acidergic. *Journal of Neuroscience Research*, *93*(10). https://doi.org/10.1002/jnr.23610